

# 1<sup>st</sup> International Conference on NMR Microscopy

## Heidelberg, September 15 - 19, 1991

Welcome to the 1<sup>st</sup> International Conference on NMR Microscopy in Heidelberg. Essential features of this conference are:

- Registration and conference activities take place at the Max-Planck-Haus, 6900 Heidelberg, Berliner Str. 10 (300 m North of the Ernst-Walz bridge across the Neckar river).
- The registration desk is open during the entire conference: Sun.: 16.00 - 20.00 o'clock, Mon. - Wed.: 9.00 - 18.00 o'clock, Thurs.: 8.30 - 13.00 o'clock.
- The posters are on display during the entire length of the conference. There is an informal poster viewing on Sunday evening from 20.00 to 22.00 o'clock.
- A welcoming cocktail party is given on Sunday from 19.00 to 20.00 o'clock in the mensa of the Max-Planck-Haus.
- Companies will exhibit their products in the Max-Planck-Haus during the meeting.
- The financial support of the vendors and industrial companies is gratefully acknowledged. It enables the participation of many students and colleagues from former east block countries in this conference.

W. Kuhn and B. Blümich

# Sponsors of the 1<sup>st</sup> International Conference on NMR Microscopy

The organizers of the 1<sup>st</sup> International Conference on NMR Microscopy would like to thank the following sponsors for their support

Varian GmbH, D-6100 Darmstadt

Deutsche Forschungsgemeinschaft (DFG), D-5300 Bonn

Bruker Analytische Meßtechnik GmbH, D-7512 Rheinstetten

Fraunhofer-Institut für Zerstörungsfreie Prüfverfahren, Hauptabteilung Medizintechnik, D-6670 St. Ingbert

Max-Planck-Institut für Polymerforschung, D-6500 Mainz

Max-Planck-Institut für Medizinische Forschung, D-6900 Heidelberg

SMIS, Guildford, United Kingdom

Oxford Instruments, D-6200 Wiesbaden

Doty Scientific, Inc., Columbia, USA

DSM Research B.V., NL-6160 MD Geelen

Boehringer Ingelheim KG, D-6507 Ingelheim

Wemhöner & Popp, D-5100 Aachen

Chemagnetics Inc., Fort Collins, USA

BASF, D-6700 Ludwigshafen

Hoechst AG, D-6230 Frankfurt-Höchst

## Transportation in Heidelberg

Heidelberg has an excellent public transportation system. The Max-Planck-Haus is located about 300 m North of the Ernst-Walz-Bridge across the Neckar river. Most hotels are South of the river. The Max-Planck-Haus can be reached by

- Bus 12, passing "Bismarck-Platz". Exit bus at "Bunsen-Gymnasium", at the corner of Berliner Strasse / Mönchhofstrasse. Turn South to the Max-Planck-Haus.
- Bus 33 passing "Bismarck-Platz" and "Hauptbahnhof". Exit bus at first stop after the bridge ("Chirurgische Klinik").
- Tram 1, passing "Bismarck-Platz" and "Hauptbahnhof". Exit at first stop after the bridge ("Chirurgische Klinik"). Continue North to the Max-Planck-Haus.
- Tram 4, passing "Hauptbahnhof". Exit at first stop after the bridge ("Chirurgische Klinik"). Continue North to the Max-Planck-Haus.

If your hotel is not close to any of these lines, connect to bus 12 or tram 1 at "Bismarck-Platz" or to buses 12, 33 or trams 1, 4 at "Hauptbahnhof". Tickets are available from the conductor in the bus or tram (DM 2.40 each), and from ticket machines located at "Bismarck-Platz" and "Hauptbahnhof" (5 tickets for DM 9.-).

## Eating and Drinking

Heidelberg has many restaurants, especially in the old part of the town. They tend to be very crowded in the evenings. The conference participants are encouraged to have lunch and dinner in the cafeteria of the Max-Planck-Haus. Tickets are available at the registration desk. Prices are DM 8.- for lunch and DM 10.- for dinner.

## Conference Guide:

**Notebook:** Abstracts for talks and posters appear in two separate sections. The Author Index references the program code and the page on which the abstract appears. An update to the directory will be provided during the conference.

**Location of Sessions:** All talks are held in the lecture hall on the upper level. The posters are on display in the library of the MPI für Völkerrecht in the same building.

**Laudatio:** At the beginning of the conference Prof. K. H. Hausser will be honored for his outstanding scientific contributions and his continuing support of magnetic resonance spectroscopy and imaging.

**Speakers and Session Chairs:** Please arrive 15 - 30 min. before your session to familiarize yourself with each other and with the audiovisual system. If using slides, please give them to the projectionist before the session begins.

**Posters:** All posters will be on display throughout the conference. Posters may be mounted beginning Sunday afternoon, 16.00 o'clock. Posters may be viewed informally on Sunday from 20.00 to 22.00 o'clock. All posters must be up by Monday noon. The poster abstracts are in the POSTERS section of this notebook. They are arranged in the same order as the session topics.

**Reception:** Participants are invited to a reception given by Dr. Korz, Bürgermeister of Heidelberg, on Tuesday, 19.00 o'clock. Busses to the reception will leave immediately after the last talk of the session on Commercial Perspectives.

**Conference Refreshments:** There is one coffee break in the morning and one in the afternoon sessions. The refreshments are sponsored by the companies supporting the conference.

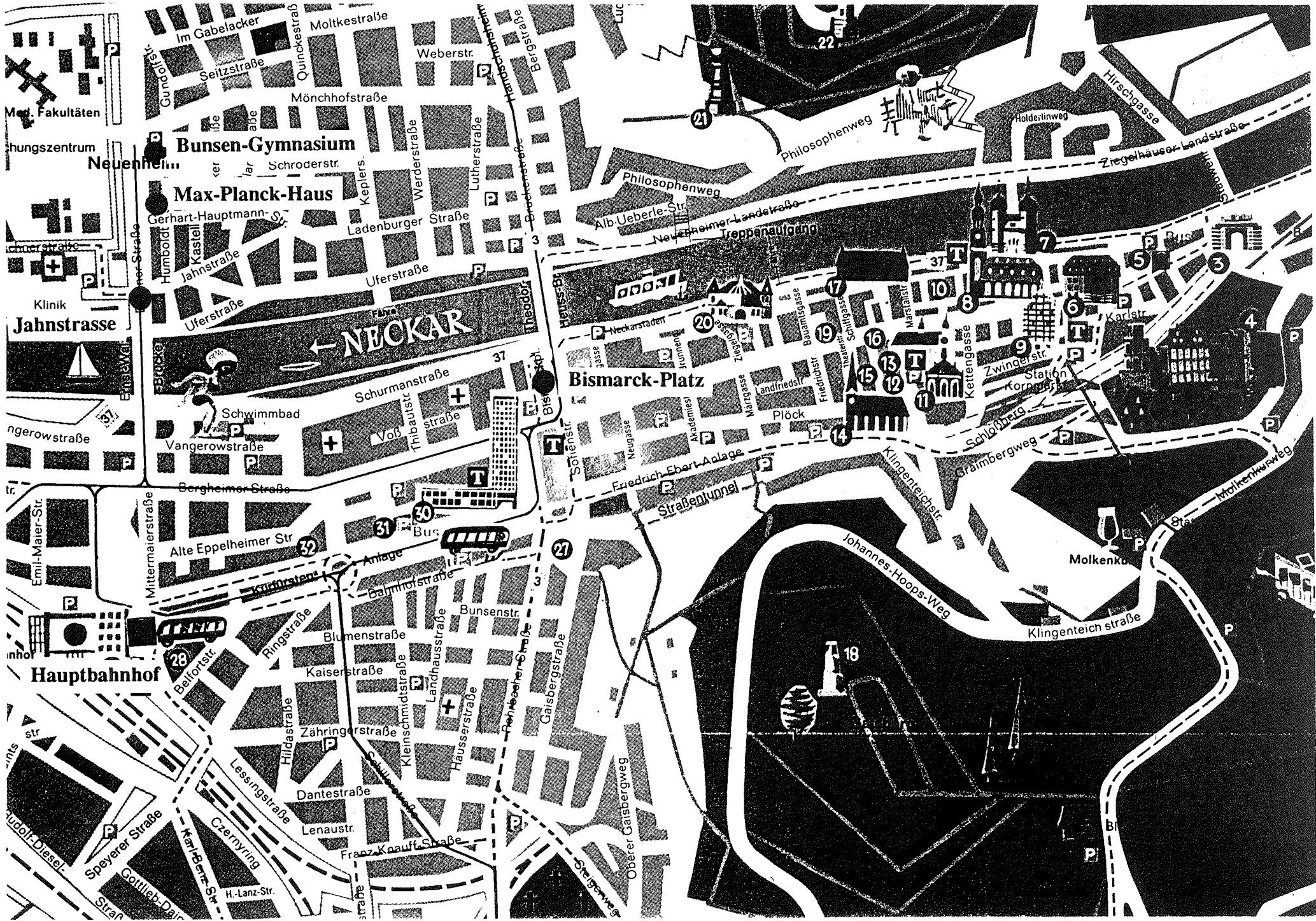
**Welcome Cocktail:** There is a welcome cocktail on Sunday from 19.00 to 20.00 o'clock in the mensa of the Max-Planck-Haus.

**Concert:** A piano concert will be given by W. E. Hull on Wednesday at 19.00 o'clock before the conference dinner in the lecture hall of the Max-Planck-Haus.

**Conference Dinner:** The conference dinner will be given in the mensa of the Max-Planck-Haus on Wednesday at 20.00 o'clock. Tickets can be purchased for DM 50.- at the registration desk.

**Regulations:**

- No smoking in the lecture hall or in the posters room.
- Registration badges must be worn during all conference activities.



**Bunsen-Gymnasium**

**Max-Planck-Haus**

**Jahnstrasse**

**NECKAR**

**Bismarck-Platz**

**Hauptbahnhof**

Med. Fakultäten

Neuenheim

Klinik

Vangerowstrasse

Emil-Mater-Str.

Belforstr.

Hudolf-Diesel-Str.

Gottlieb-Daig-Str.

Epeyerer Str.

Im Gabelacker

Seitzstr.

Mönchhofstr.

Schroderstr.

Gerhart-Hauptmann-Str.

Jahnstr.

Uferstr.

Schurmanstr.

Vangerowstr.

Alte Eppelheimer Str.

Mittermaierstr.

Bergheimer Str.

Ringstr.

Blumenstr.

Kaiserstr.

Zähringerstr.

Dantestr.

Lenaustr.

Lessingstr.

Czernyring

H.-Lanz-Str.

Franz-Knauff-Str.

Str.

Weberstr.

Werderstr.

Lutherstr.

Ladenburger Str.

Uferstr.

Schurmanstr.

Vangerowstr.

Alte Eppelheimer Str.

Bergheimer Str.

Mittermaierstr.

Bergheimer Str.

Ringstr.

Blumenstr.

Kaiserstr.

Zähringerstr.

Dantestr.

Lenaustr.

Lessingstr.

Czernyring

H.-Lanz-Str.

Franz-Knauff-Str.

Str.

Moltkestr.

Werderstr.

Lutherstr.

Ladenburger Str.

Uferstr.

Schurmanstr.

Vangerowstr.

Alte Eppelheimer Str.

Bergheimer Str.

Mittermaierstr.

Bergheimer Str.

Ringstr.

Blumenstr.

Kaiserstr.

Zähringerstr.

Dantestr.

Lenaustr.

Lessingstr.

Czernyring

H.-Lanz-Str.

Franz-Knauff-Str.

Str.

Philosophenweg

Philosophenweg

Philosophenweg

Alb-Ueberle-Str.

Neuenheimer Landstr.

Philosophenweg

Philosophenweg

Philosophenweg

Alb-Ueberle-Str.

Neuenheimer Landstr.

Philosophenweg

Philosophenweg

Philosophenweg

Alb-Ueberle-Str.

Neuenheimer Landstr.

Philosophenweg

Philosophenweg

Philosophenweg

Alb-Ueberle-Str.

Neuenheimer Landstr.

Philosophenweg

Philosophenweg

Philosophenweg

Alb-Ueberle-Str.

Neuenheimer Landstr.

Philosophenweg

Philosophenweg

Philosophenweg

Alb-Ueberle-Str.

Neuenheimer Landstr.

Philosophenweg

Philosophenweg

Philosophenweg

Alb-Ueberle-Str.

Neuenheimer Landstr.

Philosophenweg

Philosophenweg

Philosophenweg

Alb-Ueberle-Str.

Neuenheimer Landstr.

# Bus

## Universitätsplatz – Bismarckplatz – Mönchhofstraße – Bunsengymnasium – Neuklinikum – Sportzentrum Nord



**12**

montags – freitags

		♿	♿	♿	♿	♿	♿	♿	♿	♿	♿	♿	
Universitätsplatz	ab	0701	0721	0741	0801	0821	0841	0901	0921	0941	1001	1021	1041
Peterskirche	ab	0702	0722	0742	0802	0822	0842	0902	0922	0942	1002	1022	1042
Friedrich-Ebert-Platz	ab	0704	0724	0744	0804	0824	0844	0904	0924	0944	1004	1024	1044
Adenauerplatz	ab	0706	0726	0746	0806	0826	0846	0906	0926	0946	1006	1026	1046
Bismarckplatz	an	0707	0727	0747	0807	0827	0847	0907	0927	0947	1007	1027	1047
Bismarckplatz	ab	0708	0728	0748	0808	0828	0848	0908	0928	0948	1008	1028	1048
Ladenburger Straße	ab	0710	0730	0750	0810	0830	0850	0910	0930	0950	1010	1030	1050
Mönchhofplatz	ab	0711	0731	0751	0811	0831	0851	0911	0931	0951	1011	1031	1051
Mönchhofschule	ab	0712	0732	0752	0812	0832	0852	0912	0932	0952	1012	1032	1052
Wielandstraße	ab	0713	0733	0753	0813	0833	0853	0913	0933	0953	1013	1033	1053
Bunsengymnasium	an	0715	0735	0755	0815	0835	0855	0915	0935	0955	1015	1035	1055
Bunsengymnasium	ab	0716	0736	0756	0816	0836	0856	0916	0936	0956	1016	1036	1056
Blumenthalstr. West	ab	0717	0737	0757	0817	0837	0857	0917	0937	0957	1017	1037	1057
Pädagog. Hochschule	ab	0718	0738	0758	0818	0838	0858	0918	0938	0958	1018	1038	1058
Neuklinikum	ab	0719	0739	0759	0819	0839	0859	0919	0939	0959	1019	1039	1059
Studentenwohnheim	ab	0720	0740	0800	0820	0840	0900	0920	0940	1000	1020	1040	1100
Schwimmbad	ab	0721	0741	0801	0821	0841	0901	0921	0941	1001	1021	1041	1101
Bundesleistungszentrum	ab	0722	0742	0802	0822	0842	0902	0922	0942	1002	1022	1042	1102
DJK Sportplatz	ab	0723	0743	0803	0823	0843	0903	0923	0943	1003	1023	1043	1103
Sportzentrum Nord	an	0724	0744	0804	0824	0844	0904	0924	0944	1004	1024	1044	1104



Bitte berücksichtigen Sie bei der Disposition Ihrer Fahrten, daß es infolge der Bauarbeiten an der Theodor-Heuss-Brücke zu Verspätungen kommen kann.

**12**



montags – freitags

## Sportzentrum Nord – Neuklinikum – Bunsengymnasium – Mönchhofstraße – Bismarckplatz – Universitätsplatz

		♿	♿	♿	♿	♿	♿	♿	♿	♿	♿	
Sportzentrum Nord	ab	1658	1718	1738	1758	1818	1838	1858	1918	1933	1948	2008
DJK Sportplatz	ab	1659	1719	1739	1759	1819	1839	1859	1919	1934	1949	2009
Bundesleistungszentrum	ab	1700	1720	1740	1800	1820	1840	1900	1920	1935	1950	2010
Schwimmbad	ab	1701	1721	1741	1801	1821	1841	1901	1921	1936	1951	2011
Studentenwohnheim	ab	1702	1722	1742	1802	1822	1842	1902	1922	1937	1952	2012
Neuklinikum	ab	1703	1723	1743	1803	1823	1843	1903	1923	1938	1953	2013
Pädagog. Hochschule	ab	1704	1724	1744	1804	1824	1844	1904	1924	1939	1954	2014
Blumenthalstr. West	ab	1705	1725	1745	1805	1825	1845	1905	1925	1940	1955	2015
Bunsengymnasium	an	1706	1726	1746	1806	1826	1846	1906	1926	1941	1956	2016
Bunsengymnasium	ab	1707	1727	1747	1807	1827	1847	1907	1927	1942	1957	-
Wielandstraße	ab	1708	1728	1748	1808	1828	1848	1908	1928	1943	1958	-
Mönchhofschule	ab	1709	1729	1749	1809	1829	1849	1909	1929	1944	1959	-
Mönchhofplatz	ab	1711	1731	1751	1811	1831	1851	1911	1931	1946	2001	-
Ladenburger Straße	ab	1712	1732	1752	1812	1832	1852	1912	1932	1947	2002	-
Bismarckplatz	an	1714	1734	1754	1814	1834	1854	1914	1934	1949	2004	-
Bismarckplatz	ab	1715	1735	1755	1815	1835	1855	1915	1935	1950	-	-
Vincentius Krankenhaus	ab	1717	1737	1757	1817	1837	1857	1917	1937	1952	-	-
Kongreßhaus	ab	1718	1738	1758	1818	1838	1858	1918	1938	1953	-	-
Marshallstraße	ab	1719	1739	1759	1819	1839	1859	1919	1939	1954	-	-
Universitätsplatz	an	1721	1741	1801	1821	1841	1901	1921	1941	1956	weiter als Linie 10	-



Bitte berücksichtigen Sie bei der Disposition Ihrer Fahrten, daß es infolge der Bauarbeiten an der Theodor-Heuss-Brücke zu Verspätungen kommen kann.

**33**



montags – freitags

## Köpfel – Ziegelhausen – Schlierbach – Altstadt – Bismarckplatz – Hbf. – Sportzentrum Nord

		♿	♿	♿	♿	♿	♿	♿	♿	♿	♿	♿		
Karlstor	ab	0740	0800	0820	0840	0900	0920	0940	1000	1020	1040	1100	1120	1140
Rathaus/Bergbahn	ab	0742	0802	0822	0842	0902	0922	0942	1002	1022	1042	1102	1122	1142
Peterskirche	ab	0745	0805	0825	0845	0905	0925	0945	1005	1025	1045	1105	1125	1145
Friedrich-Ebert-Platz	ab	0747	0807	0827	0847	0907	0927	0947	1007	1027	1047	1107	1127	1147
Bismarckplatz	an	0749	0809	0829	0849	0909	0929	0949	1009	1029	1049	1109	1129	1149
Bismarckplatz	ab	0750	0810	0830	0850	0910	0930	0950	1010	1030	1050	1110	1130	1150
Römerstraße	ab	0752	0812	0832	0852	0912	0932	0952	1012	1032	1052	1112	1132	1152
Römerkreis West	ab	0754	0814	0834	0854	0914	0934	0954	1014	1034	1054	1114	1134	1154
Hauptbahnhof	ab	0756	0816	0836	0856	0916	0936	0956	1016	1036	1056	1116	1136	1156
Karl-Metz-Straße	ab	0757	0817	0837	0857	0917	0937	0957	1017	1037	1057	1117	1137	1157
Chirurg. Klinik	ab	0759	0819	0839	0859	0919	0939	0959	1019	1039	1059	1119	1139	1159
Kinderklinik	ab	0801	0821	0841	0901	0921	0941	1001	1021	1041	1101	1121	1141	1201
Zoo	ab	0803	0823	0843	0903	0923	0943	1003	1023	1043	1103	1123	1143	1203
Jugendherberge	ab	0804	0824	0844	0904	0924	0944	1004	1024	1044	1104	1124	1144	1204
Schwimmbad	ab	0806	0826	0846	0906	0926	0946	1006	1026	1046	1106	1126	1146	1206
Sportzentrum Nord	an	0808	0828	0848	0908	0928	0948	1008	1028	1048	1108	1128	1148	1208



## Sportzentrum Nord – Hbf. – Bismarckplatz – Altstadt – Schlierbach – Ziegelhausen – Köpfel



**33**

montags – freitags

		♿	♿	♿	♿	♿	♿	♿	♿	♿	♿		
Sportzentrum Nord	ab	1712	1732	1752	1812	1832	1852	1912	1948	-	-	-	
Schwimmbad	ab	1715	1735	1755	1815	1835	1855	1915	1951	-	-	-	
Jugendherberge	ab	1716	1736	1756	1816	1836	1856	1916	1952	-	-	-	
Zoo	ab	1717	1737	1757	1817	1837	1857	1917	1953	-	-	-	
Kinderklinik	ab	1719	1739	1759	1819	1839	1859	1919	1954	-	-	-	
Schwesternheim	ab	1720	1740	1800	1820	1840	1900	1920	1955	-	-	-	
Chirurg. Klinik	ab	1721	1741	1801	1821	1841	1901	1921	1956	-	-	-	
Karl-Metz-Straße	ab	1723	1743	1803	1823	1843	1903	1923	1958	-	-	-	
Hauptbahnhof	ab	1724	1744	1804	1824	1844	1904	1924	1959	-	-	-	
Römerkreis West	ab	1725	1745	1805	1825	1845	1905	1925	2000	-	-	-	
Römerstraße	ab	1727	1747	1807	1827	1847	1907	1927	2002	-	-	-	
Bismarckplatz	an	1730	1750	1810	1830	1850	1910	1930	2005	-	-	-	
Bismarckplatz	ab	1731	1751	1811	1831	1851	1911	1931	2007	2107	2207	2307	0007
Friedrich-Ebert-Platz	ab	1733	1753	1813	1833	1853	1913	1933	2009	2109	2209	2309	0009
Peterskirche	ab	1734	1754	1814	1834	1854	1914	1934	2010	2110	2210	2310	0010
Rathaus/Bergbahn	ab	1737	1757	1817	1837	1857	1917	1937	2012	2112	2212	2312	0012
Karlstor	ab	1740	1800	1820	1840	1900	1920	1940	2015	2115	2215	2315	0015





## Handschuhsheim – Bismarckplatz – Hauptbahnhof – Blumenthalstr. West

montags – freitags

Burgstraße	ab	0630	0730	0740	0750	0800	0810	0820	0830	0840	-	-	-
Biethstraße	ab	0631	0731	0741	0751	0801	0811	0821	0831	0841	-	-	-
OEG-Bahnhof	ab	0632	0732	0742	0752	0802	0812	0822	0832	0842	-	-	-
Froschäckerweg	ab	0633	0733	0743	0753	0803	0813	0823	0833	0843	-	-	-
Kapellenweg	ab	0634	0734	0744	0754	0804	0814	0824	0834	0844	-	-	-
Blumenthalstr. Ost	ab	0635	0735	0745	0755	0805	0815	0825	0835	0845	-	-	-
Kußmaulstraße	ab	0636	0736	0746	0756	0806	0816	0826	0836	0846	-	-	-
Mönchhofplatz	ab	0637	0737	0747	0757	0807	0817	0827	0837	0847	-	-	-
Ladenburger Straße	ab	0638	0738	0748	0758	0808	0818	0828	0838	0848	-	-	-
Bismarckplatz	an	0641	0741	0751	0801	0811	0821	0831	0841	0851	-	-	-
Bismarckplatz	ab	0642	0742	0752	0802	0812	0822	0832	0842	0852	0902	0912	0922
Adenauerplatz	ab	0643	0743	0753	0803	0813	0823	0833	0843	0853	0903	0913	0923
Poststraße	ab	0644	0744	0754	0804	0814	0824	0834	0844	0854	0904	0914	0924
Stadtbücherei	ab	0645	0745	0755	0805	0815	0825	0835	0845	0855	0905	0915	0925
Römerkreis West	ab	0646	0746	0756	0806	0816	0826	0836	0846	0856	0906	0916	0926
Stadtwerke	ab	0647	0747	0757	0807	0817	0827	0837	0847	0857	0907	0917	0927
Hauptbahnhof	ab	0648	0748	0758	0808	0818	0828	0838	0848	0858	0908	0918	0928
Karl-Metz-Straße	ab	0649	0749	0759	0809	0819	0829	0839	0849	0859	0909	0919	0929
Mittermaierstraße	ab	0650	0750	0800	0810	0820	0830	0840	0850	0900	0910	0920	0930
Chirurgische Klinik	ab	0652	0752	0802	0812	0822	0832	0842	0852	0902	0912	0922	0932
Bunsengymnasium	ab	0653	0753	0803	0813	0823	0833	0843	0853	0903	0913	0923	0933
Blumenthalstr. West	an	0654	0754	0804	0814	0824	0834	0844	0854	0904	0914	0924	0934

alle 10 Minuten

alle 10 Minuten

Bitte berücksichtigen Sie bei der Disposition Ihrer Fahrten, daß es infolge der Bauarbeiten an der Theodor-Heuss-Brücke zu Verspätungen kommen kann.

## Blumenthalstr. West – Hauptbahnhof – Bismarckplatz – Handschuhsheim



montags – freitags

Blumenthalstr. West	ab	1838	1848	1858	1908	1918	1928	1938	1948	1956
Bunsengymnasium	ab	1839	1849	1859	1909	1919	1929	1939	1949	1957
Chirurgische Klinik	ab	1840	1850	1900	1910	1920	1930	1940	1950	1958
Karl-Metz-Straße	an/ab	1842	1852	1902	1912	1922	1932	1942	1952	2000
Hauptbahnhof	ab	1844	1854	1904	1914	1924	1934	1944	1954	-
Stadtwerke	ab	1845	1855	1905	1915	1925	1935	1945	1955	-
Römerkreis West	ab	1846	1856	1906	1916	1926	1936	1946	1956	-
Stadtbücherei	ab	1847	1857	1907	1917	1927	1937	1947	1957	-
Poststraße	ab	1848	1858	1908	1918	1928	1938	1948	1958	-
Adenauerplatz	ab	1849	1859	1909	1919	1929	1939	1949	1959	-
Bismarckplatz	an	1850	1900	1910	1920	1930	1940	1950	2000	-
Blumenthalstr. West	ab	2018	2048	2118	2148	2218	2248	2318	2348	0020
Bunsengymnasium	ab	2019	2049	2119	2149	2219	2249	2319	2349	0021
Chirurgische Klinik	ab	2020	2050	2120	2150	2220	2250	2320	2350	0022
Karl-Metz-Straße	an/ab	2022	2052	2122	2152	2222	2252	2322	2352	0024
Hauptbahnhof	ab	2024	2054	2124	2154	2224	2254	2324	2354	-
Stadtwerke	ab	2025	2055	2125	2155	2225	2255	2325	2355	-
Römerkreis West	ab	2026	2056	2126	2156	2226	2256	2326	2356	-
Stadtbücherei	ab	2027	2057	2127	2157	2227	2257	2327	2357	-
Poststraße	ab	2028	2058	2128	2158	2228	2258	2328	2358	-
Adenauerplatz	ab	2029	2059	2129	2159	2229	2259	2329	2359	-
Bismarckplatz	an	2030	2100	2130	2200	2230	2300	2330	2400	-

Bitte berücksichtigen Sie bei der Disposition Ihrer Fahrten, daß es infolge der Bauarbeiten an der Theodor-Heuss-Brücke zu Verspätungen kommen kann.



## Rohrbach – Hauptbahnhof – Blumenthalstr. West

montags – freitags

Eichendorffplatz	ab	0538	0548	0558	0608	0618	0628	0638	1618	1628	1638	1648	1658	1708
Markscheide	ab	0539	0549	0559	0609	0619	0629	0639	1619	1629	1639	1649	1659	1709
Rheinstraße	ab	0540	0550	0600	0610	0620	0630	0640	1620	1630	1640	1650	1700	1710
Bethanien Krankenh.	ab	0541	0551	0601	0611	0621	0631	0641	1621	1631	1641	1651	1701	1711
Bergfriedhof	ab	0542	0552	0602	0612	0622	0632	0642	1622	1632	1642	1652	1702	1712
Franz-Knauff-Straße	ab	0543	0553	0603	0613	0623	0633	0643	1623	1633	1643	1653	1703	1713
Christuskirche	ab	0544	0554	0604	0614	0624	0634	0644	1624	1634	1644	1654	1704	1714
Römerkreis Süd	ab	0545	0555	0605	0615	0625	0635	0645	1625	1635	1645	1655	1705	1715
Römerkreis West	ab	0547	0557	0607	0617	0627	0637	0647	1627	1637	1647	1657	1707	1717
Stadtwerke	ab	0548	0558	0608	0618	0628	0638	0648	1628	1638	1648	1658	1708	1718
Hauptbahnhof	ab	0549	0559	0609	0619	0629	0639	0649	1629	1639	1649	1659	1709	1719
Karl-Metz-Straße	ab	0550	0600	0610	0620	0630	0640	0650	1630	1640	1650	1700	1710	1720
Mittermaierstraße	ab	0551	0601	0611	0621	0631	0641	0651	1631	1641	1651	1701	1711	1721
Chirurgische Klinik	ab	0553	0603	0613	0623	0633	0643	0653	1633	1643	1653	1703	1713	1723
Bunsengymnasium	ab	0554	0604	0614	0624	0634	0644	0654	1634	1644	1654	1704	1714	1724
Blumenthalstr. West	an	0555	0605	0615	0625	0635	0645	0655	1635	1645	1655	1705	1715	1725

alle 10 Minuten

## Blumenthalstr. West – Hauptbahnhof – Rohrbach



montags – freitags

Blumenthalstr. West	ab	0727	0737	0747	0757	0807	0817	1757	1807	1817	1827	1837	1847	1857
Bunsengymnasium	ab	0728	0738	0748	0758	0808	0818	1758	1808	1818	1828	1838	1848	1858
Chirurgische Klinik	ab	0729	0739	0749	0759	0809	0819	1759	1809	1819	1829	1839	1849	1859
Karl-Metz-Straße	ab	0731	0741	0751	0801	0811	0821	1801	1811	1821	1831	1841	1851	1901
Hauptbahnhof	ab	0733	0743	0753	0803	0813	0823	1803	1813	1823	1833	1843	1853	1903
Stadtwerke	ab	0734	0744	0754	0804	0814	0824	1804	1814	1824	1834	1844	1854	1904
Römerkreis West	ab	0735	0745	0755	0805	0815	0825	1805	1815	1825	1835	1845	1855	1905
Römerkreis Süd	ab	0737	0747	0757	0807	0817	0827	1807	1817	1827	1837	1847	1857	1907
Christuskirche	ab	0738	0748	0758	0808	0818	0828	1808	1818	1828	1838	1848	1858	1908
Franz-Knauff-Straße	ab	0739	0749	0759	0809	0819	0829	1809	1819	1829	1839	1849	1859	1909
Bergfriedhof	ab	0740	0750	0800	0810	0820	0830	1810	1820	1830	1840	1850	1900	1910
Bethanien Krankenh.	ab	0741	0751	0801	0811	0821	0831	1811	1821	1831	1841	1851	1901	1911
Rheinstraße	ab	0742	0752	0802	0812	0822	0832	1812	1822	1832	1842	1852	1902	1912
Markscheide	ab	0743	0753	0803	0813	0823	0833	1813	1823	1833	1843	1853	1903	1913
Eichendorffplatz	ab	0744	0754	0804	0814	0824	0834	1814	1824	1834	1844	1854	1904	1914

alle 10 Minuten



## Program Highlights

### Sunday, September 15, 1991

13.00 - 18.00 Educational Session: *J.L. Ackerman*

16.00 - 19.00 Registration

19.00 - 20.00 Welcome Cocktail

20.00 - 21.30 Informal Poster Viewing

### Monday, September 16, 1991

9.00 - 11.15 Opening Session: *U. Haeberlen*, Chair

11.45 - 12.45 Methods I: *W.S. Veeman*, Chair

14.15 - 16.30 Methods II: *W.S. Veeman*, Chair

17.00 - 18.30 EPR-Imaging: *L.J. Berliner*, Chair

20.00 - 21.30 Poster Session

### Tuesday, September 17, 1991

9.00 - 11.00 Materials Imaging: *H.W. Spiess*, Chair

11.30 - 12.45 Materials Imaging II: *H.W. Spiess*, Chair

14.15 - 16.15 Molecular Flow and Diffusion: *P.T. Callaghan*, Chair

16.45 - 18.30 Commercial Perspectives: *A. N. Garroway*, Chair

19.00 Reception by the 1. Bürgermeister of Heidelberg, *Dr. Korz*

**Wednesday, September 18, 1991**

**9.00 - 11.00 Biomedicine I: *L. W. Jelinski*, Chair**

**11.30 - 12.45 Biomedicine II: *L. W. Jelinski*, Chair**

**12.45 *L.J. Berliner: History of NMR and Imaging for Young Scientist and Accompanying Persons.***

**14.15 Excursion**

**19.00 Piano Concert by *W.E. Hull*  
(Lecture Hall of the Max-Planck-Haus)**

**20.00 Conference Dinner**

***E.R. Andrew : Magnetic Resonance Reflections.***

**Thursday, September 19, 1991**

**9.00 - 10.30 Plants and Agriculture: *W. Kuhn*, Chair**

**11.00 - 13.00 Rare Isotopes: *G.D. Mateescu*, Chair**

**14.30 - 16.30 Round Table Discussion: *A. Haase*, Chair**

**Sunday, 15. 9. 1991**

**Educational Session: *Bettina Pfeleiderer*, Chair**

- 13.00 Introduction to NMR Spectroscopy and Imaging**  
*R. A. Komoroski*  
Dept. of Radiology, Univ. of Arkansas, Little Rock,  
Arkansas, USA
- 13.55 Approaches to Chemistry and Physiologic Function in Living Systems via NMR Spectroscopy and Imaging**  
*J. J. H. Ackerman*  
Dept. of Chemistry and Radiology, Washington Univ.,  
St. Louis, Missouri, USA
- 14.50 Break**
- 15.15 Flow and Diffusion**  
*P. T. Callaghan*  
Dept. of Physics and Biophysics, Massey Univ., Palmerstone  
North, New Zealand
- 16.10 Solid State NMR Spectroscopy and Imaging**  
*W. S. Veeman*  
Laboratory of Physical Chemistry, Univ. of Nijmegen,  
Nijmegen, Netherlands
- 17.05 Coherent Averaging Techniques Applied to NMR Imaging**  
*D. C. Cory*  
Bruker Instruments Inc., Billerica, Mass. USA

**Monday, 16.09.1991**

**Opening: U. Haeberlen, Chair**

- 9.00** Welcome  
*W. Kuhn*  
St. Ingbert (Germany)
- 9.15** **Laudatio to Prof. K.H. Hausser.**  
*H.W. Spiess*  
Mainz (Germany)
- 9.45** Special Lecture:  
**Resolution and Sensitivity: the Constant Challenges of NMR.**  
*A. Pines*  
Berkeley, California, (USA)
- 10.30** Opening Lecture:  
**NMP Microscopy: History, Theory, and Applications.**  
*P.C. Lauterbur, X. Zhou, W.B. Hyslop, C.S. Potter, L.K. Hedges,  
and M.L. Bernardo, Jr.*  
Urbana, Illinois (USA)
- 11.15** **Coffee break**
- Methods: W.S. Veeman, Chair**
- 11.45** **MET 1: NMR Microscopy at 500 MHz: Cellular Resolution in Bio-Systems.**  
*P. Mansfield, R. Bowtell, J. Sharp, G. Brown, and M. McJury*  
Nottingham (United Kingdom)
- 12.15** **MET 2: Line-Narrowing Approaches for Macroscopic Solid State Imaging.**  
*J.B. Miller, D.G. Cory\*, and A.N. Garroway*  
Washington DC (USA) / \*Billerica, Massachusetts (USA)
- 12.45** **Lunch**
- 14.15** **MET 3: Spatially Resolved Material Characterization Using NMR or NQR Techniques.**  
*R. Kimmich*  
Ulm (Germany)

- 14.45      **MET 4: Magic Angle Rotating Frame NMR Imaging of Materials.**  
*B. Maraviglia*  
Rome (Italy)
- 15.15      **MET 5: NMR Imaging Studies of Velocity and Concentration Distributions in Flows.**  
*S.A. Altobelli, A. Caprihan, E. Fukushima, and P.D. Majors*  
Albuquerque, New Mexico (USA)
- 15.45      **MET 6: STRAFI: How it Works.**  
*A.A. Samoilenko*  
Moscow (USSR)
- 16.00      **MET 7: Imaging by Radiofrequency Field Gradients.**  
*P. Maffei, and D. Canet*  
Vandoeuvre les Nancy (France)
- 16.15      **MET 8: Solid State Imaging in Combination with Magic Angle Spinning.**  
*W.S. Veeman, and G. Bijl*  
Nijmegen (Netherlands)
- 16.30      **Coffee break**
- EPR-Imaging: L.J. Berliner, Chair**
- 17.00      **EPI 1: Scanning and CT-ESR Microscopes.**  
*M. Ikeya*  
Osaka (Japan)
- 17.30      **EPI 2: EPR Imaging of Polymers, Solid Materials, and Tumors.**  
*L.J. Berliner, H. Fujii*  
Columbus, Ohio (USA)
- 18.00      **EPI 3: Proton Imaging after Dynamic Polarization: Potential Applications in Biology.**  
*D. Grucker*  
Strasbourg (France)
- 18.15      **EPI 4: Spectral-Spatial Skin Imaging with Modulated Gradient and Simultaneous Field Scan (MOSS).**  
*T. Herrling, N. Groth, K.U. Thiessenhusen, and U. Ewert*  
Berlin (Germany)
- 18.30      **Dinner**
- 20.00      **Poster Session**

Tuesday, 17.09.1991

**Materials Imaging: H.W. Spiess, Chair**

- 9.00        **MAT 1: NMR Imaging of Polymeric Systems.**  
*J.L. Koenig*  
Cleveland, Ohio (USA)
- 9.30        **MAT 2: NMR Imaging of Composition and Defects in Industrial Elastomers.**  
*R.A. Komoroski, and S.N. Sarkar*  
Little Rock, Arkansas (USA)
- 10.00       **MAT 3: Gradient Modulations for Liquid and Solid State NMR Microscopy.**  
*D.G. Cory*  
Billerica, Massachusetts (USA)
- 10.30       **MAT 4: MRI Studies of in situ Polymerisation Reactions at Elevated Temperatures.**  
*T.A. Carpenter, L.D. Hall, P. Jezzard, C.J. Wiggins, N.J. Clayden\*, P. Jackson\*, N. Walton#*  
Cambridge (England), \*Middlesbrough, Cleveland (England), #Runcorn, Cheshire (England)
- 11.00       **Coffee break**
- 11.30       **MAT 5: NMR Imaging of Polymers: Methods and Applications.**  
*B. Blümich, P. Blümler, J. Jansen, G. Schauß, and H.W. Spiess*  
Mainz (Germany)
- 11.45       **MAT 6: Investigation of Aging Processes in Elastomers by Parameter Selective NMR Microscopy.**  
*E. Koeller, I. Theis, and W. Kuhn*  
St. Ingbert (Germany)
- 12.00       **MAT 7: Monitoring of Photopolymerization Processes by NMR Imaging.**  
*K. Albert, U. Günther, M. Ilg, E. Bayer, and M. Grossa\**  
Tübingen (Germany) / \*Neu-Isenburg (Germany)

- 12.15      **MAT 8: Some Applications of Pulsed-Field-Gradient NMR in Petrochemical Research.**  
*K.P. Datema, J.A. Bolt-Westerhoff, and J. Kärger\**  
 Amsterdam (Netherlands) / \*Leipzig (Germany)
- 12.30      **MAT 9: NMR Imaging of Water Distribution in Vycor Glass.**  
*G. Guillot, P. Gonord, S. Kan, S. Durand-Vidal, and O. Bruynooghe*  
 Orsay (France)
- 12.45      **Lunch**
- Molecular Flow and Diffusion:**  
*P.T. Callaghan, Chair*
- 14.15      **DIF 1: Structure Related Diffusion in Microporous Crystallites.**  
*J. Kärger, and H. Pfeifer*  
 Leipzig (Germany)
- 14.45      **DIF 2: Imaging of Dynamics Associated with the Belousov-Zhabotinski Reaction.**  
*R.L. Armstrong, A. Tzalmona\*, M. Menzinger\*, and C. Lemaire\**  
 New Brunswick (Canada), \*Toronto (Canada)
- 15.15      **DIF 3: Translational Motion Imaging with Pulsed Gradient Spin Echo NMR Methods.**  
*P.T. Callaghan*  
 Palmerston North (New Zealand)
- 15.45      **DIF 4: Approaches to Flow Statistics, Structure Correlations and 2D Spectroscopy Using Characteristic Functions.**  
*L. Frydman, G.A. Barrall, J.S. Harwood, and G.C. Chingas*  
 Berkeley, California (USA)
- 16.00      **DIF 5: Diffusion Anisotropy Measurements by 2D-FT NMR Microscopy.**  
*M. Neeman, C.F. Kirsch, J.P. Freyer, and L.O. Sillerud*  
 Los Alamos, New Mexico (USA)
- 16.15      **DIF 9: Imaging the Velocity Profiles for Water Flow through an Abrupt Contraction and Abrupt Enlargement.**  
*Y. Xia, K.R. Jeffrey\*, and P.T. Callaghan*  
 Palmerston North (New Zealand) / \*Guelph, Ontario (Canada)
- 16.30      **Coffee break**

**Commercial Perspectives:***A.N. Garroway, Chair*

- 16.50**      **CPI 1: NMR Microimaging with a Versatile Spectrometer for Diverse Applications in Biology and Materials Science.**  
*N. Schuff, and P.A. Hornung*  
Varian, Palo Alto, California (USA)
- 17.15**      **CPI 2: Some Aspects on the Commercialization of NMR Microscopy.**  
*M. Mattingly*  
Bruker Instruments, Billerica, Massachusetts (USA)
- 17.40**      **CPI 3: A View on NMR Microscopy**  
*V.J. Bartuska*  
Chemagnetics, Fort Collins, Colorado (USA)
- 18.05**      **CPI 4: Low Cost Microscopy.**  
*N. Eolas, C.F. Randell, and F. Goldie*  
SMIS Ltd., Guildford (United Kingdom)
- 18.35**      **Bus departure to the "Prinz Carl"**
- 19.00**      **Empfang durch den 1. Bürgermeister der Stadt Heidelberg, Herrn Dr. Korz, im Spiegelsaal des "Prinz Carl"**

**Wednesday, 18.09.1991**

**Biomedicine: *L.W. Jelinski*, Chair**

- 9.00**      **BIO 1: NMR Microscopy of Human Tumor Xenocrafts on Nude Mice.**  
*W.E. Hull, and K.P. Fichtner*  
 Heidelberg (Germany)
- 9.30**      **BIO 2: MR Microscopy of Disease Models.**  
*G.A. Johnson, H. Benveniste, R.R. Black\*, G.P. Cofer,*  
*S.L. Gewalt, L.W. Hedlund, R.R. Maronpot#, S.A. Suddarth,*  
*B.E. Todd*  
 Durham, North Carolina (USA) / \*Schenectady, New York  
 (USA) / #Triangle Park, North Carolina (USA)
- 10.00**      **BIO 3: Oxygen-17 Imaging and Localized Spectroscopy in Biomedical Research and its Diagnostic Potential.**  
*G.D. Mateescu*  
 Cleveland, Ohio (USA)
- 10.30**      **BIO 4: The Fourth Dimension of MRI: Obtaining Physiological Information on a Microscopic Scale**  
*L.W. Jelinski*  
 Murray Hill, New York (USA)
- 11.00**      **Coffee break**
- 11.30**      **BIO 5: High Field Localized in vivo Proton Spectroscopy.**  
*D.M. Doddrell, S. Crozier, and I. Brereton*  
 Brisbane, Queensland (Australia)
- 11.45**      **BIO 6: NMR Microscopy Imaging of Surface and Fine Structures of Cartilage and Contrast Enhancement by Manganese Ions.**  
*K. Gersonde, W. Gründer\*, K. Dannhauer\*, and Y. Kusaka*  
 St. Ingbert (Germany) / Leipzig (Germany)
- 12.00**      **BIO 7: Relaxation Time and Diffusion NMR Microscopy of Single Neurons.**  
*J.S. Schoeniger, N. Aiken, E. Hsu, and S.J. Blackband*  
 Baltimore, Maryland (USA)

- 12.15**      **BIO 8: MRI of Carbon Fibers Implants in Bones.**  
*B. Tomanek, E. Staszko, S. Sagnowski, and S. Kwiecinski*  
Krakow (Poland)
- 12.30**      **BIO 9: Q-space Imaging in Heterogeneous (Bio) Systems.**  
*H. van As, J.E.M. Snaar, D. van Dusschoten, and W.D. Palstra*  
Wageningen (Netherlands)
- 12.45**      *L.J. Berliner: **History of NMR and Imaging for Young Scientist***  
**and Accompanying Persons.**
- 13.00**      **Lunch**
- 14.00**      **Excursion**
- 19.00**      **Piano Concert by *W.E. Hull***
- 20.00**      **Conference Dinner**  
*E.R. Andrew: **Magnetic Resonance Reflections***

Thursday, 19.09.1991

**Plants & Agriculture: W. Kuhn, Chair**

- 9.00** PLA 1: **Applications of Chemical Shift Microscopy to Non-Invasive Histochemistry of Plant Materials.**  
*J.M. Pope*  
 Kensington, New South Wales (Australia)
- 9.30** PLA 2: **Some Aspects of NMR Microscopy Applications in Plant Sciences and Agriculture.**  
*V. Sarafis*  
 Richmond, New South Wales (Australia)
- 10.00** PLA 3: **The Ripening of Red Raspberry Fruits Studied by NMR Microscopy.**  
*B. Williamson, B.A. Goodman, J.A. Chudek\*, and S.N. Scrimgeour\**  
 Invergowrie, Dundee (United Kingdom) / \*Dundee (United Kingdom)
- 10.15** PLA 4: **Study of Chilled and Nonchilled Zucchini Squash by NMR Imaging.**  
*P.C. Wang, and C.Y. Wang\**  
 Washington, DC (USA) / \*Beltsville, Maryland (USA)
- 10.30** Coffee break

**Rare Isotopes: G.D. Mateescu, Chair**

- 11.00** RAI 1: **Deuterium NMR: Current and Future Uses *in vivo***  
*J.J.H. Ackerman, C.S. Bosch, J.L. Evelhoch, J.J. Nil, R.S. Hotchkiss, and S.-K. Song*  
 St. Louis, Missouri (USA)
- 11.30** RAI 2: **Oxygen-17 MRS and MRI: Theoretical and Experimental Aspects.**  
*G.D. Mateescu*  
 Cleveland, Ohio (USA)
- 11.45** RAI 3: **Heteronuclear Solid State MRI and in-situ Spectroscopy of Biological and Nonbiological Ceramics**  
*B. Pfeleiderer, Y. Wu, J.L. Ackerman, L. Garrido, and J.R. Moore,*  
 Boston, Massachusetts (USA)

- 12.15**      **RAI 4: Boron-11 MRI and MRS.**  
*G.W. Kabalka, G.-Q. Cheng, and P. Bendel\**  
Knoxville, Tennessee (USA) / \*Rehovot (Israel)
- 12.45**      **RAI 5: Spectroscopic  $^{13}\text{C}$  and  $^2\text{H}$  NMR Imaging in Solids.**  
*E. Günther, B. Blümich, and H.W. Spiess*  
Mainz (Germany)
- 13.00**      **Lunch**
- 14.30**      **Round Table Discussion: A. Haase, Chair**
- 16.30**      **Conference Adjourns**

# Lectures: Abstracts

## HISTORY OF NMR AND IMAGING FOR YOUNG SCIENTISTS AND ACCOMPANYING PERSONS.

Lawrence J. Berliner

Department of Chemistry, The Ohio State University, 120 W. 18th Avenue, Columbus, OH 43210-1173, U.S.A.

The history and jargon of NMR and ESR and imaging are new and confusing to spouses of scientist and young students. This lecture will review the salient historical aspects of NMR and ESR and explain such unusual abbreviations and terms such as MRI, IBM, Hamiltonian and others. The major useful applications of these techniques will be described in language that is clear and understandable to spouses of scientist and young students. Participants are strongly encouraged to invite their accompanying persons to this lecture.

RESOLUTION AND SENSITIVITY: THE CONSTANT CHALLENGES OF NMR

A. Pines

Lawrence Berkeley Laboratory and University of California,  
Berkeley

I shall outline three developments at Berkeley that may contribute to the enhancement of resolution and sensitivity of nuclear magnetic resonance (NMR) and nuclear quadrupole resonance (NQR) for the study of materials. The first involves zero-field resonance with a superconducting quantum interference device (SQUID). The second involves rapidly rotating a sample around two axes thereby implementing the symmetry of an icosahedron. This allows for the first time high resolution NMR of isotopes such as oxygen-17 and aluminum-27 in solids. The third involves optical pumping of gases. Applications of these techniques include the observation of quantum tunneling at low temperatures, the study of materials such as minerals, catalysts, polymers and glasses, and investigations of gas-surface interactions.

NMR Microscopy at 500 MHz: Cellular resolution in Bio-Systems.  
P. Mansfield, R. Bowtell, J. Sharp, G. Brown and M. McJury  
Department of Physics, University of Nottingham, University  
Park, Nottingham, NG7 2RD, UK.

Using the principles of NMR microscopy (1, 2) we have produced images showing cellular detail in bio-systems. These images have a best in-plane resolution of 4.5  $\mu\text{m}$  and a slice thickness of 40  $\mu\text{m}$ . The specially constructed NMR microscope is based around an 89 mm bore, 11.7 T magnet and incorporates a 'home-built' actively screened gradient coil set, of 3 cm inner diameter (3). This is capable of producing magnetic field gradients of ca. 2 G  $\text{cm}^{-1} \text{A}^{-1}$ . For imaging small samples an inductively coupled, RF, surface coil, which is built into a standard microscope slide, is used. For larger samples simple solenoidal RF coils or resonant array coils are employed.

Onion epithelial cells are large and highly vacuolated and so form a good system for investigation by NMR microscopy. We have imaged many such samples producing  $T_1$  and diffusion weighted images. We have also used the NMR microscope to follow the movement of water which takes place when epithelial cells are plasmolysed in a hyperosmotic sucrose solution. Other samples which have been investigated include the stems of vascular plants as well as rice plant calluses. In images of vascular plants it has been shown that many of the features are caused by the magnetic susceptibility effects of intercellular air spaces (3). In rice calluses, diffusion weighted images are being used as a possible method of discriminating between embryogenic and non-embryogenic tissue.

#### References

- 1) P. Mansfield and P. K. Grannell, J. Phys. C. 6, L422 (1973); Phys. Rev. 12, 3618 (1975); Phys. Med. Biol. 20, 477 (1975).
- 2) J. B. Aguayo, S. J. Blackband, J. Schoeniger, M. A. Mattingly and M. Hintermann, Nature 322, 190 (1986).
- 3) R. Bowtell, G. D. Brown, P. M. Glover, M. McJury and P. Mansfield, Phil. Trans. Roy. Soc. Lond. A 333, 457, (1990).

"Line-narrowing approaches for macroscopic solid state imaging"

J. B. Miller, D. G. Cory<sup>+</sup>, and A. N. Garroway

Code 6122, Chemistry Division, Naval Research Laboratory, Washington DC  
20375-5000, USA

<sup>+</sup> Present address, Bruker Instruments Inc, Manning Park, Billerica MA 01821

Near room temperature, random molecular motions in many materials are sufficiently rapid and almost isotropic so that the NMR resonance line is motionally narrowed: in this regime conventional or modified magnetic resonance imaging (MRI) approaches are quite adequate to produce an image. However, more rigid materials, such as engineering polymers, exhibit broad lines, whose widths are nearly comparable to their corresponding rigid lattice limits. In such rigid solids, this broader line corresponds to a surfeit of (potentially useful) information about dipolar couplings, isotropic and anisotropic chemical shifts, and magnetic susceptibility; much of this information is irrevocably lost in more mobile systems. For imaging this excess information may be undesirable and can be removed by coherent averaging schemes which artificially reduce the line widths, thus enhancing spatial resolution and improving the signal-to-noise ratio. However, the ability to switch off irrelevant parts of the Hamiltonian while highlighting important features provides an additional tool for image contrast not generally available to liquid state imaging.

We examine a hierarchy of coherent RF line narrowing techniques based on solid echoes and present representative proton images of engineering polymers including polyacrylic, Ultem (polyimide), and a fiberglass/polyester resin composite. We achieve increased spatial resolution by replacing the quasi-static magnetic gradient with pulsed (*ca* 3  $\mu$ s) gradients installed at particular windows of the pulse sequences. With 'time suspension' sequences, for which the entire average Hamiltonian is set to zero, we observe line widths quite comparable to those amenable to conventional MRI. By introducing an imaging Hamiltonian into the time suspension sequence through modest ( $< 0.3$  T/m) pulsed gradients, solid state images can be achieved with a spatial resolution comparable to that in liquids.

Thus far our demonstrations of solid state imaging have been only on 'macroscopic' (*ca* 1 cm) samples, to a resolution of about 50 microns. We speculate on the extension of such methods to much smaller sample sizes. As is well-known, molecular diffusion does not present a limit to spatial resolution for solids as it does for more liquid-like systems. Further, some of the practical problems of line-narrowing become more tractable for smaller samples.

Spatially resolved material characterization  
using NMR or NQR techniques

Rainer Kimmich

Sektion Kernresonanzspektroskopie, Universität Ulm,  
W-7900 Ulm, Fed. Rep. of Germany

A series of selected new techniques will be reported permitting the spatially resolved characterization of materials or tissue. This refers to volume-selective spectroscopy and imaging of liquid or solid materials. Apart from NMR applications, the potential use of NQR techniques will be discussed briefly.

$^{13}\text{C}$  is a nucleus scarcely employed in spatially resolved NMR because of the poor sensitivity. A technique will be presented by which the protons coupled to  $^{13}\text{C}$  nuclei are detected. Thus the distribution of coupled  $^{13}\text{C}$  nuclei can indirectly be imaged with the sensitivity of proton NMR.

The spatial resolution of solid-state NMR imaging depends on the encoding efficiency, i. e. on the length of the coherence evolution intervals after which signals can still be detected. A very favorable method in this sense is the magic-echo phase-encoding solid imaging technique (MEPSI). It provides a high spatial resolution together with the full spectroscopic information which is considered to be crucial for material characterization. Corresponding pulse sequences, the theoretical background and test experiments will be outlined.

Finally a solid-state imaging method will be presented based on pure nuclear quadrupole resonance. No static magnetic fields are used at all. Rather Hoult's rotating-frame zeugmatography method is adapted to NQR. This rotating frame NQR imaging ( $\rho\text{NQR}$ I) technique can be combined with the use of surface coils so that localized information can be obtained even with large objects. As an application, the representation of temperature distributions will be demonstrated.

## Magic Angle Rotating Frame NMR Imaging of Materials

B. Maraviglia

Dipartimento di Fisica, Università di Roma "La Sapienza"  
00185 Rome, Italy

In NMR imaging, severe constraints on the spatial resolution are imposed by the natural lineshape of the sample: both homogeneous and inhomogeneous (1) broadening of the line due to nuclear interactions affect the imaging condition  $\gamma G \Delta r \geq \Delta\omega$ , where  $\Delta r$  is the spatial resolution,  $G$  the gradient intensity,  $\Delta\omega$  the natural bandwidth of the nuclear spin system, and  $\gamma$  its gyromagnetic ratio.

All aspects of the nuclear interactions are in principle retained in solids, due to the absence of the molecular motions which average out in liquids those parts of the nuclear spin Hamiltonian which are responsible for the line broadening. In such solid systems, the imaging condition therefore usually becomes so overwhelmingly severe on  $G$  and  $\Delta r$  that performing solid-state imaging has often been considered a quite difficult goal (2).

In the last few years, however, following the efforts made in NMR spectroscopy for obtaining high-resolution spectra in solids (3-6), some groups started utilizing these methods for solid-state imaging purposes (7-10).

In this talk I will report the basis and the achievements of a group of methods which we developed recently. Among these methods special attention will be devoted to the Magic-Angle-Rotating-Frame (MARF) echo (11) technique, which is obtained by generating Audio Frequency pulses in the rotating frame.

Two other lines of development of Imaging will be discussed; one is the 2DFT in the rotating frame and a second one is an approach based on a modified Lee Goldberg sequence.

### References

1. M. Mehring, "High Resolution NMR in Solids", 2nd ed., Springer-Verlag, Berlin, 1983.
2. P. Mansfield and P.G. Morris, "Advances in Magnetic Resonance", Suppl. 2, Academic Press, New York, 1982.
3. E.R. Andrew, A. Bradbury and R.G. Eades, Nature (London) 182, 1659 (1958).
4. M. Lee and W.I. Goldberg, Phys. Rev. 140, 1261 (1965).
5. J.S. Waugh, L.N. Huber and U. Haeberlen, Phys. Rev. Lett. 20, 180 (1968).
6. A.E. Mefed and V.A. Atsarkin, Sov. Phys. JEPT 47, 378 (1978).
7. D.G. Cory, J.W.M. Van Os and W.S. Veeman, J. Magn. Reson. 76, 543 (1988)
8. G.C. Chingas, J.B. Miller and A.N. Garroway, J. Magn. Reson. 66, 530 (1986)
9. F. De Luca and B. Maraviglia, J. Magn. Reson. 67, 169 (1986)
10. F. De Luca, C. Nuccetelli, B.C. De Simone and B. Maraviglia, J. Magn. Reson. 69, 496 (1986)
11. F. De Luca, C. Nuccetelli, B.C. De Simone and B. Maraviglia, Solid State Commun. 70, 797 (1989)

## NMR Imaging Studies of Velocity and Concentration Distributions in Flows

S. A. Altobelli, A. Caprihan, E. Fukushima, and P. D. Majors\*  
Lovelace Medical Foundation and \*University of New Mexico  
Albuquerque, New Mexico, U. S. A.

This is a review of the various NMR imaging (NMRI) techniques to non-invasively study concentration and hydrodynamic parameters in flowing systems, mostly liquids, as well as a survey of the applications of NMR to flow problems. It will show that NMR imaging is well suited to a wide variety of flow problems in many fields with applications in physics, biology, botany, rheology, geology, etc. The parameters that can be directly measured by NMR include density, velocity, acceleration and other derivatives of displacement, diffusion, and other fluctuations. The experiments can be conducted to yield these parameters as a full three-dimensional array or any subset thereof down to just an average over the region with commensurate trade-off in data acquisition and processing times.

We begin by discussing the magnetic resonance phenomena of nuclear spins in motion. A survey will be made of the evolution of NMR flow studies leading up to images of appropriate hydrodynamic parameters. Different strategies for obtaining flow information will be covered and will lead into a review of NMR imaging as it is affected by moving nuclei. Specific examples of density and velocity imaging of flowing spins will be given with discussions of practical problems and limitations.

Two major velocity imaging techniques, time-of-flight (TOF) and phase methods, will be discussed. The simplest TOF experiment is to tag a slice in the flowing medium and recall an echo only from the tagged spins after the tag has moved a short distance. Because the tag will only occupy one plane of the sample, this scheme works best in spatially uniform flow. An embellishment of this basic idea which greatly broadens the usefulness of the method is to spatially replicate the slice so that the tags are multiple.

It is well known that phase effects can affect signal amplitudes as well as the average phase for an assembly of spins. The variation in image intensity of flows found in clinical medical images are caused by the distribution of spin phases in each voxel but this effect is difficult to quantify. The standard phase method for velocity measurements relies on the fact that the average phase within a voxel can be made proportional to the velocity component along a field gradient. Such an experiment can yield velocity and other information everywhere within the region of interest but at some cost in time.

Applications of flow imaging with little or no velocity information include density images of flowing spins such as magnetic resonance angiograms which show only the flowing liquid (blood) and multiphase slow flows in porous media in which the different phases are tracked by chemical shift imaging. Another example of a density image is the concentration profile of different phases in multiphase flows and some examples of such flow studies will be described. Several examples of velocity images will be given in single and multiphase flows including flows in the presence of growing biofilms, flows of concentrated suspensions, etc.

## STRAFI: HOW IT WORKS?

A.A.Samoilenko

Institute of Chemical Physics, USSR Academy of Sciences,  
117977 Moscow, USSR

## ABSTRACT

The techniques of solid state imaging in a stray field of superconducting solenoid (STRAFI) at a very high magnetic field gradients is described. The conditions and procedure of the corresponding experiments are discussed.

## INTRODUCTION

Several methods to obtain NMR images of solid samples have been proposed. An approach based on experiments in a stray field at the edges of superconducting magnets /1/ was demonstrated to be an universal way to take high resolution (about 100 microns) pictures of various objects containing protons /2/, /3/, /4/. This method is based on the one-dimensional projections formation. Each of these projections is prepared by subsequent detection of signals from the selectively excited thin slices crossing a sample moving along the magnet axis. A set of projections taken for different sample orientations relative to the magnet axis can be transformed via background routine into 2D or 3D pictures.

## RESULTS

A topology of magnetic field at the edge of superconducting solenoid as a source of strong magnetic field gradient  $G_p$  has been studied. Numerical calculations show a presence of a constant field  $B_p$  flat surface close to the edge of solenoid with the following parameters:  $B_p = 0.4 B_o$ ,  $G_p = B_p/R$ , where  $B_o$  is a field at the magnetic center and  $R$  is a solenoid radius.

A methodology of microscopic imaging experiments including pulse sequence, signals detection, data evaluation and treatment and the mechanical arrangement of sample motion to take 1D, 2D and 3D pictures is discussed in detail.

Diffusion of water in PMMA is studied /5/. Activation energy of diffusion of  $54 \pm 3$  kJ/mol is calculated.

Possible applications and future developments of the proposed technique in material science are discussed.

#### CONCLUSIONS

This method is an universal tool for producing high quality high resolution images of solid samples containing magnetic nuclei. Relatively complicated mechanical arrangement of experiments is compensated by a wide variety of possible applications in materials research.

#### REFERENCES

- /1/ A.A.Samoilenko, D.Yu.Artemov and L.A.Sibeldina, JETP Lett. 47, 348 (1988).
- /2/ A.A.Samoilenko, D.Yu.Artemov and L.A.Sibeldina, Bruker Report, Vol.2, pp.30-31 (1987).
- /3/ A.A.Samoilenko and K.Zick, Bruker Report, Vol.1, pp.40-41 (1990).
- /4/ Proc. of 25 Congress Ampere, Stuttgart 1990, pp.92-93.
- /5/ D.Yu.Artemov, A.A.Samoilenko and A.L.Iordansky, Sov.Polym.J., AXXXI, N 12, 2473-2476.

## Imaging by radio-frequency field gradients.

P. Maffei and D. Canet  
Lab. Method. RMN  
Université de Nancy I  
B.P. 239  
54506 Vandoeuvre les Nancy cedex  
France

Novel procedures for imaging small objects by means of two coils have been developed. The first coil is the classical saddle shaped coil in the probe of a vertical cryomagnet (in the present case, the spectrometer operates at 200 Mhz). It is used for the creation of homogeneous pulses and for detection purposes. The other one is a single turn coil whose axis is perpendicular to the axis of the saddle shaped coil and which produces a linear rf gradient across the object under investigation.

Images result from NMR data that are obtained by a  $90^\circ$  rotation of the object (or of the coil assembly) within an appropriate pulse sequence. The Y direction (of the laboratory frame) is first labeled by a rf gradient applied for a time  $t_1$ ; after the above mentioned  $90^\circ$  rotation the X direction is sampled in a second time domain  $t_2$  with a train of rf gradient pulses, including a detection window between two consecutive pulses. Images are then obtained by a double Fourier transformation of the "pseudo fids" which arise from this particular detection mode. A further advantage is the ability to separate, from a single experiment, images of two chemically shifted species.

Finally, the procedure allowing a slice detection in the Z vertical direction will be described. It is based on the  $B_1$  inhomogeneity of the saddle shaped coil along Z and employs a DANTE-like selectivity sequence.

The performance and the interest of the method will be discussed through several examples.

Solid state imaging in combination with magic angle spinning

W.S. Veeman and G. Bijl  
Physical Chemistry  
University of Nijmegen  
6525 ED Nijmegen  
Netherlands

Abstract.

In general the resolution in solid state imaging suffers from the large solid state NMR linewidth. Solutions to overcome this problem vary from the use of very large gradient fields to various line narrowing techniques.

In this presentations our efforts to combine imaging with magic angle spinning NMR will be reviewed, together with recent work on the combination of imaging with magic angle spinning and selective excitation.

## SCANNING AND CT-ESR MICROSCOPES

Motoji IKEYA ,

Department of Earth and Space Science, Faculty of Science, Osaka University, Toyonaka, Osaka 560, Japan

Electron spin resonance (ESR) microscopy is based on (1) a large field gradient (CT-ESR) for high resolution as CT-NMR(MRI) or on (2) scanning either a localized magnetic field or microwave field. Spatial imaging of the concentration of paramagnetic impurities and radiation-induced radicals provides insight into the physical chemical and biomedical natures of materials. Valencies and states of paramagnetic impurities such as transition metal ions and rare earth ions clarify the enzymatic and catalytic reactions. ESR radiation dosimetry of human extracted teeth used to assess the exposure of Chernobyl residents and A-bomb survivors at Hiroshima and Nagasaki can be imaged to separate the dental radiation dose if the resolution is increased. Geological and archaeological applications of ESR as a chronological dating method based on natural radiation effect can be also given as images for rocks and minerals grown in a long time. Local radiation environment may be imaged. Pyrolytic radicals in foods may be also objects of ESR microscope. Both the hardwares (methods and apparatus) and softwares (applications) of ESR microscopes are reviewed for the future development of this methods in wide area of sciences.

**EPR IMAGING OF POLYMERS, SOLID MATERIALS, AND TUMORS.**Lawrence J. Berliner and Hirotsada Fujii\*

Department of Chemistry, The Ohio State University, 120 W. 18th Avenue, Columbus, OH 43210-1173, U.S.A.

EPR(ESR) imaging shows much promise in the field of materials research with the promise of observing naturally occurring free radicals due to fissures, oxidation, etc. The measurement of general diffusion properties through membranes, liquid crystals, polymers, etc. is of interest in studying both homogeneous and nonhomogeneous diffusion and their rates. Model systems described are polyacrylamide gels containing lossy electrolyte solutions and the visualization of non-homogeneous solvent induced swelling in polycarbonate and polystyrene molded rods, revealing rod expansion and crack development. As an example of imaging naturally occurring organic radicals, the paramagnetic composition in solid coal rods was monitored during mild pyrolysis at 150°C in air. Lastly, the manifestation of diffusion and bioreduction in whole animals by ESR imaging is demonstrated in a mouse tumor model. This work was supported in part by a grant from the NIH (RR03126).

\* Current address: The Tokyo Metropolitan Institute of Medical Science, 18-22 Honkomagome 3-chome, Bunkyo-ku, Tokyo 113 JAPAN

PROTON IMAGING AFTER DYNAMIC POLARIZATION  
POTENTIAL APPLICATIONS IN BIOLOGY

D. GRUCKER, Institut de Physique Biologique, URA 1173 du CNRS, 4 Rue Kirschleger  
67085 STRASBOURG CEDEX, FRANCE

The considerable development of NMR imaging has negated the main drawback of NMR : the lack of sensitivity. Sensitivity of NMR is usually enhanced by increasing the main magnetic field ; double resonance technique is another way to reach this goal. Magnetic resonance microscopy is confronted with the low spin content of an image pixel. If the increase of the magnetic field is not an adequate way to increase sensitivity, the nuclear enhancement arising from saturation of the electron paramagnetic resonance of a dissolved free radical can be used. This well-known concept of double resonance will be presented here with the aim of biological application. As a matter of fact, the water presence and the biological reduction of stable free radicals involve a specific approach.

Dynamic polarization is a double resonance method based on the Overhauser effect, whereby it is possible to increase the difference in populations between two energetic levels many times above its thermal equilibrium value. In the presence of two spins, **H** and **S**, belonging to two different species, the saturation of the resonance of spin **S** enhances the population difference between the energetic levels of spin **H** due to a coupling between them. If **S** is an electronic spin, the dynamic polarization of the nuclear spin may reach 330 times the equilibrium level in the case of a free electron coupled to a proton by a dipole-dipole interaction.

Dynamic polarization can be regarded as a spin preparation period after which all of the NMR imaging sequences can be used. In this case, the contrast of the image is predominantly governed by the proton polarization of water which is proportionnal to the free-radical concentration and the degree of saturation of the EPR resonance. Such an imaging method after dynamic polarization might be called Overhauser imaging.

The interest in Overhauser imaging lays in the possibility to perform indirect EPR imaging in large aqueous samples. EPR is a very sensitive tool for detecting free radicals and for *in vivo* oximetry. Unfortunately, EPR imaging is limited to small biological samples due to non-resonant absorption and that the short electron relaxation times need a very high magnetic gradient in order to perform imaging. On the contrary, Overhauser imaging, performed in low magnetic field ( $B_0 < 20$  mT), allows imaging of free radical in large aqueous sample with conventional MRI methods. Biological application of Overhauser imaging has been devoted to oximetry and free radical detection.

Overhauser imaging sensitivity to dissolved oxygen comes from the paramagnetism of  $O_2$  which broadens the EPR and the NMR lines. Therefore, in the presence of oxygen, the degree of EPR

saturation is reduced at constant r.f. power and moreover the coupling between dissolved free radicals and water protons is reduced. These two effects give a lower NMR signal enhancement than that in the absence of oxygen. Therefore, Overhauser imaging has the potential to detect ischemic region via an increase in the NMR signal.

Detection of endogenous free-radical production is the second goal of Overhauser imaging. Free radical such as  $\text{OH}\cdot$  are involved in many disease states. The lifetime of hydroxyl radicals is too short to allow their direct detection. A dissolved diamagnetic spin-trap molecule can interact with short-living radicals to give a sufficiently stable free radical to perform Overhauser imaging. The feasibility of this method has been reported by UV-generated spin-trapped hydroxyl free radical (Lurie D.J. et al. 8th ESMRMB Congress 1991).

Overhauser imaging is a very new technique which looks promising, but it is now confronted with three main difficulties : firstly, the overheating due to non-resonant r.f. energy absorption during the electron resonance saturation period ; secondly, the lack of stability in biological fluids of the free radical; thirdly, the possible toxicity of the stable-free radicals used.

The work in progress for overcoming these difficulties can be roughly classified in two categories. The first one is based on physical developments such as field cycling or electron rotary saturation. The second approach is based on the chemical structures of the free radicals used for Overhauser imaging. Isotope substitution of nitroxides causes the narrowing of EPR lines and even the reduction of the number of lines. In this case, saturation of EPR is reached more easily and overheating is reduced compared to conventional nitroxides. The use of other free radicals is discussed.

The Overhauser imaging method is theoretically a way to allow imaging of unfavorable isotopes to a NMR point of view, due to low natural abundance and small gyromagnetic ratio. In non-aqueous sample where overheating by the EPR saturation wave is not the main problem, the usefulness of Overhauser imaging compared to conventional NMR imaging in high magnetic field, has to be discussed in regard of the penetration of EPR frequency waves and the possibility to introduce free radicals into the sample. At the present time, this new imaging technique is mainly dedicated to aqueous sample where the proton abundance allows the indirect imaging of an electron spin system with very short relaxation times by a nuclear spin system with long relaxation times which permits high resolution images with in vivo acceptable gradient strengths.

Spectral - Spatial Skin Imaging with MOdulated Gradient and Simultaneous Field Scan (MOSS)

Th. Herrling, N. Groth, K.U. Thiessenhusen, U. Ewert  
Centre of Scientific Instruments  
Rudower Chaussee 6, Berlin 1199

Spectral spatial EPR imaging is the most direct approach to investigate the spatial distribution of biochemical and biophysical processes in skin in order to characterize proteins, lipids and cell membranes.

A two dimensional MOSS-Image (128x128 points) is measured by using modulated gradient with a simultaneous field scan. The image is obtained by measuring the EPR spectrum for a series of 128 sequential positions. The minimum distance applied was 10  $\mu\text{m}$  between two positions. A fast field scan of 2 s with a scan range of 10 mT enables a short registration time of about 4 minutes for a 2D image.

We studied MOSS images in skin biopsies of hairless mice. Our imaging technique utilized modulated field gradient to obtain cross sectional images perpendicular to the skin surface. Employing free nitroxide radicals, this technique allows the analysis of biophysical and biochemical phenomena within the micron range. By spin labeling of drugs, pharmacokinetic properties of the labeled compounds can be monitored in skin. We suggest that EPR imaging has a broad application potential in dermatologic research.

## ABSTRACT

## NMR IMAGING OF POLYMERIC SYSTEMS

by

J. L. Koenig  
Department of Macromolecular Science  
Case Western Reserve University  
Cleveland, Ohio 44106

NMR imaging is one of the few tools which allows a determination of the spatial distribution of structures in a heterogeneous polymer sample. NMR imaging is a method whereby the stimulated signal is spatially encoded using linear magnetic gradients so that a 2D image can be reconstructed showing the distribution of nuclei in the sample. Other than spatially encoding the signal, imaging works on the same principles as standard NMR. Consequently, not only can the nuclei density be determined but differences and the distribution of the molecular mobility as well. The NMR imaging technique depends on the differences in the environment of the nuclei, and the environments are influenced by a wide variety of chemical and physical effects, so the potential applications of the MRI technique to materials are very large including:

- Adsorption and diffusion processes of fluids in materials
- Detection of internal defects and voids
- Characterization of heterogeneous mixtures of different materials
- Study of molecular interactions between materials
- Detection of internal gradients in materials
- Determination of spatially distributed structural changes
- Composition profiling from surfaces and other sources
- Study variations in molecular mobility throughout the sample
- Evaluation of homogeneity of mixing processes
- Determination of internal flow processes

With our imaging equipment, samples with an external diameter of 60 mm can be imaged and the sampling technique consists of simply placing the sample in the image probe. We have been studying a variety of polymeric systems. These preliminary results suggest that NMR imaging will have a large impact on our future knowledge of the polymeric behaviour.

NMR Imaging of Composition and Defects in Industrial  
Elastomers

Richard A. Komoroski and Subhendra N. Sarkar  
University of Arkansas for Medical Sciences  
Little Rock, AR 72205 U.S.A.

ABSTRACT

Multiple slice 3D  $^1\text{H}$  imaging at medium resolution (100-200  $\mu\text{m}$ ) and short echo times (0.5-2 ms) has been applied to composite tire sections. Various rubber layers and the cords were visualized at 200  $\mu\text{m}$  resolution with contrast from  $T_2$  differences. MAS NMR characterization of samples from each layer provided information on elastomer composition that supported the image intensity variations. The limit on detecting composition variation in actual tires was estimated by imaging well characterized diblends of cis-polybutadiene (BR) and styrene-butadiene (SBR) rubbers of variable composition. From their  $T_2$  weighted images or from the total intensity profiles, a 10-20% difference in blend composition was distinguishable. 3D images of experimental tire sections could distinguish those with good and poor carbon black dispersions at 150  $\mu\text{m}$  in-plane resolution. Artifactual intensity patterns arising from bulk magnetic susceptibility differences between various defects and the surrounding matrix were observed in most carbon-black-filled samples, and may be useful for identification of the defect.

## Gradient Modulations for Liquid and Solid State NMR Microscopy

David G. Cory  
Bruker Instruments, Inc.  
19 Fortune Drive  
Billerica, MA 01821

The role of gradient modulation in NMR microscopy will be explored with applications to both liquid and solid state studies. The possible benefits of gradient modulation include: (1) the separation of the gradient Hamiltonian from inhomogeneous Hamiltonians with similar functionalities, (2) the suppression of undesired cross terms during coherent averaging, and (3) the circumvention of gradient imposed diffusion and sensitivity limits to resolution.

## MRI STUDIES OF IN-SITU POLYMERISATION REACTIONS AT ELEVATED TEMPERATURES

T.A. Carpenter, L.D. Hall, P. Jeppard, C.J. Wiggins.  
The Herchel Smith Laboratory for Medicinal Chemistry,  
University Forvie Site, Robinson Way, Cambridge, CB2 2PZ, England.

N.J. Clayden and P. Jackson,  
Wilton Materials Research Centre,  
ICI, PO Box 90, Wilton, Middlesbrough, Cleveland, TS6 8JE, England.

N. Walton,  
ICI Chemicals and Polymers Limited,  
PO Box 8, The Heath, Runcorn, Cheshire, WA7 42D, England.

Although Magnetic Resonance Imaging has been successfully used to study some aspects of materials science, little attention has been directed towards polymer chemistry. As part of a joint venture between Cambridge and ICI, NMR results have been obtained using a variety of polymerisation schemes. This paper will discuss two illustrative examples of what can be achieved using an MRI system based on a 2 Tesla, 31cm bore magnet fitted with fast switching gradient coils which surround a large, heated processing oven.

Moulds have been developed which fit inside the oven, into which liquid methylmethacrylate-based systems can be injected. Imaging experiments allow the thermally-induced formation of polymethylmethacrylate to be mapped in both space and time. Such studies provide new insight into the formation of defects, such as voids or optical imperfections which are induced when the processing conditions are unfavorable.

Similar equipment has been used to follow the high-temperature curing of structures made from an advanced aerospace composite, manufactured from a continuous carbon-fibre reinforced epoxy resin. The resulting images can be used to monitor the cure state of the polymer phase, and defects introduced in the initial laying-up process can be detected.

In addition to allowing the monitoring of such high-temperature reactions, operation at elevated temperatures also offers further advantages in materials science studies. By increasing the mobility of the molecules of interest, it is possible to generate enhanced images from, for example, solvents ingressed into polymers and composites, and from amorphous regions within solid polymer objects. Work on water ingress into nylon blocks and direct imaging of a solid polypropylene component will be described to illustrate these fields.

# NMR Imaging of Polymers: Methods and Applications

B. Blümich, P. Blümmler, E. Günther, J. Jansen, G. Schauß, and H. W. Spiess

Max-Planck-Institut für Polymerforschung, Postfach 3148, W-6500 Mainz, Germany

The development of polymer materials with extraordinary properties is of particular interest in present polymer research. In many applications the material properties of interest are tailored to vary as a function of space. Examples are different rubber layers in car tires, morphological changes in drawn polymers, and flow induced orientation of injection molded parts. Furthermore, mere use of the product can induce chemical or physical change as a function of stress, time and environmental conditions in exposed areas. Therefore, methods which provide information on the spatial distributions of physical and chemical parameters are in need.

NMR imaging is particularly suited for this, because it combines the rich information contents of NMR spectroscopy with spatial resolution. On the other hand, from the point of NMR, polymers are interesting candidates for imaging, because they are rich in protons. However, conventional imaging methods can only be applied to solids such as many elastomers, which exhibit high molecular mobility. Imaging of more rigid solids requires the development of special methods to overcome the linewidth problem which limits the spatial resolution.

We have exploited conventional imaging methods and developed solid state methods for  $^1\text{H}$ ,<sup>1-3</sup>  $^2\text{H}$ ,<sup>3-5</sup> and  $^{13}\text{C}$ ,<sup>6</sup> which provide detailed information on 1) heterogeneities in elastomers based on chemical composition, and chemical and mechanical aging,<sup>1-3</sup> 2) molecular order and morphology of drawn tensile bars,<sup>6</sup> 3) molecular mobility as influenced by differences in plasticiser concentration,<sup>2,3</sup> and 4) sample deformation as a result of applied external forces.<sup>2</sup> The methods used are spin echo techniques,<sup>1-3,6</sup> double quantum imaging,<sup>2-4</sup> and MAS imaging.<sup>5,7</sup> They are combined with different filter preparation periods and spectroscopic resolution for contrast enhancement and parameter-selective imaging. For examining large objects 1D and 2D spectroscopic imaging with stochastic excitation is investigated.<sup>8</sup>

## References:

- 1 P. Blümmler, B. Blümich, *Macromolecules* 24 (1991) 2183.
- 2 B. Blümich, P. Blümmler, E. Günther, G. Schauss, *Makromol. Chem., Macromol. Symp.* 44 (1991) 37-45.
- 3 B. Blümich, P. Blümmler, E. Günther, G. Schauss, *Bruker Report* 2 (1990) 22.
- 4 E. Günther, B. Blümich, H. W. Spiess, *Molec. Phys.* 71 (1990) 477.
- 5 E. Günther, B. Blümich, H. W. Spiess, *Chem. Phys. Lett.* xx (1991) xxx.
- 6 E. Günther, B. Blümich, H. W. Spiess, *Macromolecules* xx (1991) xxx.
- 7 G. Schauss, B. Blümich, H. W. Spiess, *J. Magn. Reson.* xx (1991) xxx.
- 8 B. Blümich, *J. Magn. Reson.* 90 (1990) 535.

## INVESTIGATION OF AGING PROCESSES IN ELASTOMERS BY PARAMETER SELECTIVE NMR MICROSCOPY

E. Koeller, I. Theis and W. Kuhn

Fraunhofer-Institute for Nondestructive Testing, Ensheimer  
Straße 48, D-6670 St. Ingbert, Germany

Technical elastomers such as carbon filled natural rubbers experience in their practical application many different aging processes resulting in changes of their molecular and mechanical properties. Alterations of the molecular mobility can be detected by the measurement of the proton relaxation times  $T_1$ ,  $T_{1\rho}$  and  $T_2$ . The relaxation times cover a range of  $10^{-3}$ s up to  $10^{-12}$ s in molecular correlation times.

The combination of relaxation measurements with imaging techniques leads to parameter selective images. Image analysis with respect to the relaxation times allow their spatially resolved determination and gives information on crosslink density and their inhomogeneities caused by aging processes.

According to our experience the measurement of the  $T_{1\rho}$  relaxation times at different spin lock fields in a range between 4 kHz and 200 kHz is more sensitive to changes of the network structure than  $T_1$  and  $T_2$ , since the molecular motion takes place predominantly in this range.

We can show that oxidative aging on polysulfidic cured rubber leads to significant changes in  $T_1$ ,  $T_{1\rho}$  and  $T_2$ . By means of parameter selective image analysis it is possible to determine the thickness of the aged regions in a rubber sample.

Moreover we are able to characterize mono- and polysulfidic materials and different curing conditions by their spatially resolved distribution of  $T_{1\rho}$  relaxation times. The differences in  $T_{1\rho}$  for different curing conditions are up to a factor of 2.5.

Thermal as well as oxidative aging processes can lead to remarkable changes in  $T_1$ ,  $T_{1\rho}$  and  $T_2$ . Typical results for samples aged at different thermal and oxidative conditions will be shown.

## MONITORING OF PHOTOPOLYMERIZATION PROCESSES BY NMR IMAGING

Klaus Albert<sup>1</sup>, Ulrich Günther<sup>1</sup>, Martin Ilg<sup>1</sup>, Ernst Bayer<sup>1</sup>, and Mario Grossa<sup>2</sup>

<sup>1</sup> Institut für Organische Chemie, Auf der Morgenstelle 18, D-7400 Tübingen, FRG

<sup>2</sup> Du Pont de Nemours (Deutschland) GmbH, Dornhofstr. 10, D-6078 Neu-Isenburg, FRG

Photopolymers are of great technical importance in many fields, e g. in microelectronics and in printing processes. While the mechanism of photopolymerization is largely understood, only little information upon the amount and the spatial progress of polymerization in an irradiated sample is available. For this reason it is of considerable interest to monitor the spatial process of polymerization.

We have conducted three different types of NMR imaging experiments in order to obtain more information upon this important reaction.

1) An *in situ* monitoring of the photopolymerisation process was carried out by inserting a light guide directly into the 10 mm Helmholtz insert of our microimaging probehead. The source of light was a halogen lamp delivering light with a wavelength from about 340 nm to above 550 nm. The bottom of a flat 10 mm NMR tube filled with an acrylate sensitive to this wave length region was thus irradiated. Four different states of the photopolymerisation could be observed by spin-echo imaging with an in-plane resolution of 50  $\mu\text{m}$ .

2) Detailed information was obtained by chemical shift selective imaging with a 3 mm i d. solenoidal coil yielding an in-plane resolution of 20  $\mu\text{m}$ . The images of the vinylic protons proved to be a very sensitive indicator for the gel-like state of the sample.

3) The exposed region within a printing plate was viewed in a weighted  $T_2$  spin-echo image. Here the depth of polymerization could be judged from the image.

The result of these different experiments show that magnetic resonance imaging is a valuable technique for noninvasive examination of photopolymerisation processes.

Abstract of a paper to be presented at the International Conference on NMR Microscopy to be held at Heidelberg, Germany, from 16 to 19 September 1991.

SOME APPLICATIONS OF PULSED-FIELD-GRADIENT NMR IN PETROCHEMICAL RESEARCH

by

K.P. Datema, J.A. Bolt-Westerhoff and J. Karger\*

Koninklijke/Shell-Laboratorium, Amsterdam  
(Shell Research B.V.)  
Badhuisweg 3, 1031 CM Amsterdam, The Netherlands

\* Universität Leipzig, Germany

Some recent applications of (self-)diffusion measurements by means of NMR are presented. At KSLA, the pulsed-field-gradient NMR technique has now developed into a well-established analytical tool in catalysis and polymer research.

The technique has been used for detailed analysis of the diffusion of sorbed species in heterogeneous catalysts, e.g. light n-alkanes (methane, n-butane, n-pentane) in zeolite ZSM-5. The main object of this NMR study<sup>1</sup> was to make a comparative study, using the same systems of results obtained by molecular dynamics calculations and uptake measurements. Among the more liquid-like (polymer) systems that were investigated are pure liquids, liquid mixtures, polymers in solution, polymer networks and several micellar systems, such as detergents and surfactants. In the latter case the technique has provided insight into the aggregation state and size of the micelle<sup>2</sup>.

1. K.P. Datema, C.J.J. den Ouden, D.W. Ylstra, H.P.C.E. Kuipers, M.F.M. Post and J. Karger (1991) J. Chem. Soc. Faraday Trans II, 12, in press.
2. K.P. Datema, J.A. Bolt-Westerhoff, A. Jaspers, G.J.R. Daane and L.A.M. Rupert, submitted for publication.

Amsterdam, June 1991

## NMR Imaging of water distribution in vycor glass

G. Guillot, P. Gonord, S. Kan, S. Durand-Vidal, O. Bruynooghe

Institut d'Electronique Fondamentale CNRS URA 22

Bâtiment 220 Université Paris-Sud 91405 ORSAY CEDEX FRANCE

We have obtained 2D and 3D NMR images of water distribution in vycor glass samples at 8.5 T with a resolution  $100\ \mu\text{m} \times 100\ \mu\text{m} \times 1\ \text{mm}$ . Vycor is a porous glass distributed by CORNING of great importance in catalysis. From its well controlled manufacturing process, it is mainly composed of silica, which is a prominent advantage for NMR experiments as compared to other natural mineral porous materials such as rocks, cements, etc... with uncontrolled paramagnetic centers. It has a high porosity (28%) and fairly small pores (diameter  $40\ \text{\AA}$ ). Thus it is an interesting model system of fine porous materials and has already been used by physicists to investigate the dynamic properties of confined liquids and gases [1].

Images of water distribution have been obtained 1) for homogeneous distributions in fully or partially saturated samples, 2) for inhomogeneous distributions attained in imbibition, drying, or water uptake experiments. The images show various interesting phenomena such as

- i) evidence of early crack formation during drying in large samples (diameter 9.5 mm, length 20 mm),
- ii) stability (several days) of inhomogeneous water distributions after drying by nitrogen gas flushing and leaving the sample in a tube isolated from ambient atmosphere,
- iii) water uptake from the sample sides leaving the sample in a water vapor atmosphere.

Moreover, the relaxation times have been measured in conventional experiments, without imaging, and from sets of images adequately weighed in  $T_1$  and  $T_2$ . These measurements will be presented and discussed.

[1] J. M. Drake, P. Levitz, J. Klafter, N. Turro, K. Nitsche, K. Cassidy

Phys. Rev. Lett. **61**, 865 (1988)

## Structure Related Diffusion in Microporous Crystallites

Jörg Kärger and Harry Pfeifer  
Sektion Physik der Universität Leipzig  
O 7010 Leipzig, Linnéstr.5, Germany

Pulsed field gradient (PFG) NMR spectroscopy is shown to provide a variety of direct information about molecular mass transfer in microporous adsorbents. The coefficient of *intracrystalline self-diffusion* is found to depend decisively on the adsorbent structure and the concentration of the adsorbed molecules. In adsorbents of non-cubic structure (e.g. zeolites of type ZSM-5) *diffusion anisotropy* may be investigated by either an analysis of the shape of the NMR signal attenuation or by PFG NMR measurements with oriented crystallites. *Co-adsorption* of other molecular species leads to a substantial reduction of the molecular mobility.

For root mean square displacements sufficiently enhancing the crystallite diameters, PFG NMR yields the rate of molecular self-diffusion through the bed of crystallites (*long-range self-diffusion*). In contrast to the intracrystalline diffusivities, the long-range diffusivities are substantially affected by the bed density and by the presence of inert (carrier) gases.

A study of the transition between the regimes of intracrystalline and long-range self-diffusion yields direct information about the *mean life time* of the molecules in the interior of the individual crystallites (*NMR tracer desorption technique*). These data may be compared with an estimate of the intracrystalline mean life time on the basis of the intracrystalline diffusivities. Any enhancement of the real mean life times in comparison to the estimates indicates the existence of transport resistances on the surface of the individual crystallites ("*surface barriers*"). Surface barriers may be evoked by co-adsorbed molecules, which are too large to penetrate into the intracrystalline pore system, or by subjecting the zeolite crystallites to an appropriate pretreatment (as, e.g. coking or steaming).

The *propagator representation* as following from the Fourier transform of the NMR signal attenuation in dependence on the gradient intensity provides a straightforward means for visualizing the main features of molecular migration on a microscopic scale.

# Imaging of Dynamics Associated with the Belousov-Zhabotinski Reaction

Robin L. Armstrong\* (University of New Brunswick), Canada, Ahron Tzalmona, Michael Menzinger, and Claude Lemaire (University of Toronto)

Magnetic Resonance Imaging techniques have been used to detect chemical waves associated with the  $\text{Mn}^{2+}$  catalyzed Belousov-Zhabotinski (BZ) reaction. The dynamics of quasi-two-dimensional structures has been recorded at 20 second intervals by means of proton relaxation time-weighted images using the spin-echo technique. Convection was suppressed by using agar to increase the viscosity; the formation of bubbles was minimized by allowing pressure to build up in the tightly closed reaction vessel. For low concentrations of manganese the propagating structures are replaced by stationary spools. In smaller diameter tubes plane waves are observed and one-dimensional projections can be recorded at 100 msec intervals. Without agar, velocity anomalies are observed in the form of sudden jumps, presumably a manifestation of the nonlinear thermodynamics. Spectroscopic studies of solution containing these self-organized spatial structures have revealed interesting results. Separate water proton lines associated with  $\text{Mn}^{2+}$  and  $\text{Mn}^{3+}$  are observed and the  $^{31}\text{P}$  resonance of the  $\text{H}_3\text{PO}_4$  is strongly dependent on the concentration of manganese.

Translational Motion Imaging  
with Pulsed Gradient Spin Echo NMR Methods

P.T. CALLAGHAN

Department of Physics and Biophysics

Massey University

Palmerston North, New Zealand.

**Abstract**

The use of spin echoes to measure molecular motion is almost as old as NMR itself. However in recent years some specialist adaptations of the method have been developed. For example when two short magnetic field gradient pulses are used in the Pulsed Gradient Spin Echo (PGSE) experiment, the resulting echo attenuation has a behaviour analogous to the scattering cross-section in neutron diffraction. Apart from yielding the spectrum of the motion the PGSE experiment can be used to examine the structural morphology in porous materials since the motions of molecules within the pore is restricted by the surrounding boundaries. This experiment formally resembles X-ray diffraction. Recently we have used this approach to study internal motion in random coil polymers.

When PGSE methods are applied as a contrast in micro-imaging experiments, it becomes possible to measure the motional spectrum of molecules in each pixel of an image. We have used this phase encoding experiment (Dynamic NMR Microscopy) to obtain velocity and self-diffusion maps for plant vascular tissue, measuring velocities as low as  $10 \mu\text{m s}^{-1}$ . The technique is capable of providing some useful insights in materials science. In particular it is ideally suited to the precise measurement of flow profiles and has been used to measure water motion in complex geometries as well as the shear-thinning of entangled polymer random coils in semi-dilute solution. Measurements of the polymer self-diffusion at different shear rates have been used to test fundamental theories of reptation dynamics.

**Approaches to Flow Statistics, Structure Correlations and 2d Spectroscopy  
Using Characteristic Functions**

L. Frydman, G. A. Barrall, J. S. Harwood and G. C. Chingas

Materials and Chemical Sciences Division  
Lawrence Berkeley Laboratory  
Berkeley California 94720

Although an NMR signal may contain a great deal of information, its complexity often hinders interpretation. In many cases, this information appears as statistical distributions of physical variables, whose characteristic functions are sampled during data acquisition. This fact can be helpful for synthesizing procedures to extract such information, for elucidating signal content, for devising new sequences, and for interpreting experimental results. Applications of this viewpoint will be illustrated with examples of flow statistics, NMR diffraction, and spectroscopy.

## Diffusion anisotropy measurements by 2D-FT NMR Microscopy

Michal Neeman, Claudia F. Kirsch, James P. Freyer and Laurel O. Sillerud  
Life Sciences Division, Los Alamos National Laboratory, Los Alamos NM 87545, USA

### Introduction

The attenuation of water signal due to diffusion, in a 2DFT -Pulsed Field Gradient (PGSE) experiment, depends on the magnitude of the applied diffusion gradients, the imaging gradients and the cross terms between the diffusion gradients and the imaging or background gradients (1,2). The magnitude of the cross terms is different when the direction of the diffusion gradient is changed, leading to changes in signal intensity for isotropic samples (3). In this work we report the methodology for studying diffusion anisotropy in the presence of large imaging background gradients. The method is demonstrated in the isotropic diffusion of water and anisotropic diffusion of water in celery and applied to studies of experimental compression injury in the rat spinal cord.

### Methods

NMR studies were performed at 22°C on a Bruker AM-WB 400 MHz spectrometer equipped with microimaging accessory, using standard 5 mm NMR tubes. Voxel size was 50x50x200 μm. Detection of diffusion anisotropy was done by obtaining the geometric average of images obtained with opposite polarity of the diffusion gradient. These geometric averages cancel the effect of cross terms due to the imaging or background gradients and can be applied in combination with any NMR sequence. Images obtained with the diffusion gradient applied along the X, Y or Z directions were compared for differences in signal intensity. A full diffusion map for each direction was then reconstructed from a set of 8-16 images with incremented diffusion gradients. The effect of the cross terms was demonstrated by looking at images of water obtained with diffusion gradients applied along the X, Y or Z directions. The geometric averaged images showed very good cancellation of the effect of the cross terms. The applicability of this method in studying diffusion anisotropy was tested in celery. Diffusion anisotropy could be observed for the water in the vascular bundles, with faster diffusion along the direction of the fibers (Z) relative to the perpendicular direction (X and Y).

### Results

Diffusion anisotropy in the rat spinal cord was observed for the white matter, but not for the gray matter, as previously observed in low resolution images of the brain (4,5). The diffusion coefficient for water was  $0.10 \times 10^{-5}$  cm<sup>2</sup>/s in the gray matter,  $0.06 \times 10^{-5}$  cm<sup>2</sup>/s in the X and Y directions in the white matter and  $0.13 \times 10^{-5}$  cm<sup>2</sup>/s in the Z direction (along the cord main axis). Compression injury of the cord resulted in a significant shortening of T<sub>2</sub> in the center of the cord, correlating with central hemorrhagic necrosis (6), but did not result in any significant change in water diffusion in the cord. The hemorrhagic areas were highly visible in FLASH images. The fact that the diffusion rates did not change following compression injury implies that the damage did not destroy the morphology of the myelin to a large extent. A larger effect is expected in cases where the apparent diffusion anisotropy is due to oriented capillary structure that is more vulnerable to compression damage.

### Conclusions

Diffusion anisotropy is a very sensitive parameter for detection of system symmetry and directional ordering. This type of information is unique to NMR microscopy, and may prove to be of substantial biological significance. The effect of large cross terms between the imaging gradients and the diffusion gradients can be canceled by obtaining the geometric average of images obtained with opposite diffusion gradients.

### References:

1. M. Neeman, J. P. Freyer and L.O. Sillerud. *J. Magn. Reson.* **90** 303 (1990).
2. M. Neeman, K.A. Jarrett, L.O. Sillerud and J.P. Freyer. *Cancer Research* (1991) In Press.
3. M. Neeman, J.P. Freyer and L.O. Sillerud. *Magn. Reson. Med.* (1991) In press.
4. M.E. Moseley, Y. Cohen, J. Kucharczyk et al. *Radiol.* **176** 439 (1990).
5. T.L. Chenevert, J.A. Brunberg and J.G. Pipe. *Radiol.* **177** 401 (1990).
6. C.F. Kirsch, L.O. Sillerud et al 9th Ann. Meeting SMRM, pp 49 (1990).

# *Imaging the Velocity Profiles for Water Flow through an Abrupt Contraction and Abrupt Enlargement*

Y Xia, K R Jeffrey\* and P T Callaghan

Department of Physics and Biophysics, Massey University  
Palmerston North, New Zealand

\*Department of Physics, University of Guelph  
Ontario, Canada

## **Abstract**

The ability to measure velocity profiles experimentally is of importance in the study of rheology and fluid mechanics. Knowledge of the complete velocity field can be used to check numerical calculations of the Navier-Stokes equations or the validity of the constitutive equations in the case of non-Newtonian fluids. Dynamic NMR Microscopy offers a number of advantages over all conventional methods for the determination of the velocity field. As a demonstration of the use of the dynamic NMR imaging technique for the measurement of the complete velocity field, experimental measurements were carried out on the flow of water through an abrupt contraction and abrupt enlargement. The NMR imaging technique, the imaging instruments and sample system employed in this study are described and the velocity imaging results for both the longitudinal and transverse directions are presented. Numerical solutions of the Navier-Stokes equations describing the experimental situation were performed using the finite element difference method. For these complex flow fields, the experimental results are in excellent agreement with the numerical simulations.

# **NMR Micro-Imaging with a Versatile Spectrometer for Diverse Applications in Biology and Materials Science**

N. Schuff and P.A. Hornung  
Varian Associates, Palo Alto CA 94304, U.S.A

## **Purpose**

The traditional classification into NMR in liquids, solids and imaging is still reflected in the design of many commercial NMR spectrometers. The technical performance in these systems has been optimized for one application but is generally not usable to another without sacrificing quality. In recent years, however, a steadily growing number of applications have been proposed requiring to merge NMR techniques from various fields. Frequency selective excitation, spectroscopic imaging and pulsed field gradient spectroscopy are a few examples. They demand a new spectrometer concept that addresses the broad borderline between liquids, solids and imaging applications with all kind of mesophases.

We report here the adoption of a micro-imaging module to a commercial Varian UNITY NMR research spectrometer with the capability of combining imaging investigations with high resolution and solid state spectroscopy.

## **Basic system concept**

The modular design of the UNITY spectrometer is the key to allow the assembling of the micro-imaging module to a standard console.

Programmable waveform units with a similar conceptional design to generate shaped RF and shaped gradient pulses provide the greatest degree of experimental flexibility and performance by allowing accurate timing and continuous amplitude and phase control. Stable hard pulses, shaped pulses, spin locking and CW irradiation can all be accomplished with the same linear RF amplifier assuring seamless operation over a wide range of experimental conditions.

The waveform signals for the three gradient channels are fed into bipolar power amplifiers which can drive a variety of different gradient coil sets. The standard configuration consists of an external gradient coil set which is mounted inside the room temperature shims of a vertical wide-bore superconducting magnet and is used for first order shimming as well as for the generation of the imaging gradients of up to 80 G/cm strength. The inner diameter of the gradient coil set is large enough to insert a imaging probe with 25mm inner diameter or a variety of standard RF probes for variable temperature liquids and solid state experiments. Other gradient coil sets provide active shielding and higher gradient field strength.

The data system for imaging shares the same software and user interface which has been built to allow operations and data processing for spectroscopy.

## **Applications**

Examples of specific applications of micro-imaging in the field of biological and materials research are presented. Perspectives of future directions for commercial spectroscopic micro-imaging systems will be addressed.

## **Some Aspects on the commercialization of NMR Microscopy.**

M. Mattingly

Bruker Instruments, 19 Fortune Drive, Billerica, MA 01821, USA

A commercial microimaging accessory to perform NMR imaging in submillimeter spatial units was first made available by Bruker in 1986. Although several "homemade" instruments existed before that none were truly integrated products that had the capability of large gradient strengths (ca. 50 G/cm), a variety of RF coils to accommodate a large variety of samples and fully integrated software to perform most modern imaging protocols. Within the first two years over 30 of these systems were delivered. Unlike clinical imaging systems most of these "imagers" were purchased as accessories by scientists that were already using high field NMR systems. Medical research, materials science, polymer science, and oil core analysis researchers were the buyers of these systems in the areas of gradients to enhance both spectroscopy and imaging experiments, general shaping of RF pulses and multidimensional processing of data.

# A View on NMR Microscopy

Victor J. Bartuska

Chemagnetics, Inc., 255 Midpoint Drive, Fort Collins, Colorado 80525, USA

A brief survey of the state and prospects of solid state imaging will be presented. The main discussion will focus on the many considerations and factors which were used to determine product commercialization.

## **LOW COST MICROSCOPY**

**N. Bolas, C F Randell, F Goldie - SMIS Ltd Alan Turing Road Surrey Research Park Guildford GU2 5YF**

**Ultra High Resolution Nuclear Magnetic Resonance Imaging or NMR Microscopy has a wide range of applications with resolution requirements from 10's  $\mu\text{m}$  to sub  $10\mu\text{m}$ .**

**NMR factors effect the resolution limit, these include relaxation time, diffusion, susceptibility and the inherent signal-to-noise. Experimentally, field strength and gradient strength are traded against the resolution required; for higher resolution you require higher field and gradient strengths and this currently means reduced sample size.**

**SMIS have developed an imaging and in-vivo spectroscopy system where a double gradient set is used. One gradient set for larger objects with a lower resolution plus a second set for smaller objects which provides a high resolution. Results from a 7T/150 horizontal system will be presented.**

**SMIS have a range of options available to the experimenter to provide a microscopy facility on a range of vertical or horizontal bore magnets. Results from a 7T vertical system which has been upgraded to provide such a facility will be discussed.**

## NMR Microscopy of Human Tumor Xenografts on Nude Mice

William E. Hull & Klaus-Peter Fichtner  
Central Spectroscopy Dept., German Cancer Research Center,  
Neuenheimer Feld 280, W-6900 Heidelberg, FRG

In cancer research animal model tumors in rats and mice are generally used to study tumor metabolism and growth and to test new diagnostic schemes or therapies that may then be scheduled for clinical testing and application. Although such animal tumors are well characterized and provide a convenient basis for experimentation, there are a number of significant disadvantages that need to be considered. First, there is no guarantee that the growth and metabolic characteristics of these tumors provide a representative model for human tumors, in particular with regard to therapy response. Second, these animal tumors often show very rapid, aggressive growth; they quickly (within a few days) develop hypoxic and necrotic regions by outgrowing their vascularization. The metabolic properties change almost daily, making changes caused by therapy, for example, more difficult to detect. Finally, these tumors can relatively quickly present a severe health burden for the animals and are often invasive with the formation of metastases. Therefore, it is of interest to concentrate research efforts on *human* tumors that are implanted into immune-deficient nude mice. These tumors generally grow more slowly, are less invasive and should represent a better model for metabolic studies.

We have begun to study such human xenografts using high-field NMR imaging and spectroscopy at 7 Tesla (Bruker AM-300 super-wide-bore system with 15 cm vertical magnet, Bruker wide-bore microscopy probehead with 25 mm resonator and integrated gradient coils). Typically, tumors are implanted in the hind leg (thigh) of a mouse and grow to a diameter of 3 - 15 mm over a period of 3 - 8 weeks. With the tumor-bearing leg extended the animal can be placed in a ca. 25-mm diam. plastic tube which is inserted into the resonator so that the tumor region is centered while the thorax and head of the mouse extend outside. With the leg fixed to a support, it is even possible to perform experiments without anesthesia. Multi-slice imaging can thus be done on just the tumor-bearing leg with an optimized field of view. A variety of spin-echo and gradient-echo techniques have been tested and planar resolution of 50-100  $\mu\text{m}$  for 500  $\mu\text{m}$  slices can be routinely achieved in 15-30 min for spin-echo sequences. In the first weeks of growth the tumors were homogeneous and easily discriminated from muscle tissue, mainly on the basis of their ca. 50% higher spin density (more extracellular water). Tumors with > 10 mm diam. showed more heterogeneity; necrotic regions appeared with low spin density. Using < 0.01 mm<sup>3</sup> voxels heterogeneity in  $T_1$  (1.5 - 2.5 s) and  $T_2$  (30 - 80 ms) relaxation times could be detected for both muscle and tumor and was more pronounced in older tumors. Preliminary results indicate that the local relaxation times increase with increasing spin density.

To facilitate these studies a number of methodological developments were required. These will be treated in more detail in a poster and include: rapid interactive pre-emphasis adjustment, volume-selective shimming, water-selective multi-slice imaging using fat presaturation, accurate  $T_1$  determinations using a progressive-saturation spin-echo sequence. The quality of gradient-echo images is limited by the high local field gradients inherent with the small irregular object being examined (a tumor-bearing mouse leg); very short  $t_e$  values (< 4 ms) are required and place stringent requirements on gradient strengths and rf power.

## MR Microscopy of Disease Models

G. A. Johnson, Ph.D., H. Benveniste, M.D., R.R. Black, Ph.D.<sup>1</sup>, G.P. Cofer, M.S.,  
S.L. Gewalt, M.S., L.W. Hedlund, Ph.D., R.R. Maronpot, D.V.M.<sup>2</sup>,  
S. A. Suddarth, M.S., B.E. Todd, B.S.

Center for *In Vivo* Microscopy  
Duke University Medical Center  
Durham, North Carolina 27710

<sup>1</sup>General Electric Corporate Research Center  
Schenectady, New York

<sup>2</sup>National Institute of Environmental Health Sciences  
Research Triangle Park, N. Carolina 27710

The pioneers of MR imaging realized the potential to extend the technique to the microscopic domain [1], [2]. Over the last several years a number of investigators have reduced the technical possibility to practice. The Center for *In Vivo* Microscopy has applied MR microscopy in a wide range of the basic sciences. The focus of this paper will be a review of applications in models of disease. Since we are applications-oriented, we will focus on the technique developments required for the specific disease models. The models are (a) stroke, (b) lung toxicology, and (c) liver histopathology. All work is performed on either a 2.0 T, 30-cm horizontal system, or a 7.0 T, 15-cm bore horizontal system, both of which are interfaced to GE Omega consoles (GE NMR Instruments, Fremont, Calif.).

Moseley's discovery of immediate diffusion changes in a cat model of cerebral ischemia has raised a number of interesting areas for investigation [3]. The accurate measurement of diffusion is a nontrivial problem in an imaging environment, particularly *in vivo*. Gradients employed for diffusion weighting make most sequences susceptible to motion artifacts. In the body, respiratory and cardiac motion can be particularly troublesome. We describe a motion-compensated sequence that minimizes these effects [4]. Diffusion measurements have been undertaken in rat models of cerebral ischemia. Through a combination of *in vivo* microdialysis and MR microscopy we have quantitated these changes to more clearly understand the mechanism of diffusion in stroke [5].

MR microscopy of the lung is another nontrivial technical challenge. Respiratory and cardiac motion coupled to the exceptionally short T<sub>2</sub> of lung parenchyma, are but a few of the difficulties. Macroscopic motion has been controlled through scan-synchronous ventilation and cardiac gating [6]. More recently, we have exploited projection reconstruction encoding [7]. Self-refocused pulses have been employed with shielded-gradients that limit the eddy currents so that fid acquisition can begin < 100 μsec after the selective excitation. The technique shows particular promise in chronic lung toxic insults where changes in T<sub>2</sub> are subtle.

The limits of resolution have been discussed by a number of authors. The practical limit that we encounter in performing microscopy of formalin-fixed histology specimens is the limited signal-to-noise ratio. A combination of 3DFT imaging with large arrays ( $256^3$  or  $512^2 \times 64$ ) with specially-designed "specimen" coils has enabled us to acquire images of a range of liver pathologies with resolution down  $10 \times 10 \times 10 \mu\text{m}$ , and signal-to-noise to yield relevant structural details about the pathologies. Correlation with conventionally-stained and sectioned specimens demonstrated that MR microscopy reveals information clearly sufficient to differentiate several subtle pathologies. The nondestructive 3D nature of MR opens entirely new methods to visualize and quantitate such pathology suggesting broader applications in the pathology laboratory.

## REFERENCES

1. Mansfield, P. and Grannell, P.K.. Diffraction in microscopy in solids and liquids by NMR. *Phys. Rev. B* 1975. **12**:3618. 1975.
2. Lauterbur, P.C. New direction in NMR imaging. *IEEE Trans. Nucl. Sci.* **NS-31**(4):1010, 1984.
3. Moseley, M.E., Cohen Y., Montorovitch, J. et al. Early detection of regional cerebral ischemia in cats; comparison of diffusion and T2 weighted MRI and spectroscopy. *J. Magn. Reson.* **14**:330-345, 1990.
4. Johnson, G.A. and Maki, J.H. Measuring diffusion in the presence of coherent motion. *Invest. Radiol.*, in press, 1991.
5. Benveniste, H., Hedlund, L., and Johnson, G.A.. Acute cerebral ischemia: mechanisms of detection by diffusion-weighted magnetic resonance microscopy. Submitted to *Nature*, 1991.
6. Hedlund, L.W., Cofer G., Suddarth, S.A., and Johnson, G.A. Small animal anesthesia and monitoring during extended MR microscopy. *Invest. Radiol.* **22**:77, 1987.
7. Gewalt, S.L., Glover, G.H., MacFall, J.R., Hedlund, L.W., and Johnson, G.A. Projection reconstruction microscopy of the rat lung. *Soc Magn Reson Med.* San Francisco, CA, 1991.

OXYGEN-17 IMAGING AND LOCALIZED SPECTROSCOPY IN BIOMEDICAL RESEARCH  
AND ITS DIAGNOSTIC POTENTIAL

Gheorghe D. Mateescu, Department of Chemistry  
Case Western Reserve University, Cleveland, Ohio 44106, USA

Although proposed as early as 1987 (1-4),  $^{17}\text{O}$  MRI & MRS did not attract the attention of specialists until the recent demonstration of its ability to determine, *in vivo*, the nascent mitochondrial (metabolic) water in respiration experiments with  $^{17}\text{O}$ -enriched air (5-7). The free energy necessary for cell function in organs and tissues comes from the reaction of hydrogen (provided by foodstuff metabolism) with oxygen (carried from the lungs to cells by hemoglobin),



which is coupled with the ADP  $\rightarrow$  ATP reaction. Thus, the quantity of water produced in oxidative phosphorylation (which we call "nascent mitochondrial water" to emphasize its site and time of formation) is a direct measure of oxygen utilization. This, in turn, is a direct measure of the normal or pathophysiological state of the cells (i.e., the organs and tissues they form). The potential of this method for biomedical research and diagnostic cannot be overemphasized. We present results obtained with mice breathing in atmospheres which contained 21 - 98 %  $\text{O}_2$  enriched in  $^{17}\text{O}$  from 9.5 to 45 atom percent. Preliminary experiments show that the rates of appearance of  $^{17}\text{O}$  labelled mitochondrial water are very sensitive to the physiological activity of the animal. In particular, there is a dramatic difference between animals first subjected to muscular activity while breathing  $^{17}\text{O}_2$  and those first anesthetized and then placed in a probe continuously ventilated with  $^{17}\text{O}_2$ . Significant differences were also found between animals anesthetized with different doses of chloral hydrate. This method offers an unprecedented opportunity to test the respiratory function of cells in organs and tissues. It has the potential to become a valuable test for the (possibly early) diagnostic of a wide array of diseases (cancer, ischemia, Alzheimer, etc.) and treatment efficiency.  $^{17}\text{O}$  is non-toxic. Being a stable isotope it allows long term experiments (unlike its radioactive counterpart,  $^{15}\text{O}$ , which has a half-life of only 124 s). It is possible to register  $^{17}\text{O}$  images with high resolution  $^1\text{H}$  images in a double-tuned microimaging probe. Volumes smaller than  $0.5 \text{ cm}^3$  yield satisfactory spectra for quantitative analysis. This suggests even better results could be obtained with larger animals and humans. Other biomedical applications of  $^{17}\text{O}$  MRI/MRS (e.g., blood volume and blood flow determination, water diffusion in tissues, inorganic phosphate metabolism) will be described.

#### References.

1. G.D. Mateescu & T. Dular, Experimental NMR Conference (ENC) 28, MF73a (1987).
2. G.D. Mateescu, G.M. Yvars & T. Dular, Soc. Magn. Reson. Med. 6, 929a (1987).
3. G.D. Mateescu, G.M. Yvars & T. Dular, in *Water and Ions in Biological Systems*, eds. P. Lauger, L. Packer & V. Vasilescu, Birkhauser, Basel, Boston, 1988, pp 239-250.
4. G.D. Mateescu, G.M. Yvars, I. Pazara, A. Alldridge, J.C. LaManna, W.D. Lust, M. Mattingly & W. Kuhn, in *Synthesis and Applications of Isotopically Labeled Compounds*, eds. T.A. Baillie & J.R. Jones, Elsevier, Amsterdam, 1989, pp 499-508.
5. G.D. Mateescu, 4th Workshop on *in vivo* MRS, St. Louis, April 4-7, 1991.
6. G.D. Mateescu, J.C. LaManna & W.D. Lust, ENC, 32, 194a (1991).
7. G.D. Mateescu, Spectroscopy International, 3 (3), 14-18 (1991).

## The Fourth Dimension of MRI: Obtaining Physiological Information on a Microscopic Scale

*Lynn W. Jelinski  
AT&T Bell Laboratories  
Murray Hill, NJ 07994 USA*

We have been exploring the application of microscopic MRI to obtain an additional dimension of information — information about chemistry, rheology, dynamics, or flow.

We report stroboscopic nuclear magnetic resonance images at 33  $\mu\text{m}$  resolution of the carotid arteries of 80-gram rats. The dimensional changes in the artery were correlated with the absolute blood pressure to determine Young's modulus, a measure of arterial stiffness. Phase angle images were produced from the spin echo data. They enabled us to measure arterial blood flow throughout the heart cycle and under various pathological conditions of reduced blood flow. Microscopic SPAMM (spatially modulated magnetization) techniques were developed which produced stripes as narrow as 41  $\mu\text{m}$ . This technique is useful for measuring ultra-slow flow and anisotropic diffusion in plants.

Taken together, these results illustrate the types of new information that can be obtained with microscopic MRI and portend a bright future for its application to non-clinical problems in biophysics.

HIGH FIELD LOCALIZED IN VIVO PROTON SPECTROSCOPY

David M. Doddrell, Stuart Crozier and Ian Brereton

[Centre for Magnetic Resonance, University of Queensland,  
Brisbane, Queensland 4072, Australia]

Although technically difficult, localized proton spectroscopy at high magnetic field strengths allows the acquisition of signals with increased resolution and from small voxels than at lower fields. 2-D *in vivo* spectroscopy also is of value in increasing the achievable resolution of localized spectroscopy provided the spin-spin relaxation times are sufficiently long compared to  $1/2J$ .

Data will be presented illustrating the applicability of localized proton spectroscopy (including 2-D applications) recorded at 4.7 and 11.7T. The most serious technical difficulty appears to arise from the availability of sufficient rf power rather than achieving high gradient strengths. The physical constraints of fitting an animal into a suitable probe in the vertical bore magnets (130mm at 4.7T and 54mm at 11.7T) used in the studies to be presented has meant the use of distance-decoupled gradient sets combined with gradient pre-emphasis. The most serious gradient-induced difficulty arises from  $B_0$  errors. Eddy current effects need to be addressed if accurate relaxation time data are to be measured.

D.M. Doddrell, J. Field, S. Crozier, I. Brereton, G. Galloway and S.E. Rose, Magn. Reson. Med. **13**, 518 (1990).

S. Crozier, I.M. Brereton, S.E. Rose, J. Field, G.F. Shannon and D.M. Doddrell, Magn. Reson. Med. **16**, 496 (1990).

S. Crozier, J. Field, I. Brereton, L. Moxon, G. Shannon and D.M. Doddrell, J. Magn. Reson., in press (Aug. 1991).

## NMR Microscopy Imaging of Surface and Fine Structures of Cartilage and Contrast Enhancement by Manganese Ions

K.Gersonde, W.Gründer\*, K.Dannhauer\*, Y Kusaka. Hauptabteilung Medizintechnik, Fraunhofer-Institut für zerstörungsfreie Prüfverfahren, D-6670 St.Ingbert and Fachrichtung Medizintechnik, Universität des Saarlandes, D-6650 Homburg/Saar. \*Institut für Biophysik, Universität Leipzig, D-7010 Leipzig, Germany.

### Introduction

The functions of joint cartilage are shock absorption and lubrication in a joint. An examination of joint cartilage should focus on two aspects: 1. Visualization of surface and space of joints and 2. representation of fine structures of cartilage. Here, we demonstrate, that this information can be obtained by NMR microscopy employing contrast agents, such as  $Mn^{2+}$  solutions and  $Mn^{2+}$ -entrapped lipid vesicles, respectively. The smoothness of the surface and the fine structures of cartilage cannot be visualized by routine NMR imaging without employing contrast agents. Arthrotic changes of the joint cartilage could be indicated by the roughness of the cartilage surface and by changes in the fine structure of the cartilage. The cartilage functions are based on the high water content due to the interaction of water with the negative charges (carboxyl and sulfate groups) of the proteoglycans (PG). In addition, the negative groups in the cartilage matrix attract cations resulting in an excess of  $Na^+$ ,  $Ca^{2+}$  etc., which therefore also contribute to the viscoelasticity of cartilage. Hence, the PG in cartilage plays an important role. A loss of PG during progressive degeneration of cartilage results in a lack of water and in dysfunction. In this study, we used free  $Mn^{2+}$  ions to replace other cations in the cartilage and to influence the relaxation behaviour of water. The paramagnetic ions enhance the contrasts within the cartilage and allow the differentiation of internal structures, correlated with cartilage functions. For the examination of the smoothness of the cartilage surface it is necessary, to avoid the diffusion of the paramagnetic cations into the cartilage matrix. Hence,  $Mn^{2+}$ -entrapped lipid vesicles could be very useful.

### Materials and Methods

Temporomandibular joints (TMJ) of neonatal pigs were investigated after intraarticular injection of 0.1 ml 0.75 mM  $MnSO_4$  solution and of 0.1 ml 2 mM  $MnCl_2$ , entrapped in egg yolk lecithine (20 mg/ml) vesicles. The medium of the contrast agents was isotonic saline. MR microimaging was performed on the MSL 400 spectrometer (Bruker) operating at 9.4 T. A spinecho sequence with TR = 500 ms and TE = 9 ms was employed. Pixel resolution and slice thickness were 70  $\mu m$  and 270  $\mu m$ , respectively.

### Results and Discussion

Before injection of any contrast agent, TMJ showed poor contrast between cartilage, space fluid, and surrounding tissues. Internal structures of cartilage can not be observed. Spongy bone, however, is well differentiated. Intraarticular injection of  $Mn^{2+}$ -entrapped vesicles results in an tremendous enhancement of the joint space for a relatively long duration. The space is 300 min after injection still visible. During this period no diffusion of  $Mn^{2+}$  into the cartilage occurred. The surface of the cartilage is clearly observable. As expected in this joint of an healthy animal, the surface is completely smooth. After injection of free  $Mn^{2+}$  into the joint space, sequential microimaging demonstrates the diffusion of  $Mn^{2+}$  from the joint surface into the cartilage matrix and into the joint meniscus. About 60 to 120 minutes after injection a maximum contrast was achieved and internal structures became visible. We have strong evidence, that the contrast enhancement is based on the electrostatic interactions between the negatively charged groups of the PG's and the paramagnetic cations. Zones with higher signal intensity are indicative for the accumulation of manganese ions and hence for higher PG density.

### Conclusion

The partial replacement of the accumulated cations in joint cartilage by  $Mn^{2+}$  leads to MR microimages with clearly enhanced joint cartilage and to the visualization of internal structures. By means of  $Mn^{2+}$ -entrapped lipid vesicles the quality of the cartilage surface can be assessed. Thus both contrast agents in combination could improve the diagnosis of joint cartilage degeneration at its early stage.

Relaxation Time and Diffusion NMR Microscopy of Single Neurons.

J.S.Schoeniger, N.Aiken, E.Hsu, S.J.Blackband,

Department of Radiology, Johns Hopkins School of Medicine, Baltimore MD 22105.

**Introduction:** Applications of NMR microscopy have focussed on its ability to non-invasively examine structure. However, given the much better spatial and temporal resolutions achievable using other techniques, it seems unlikely that NMR microscopy will be competitive for the direct examination of cellular structure in individual cells. We will present further developments in NMR microimaging of single cells and investigate in particular its inferences with regard to cellular structure through the measurement of NMR relaxation times and diffusion coefficients.

**Methods:** The L7 neurons (3-400 micron diameter) from the abdominal ganglia of *Aplysia californicus* were extracted by standard techniques (1) and placed in glass capillary tubes 0.6 mm in diameter. A standard dye exclusion method determined cell viability to be at least 7.5 hours the capillaries.

Imaging studies were performed using a homebuilt imaging probe consisting of a set of quadrupolar field gradients and a solenoidal receiver/transmitter radiofrequency coil supported in a novel concentric tuning assembly. Sets of T1, T2 and diffusion weighted images were obtained from which T1, T2 and diffusion maps were calculated on a Sun computer using a non-linear least squares fitting routine based on the Marquart algorithm. Spatial resolution was relaxed to 30x30x100 microns so that images could be obtained in only 13 minutes, allowing several weighted images to be obtained for good curve fitting.

Cells were perturbed by (a) allowing them to deteriorate inside the capillary tube or (b) by changing the external environment of the cell from sea water to distilled water or a manitol solution. A perfusion system has been constructed which allows these environmental changes to be performed in situ.

**Observations:** The T1, T2 and diffusion maps imply that there is less non-water material in the nucleus relative to the cytoplasm, and that the nuclear material reduces the translational diffusion of water only slightly, indicating that the nuclear structure is a relatively dilute and open matrix or solution. The cytoplasmic material hinders water diffusion significantly, indicating that the cytoplasmic structure is a concentrated and closed matrix or solution. Preliminary analysis of cytoplasmic and nuclear heterogeneity will be presented. After cell death the T2 in the cytoplasm of the cell increases two-to threefold as a consequence of a loss of the osmotic gradient and causing the cell to swell and "diluting" the cytoplasm, resulting in an increased cytoplasmic T2. These data will be compared with those obtained on single oocytes (2) and image contrast variations related to differences in cellular structure.

**Conclusions:** Measurement of relaxation times and diffusion coefficients by NMR microscopy on single cells provides insights regarding cellular structure and may be monitored non-invasively as the cell is perturbed. Further, a more thorough understanding of NMR parameters at the cellular level should lead to a greater understanding of similar measurements on macroscopic assemblies of cells and provide the basis for suitable models of relaxation times and diffusion coefficients in normal and diseased tissues.

**Acknowledgement:** This work was supported by NIH grant number R29-CA-45308.

**References.**

1. W.T.Frazier et al, *J.Neurophysiol*, 30,1288(1967).
2. Aguayo et al, *Nature* 322:190-191 (1986).

## MRI OF CARBON FIBERS IMPLANTS IN BONES

B.Tomanek\*, E.Staszko<sup>+</sup>, S.Sagnowski\*, S.Kwiecinski\*

\*Institute of Nuclear Physics, Radzikowskiego 152,  
31-342 Krakow, Poland

<sup>+</sup>Stefan Zeromski Hospital, Sieroszewskiego 66, Krakow, Poland

Carbon-carbon composites, made of carbon fibers, have been studied as an implant material in many laboratories [1,2,3,4]. The results of investigations indicated that only certain kinds of carbon fibers are well accepted by an organism. It has been shown that the replacement of the broken bone by carbon - carbon composites gives rise to the ingrowth of surrounding tissues into the artificial material. The time, required by tissue for its complete reconstruction, depends on the kind of c-c composite and the surrounding tissue. fibrous carbon implants have been already used in clinical application [9], but the phenomenon of carbon resorption is still far away from being fully understood. The variety of methods have been used to study the process of carbon resorption: i.e. histological examination, labeled samples, X-ray, analysis of bacterial colonization kinetics and bacterial binding capacity to the porous vitreous carbon.

However, none of these methods is capable of the monitoring of carbon erosion. Although the carbon element is invisible for <sup>1</sup>H MRI, the tissue surrounding it can easily be seen through this method, enabling us to study the effects of carbon implants on tissues. Moreover, the observation of the gradual ingrowth of the tissue in carbon implant is also possible making MRI method the attractive technique and convenient tool to investigate tissue reconstruction and carbon resorption processes.

The first *in vitro* results, namely: series of cross-sections of rabbit bone tissues with implemented carbon-carbon composites following various time periods after operation, are presented.

## LITERATURE:

1. Jenkins D., Forster I., McKibbin B., Ralis Z., "Introduction of tendon and ligament formation by carbon implants"., J.Bone Joint Surg [Br] 1977:59-B:53-57
2. Jenkins D., McKibbin B., "The role of flexible carbon-fibre implants as tendon and ligament substitutes in clinical practice. J.Bone Joint Surg [Br] 1980:62-B:497-499
3. Tayton K., Phillips G., "Long term effects of carbon fibers on soft tissues." J.Bone Joint Surg [Br] 1982:64-B:112-113
4. Wood T., Minns R., Stover A., "Replacement of the rabbit medial meniscus with a polyester-carbon fibre bioprosthesis", Biomaterials, 1990, 11, 13-16.

## Q-space imaging in heterogeneous (bio)systems

H. Van As, J.E.M. Snaar, D. van Dusschoten and W.D. Palstra  
 Lab. of Molecular Physics  
 Wageningen Agricultural University  
 Wageningen, the Netherlands

Pulsed Field Gradient (PFG) NMR diffusion measurements have recently been proposed for q-space imaging (1). By determining the diffusion displacement profile the structure in which the fluid diffuses is probed, i.e. by the conditional probability function ( $P_S$ ), describing that a spin originating at  $r$  at the time of the first gradient pulse will migrate to  $r'$  during the time  $\Delta$  between the two gradient pulses. This has been demonstrated for water diffusion in loosely packed monodisperse polystyrene spheres (1) and for dispersive flow of water in loosely packed monodisperse glass bead beds as a function of velocity, observation time ( $\Delta$ ) and glass bead diameter (2).

If we apply q-space imaging to heterogeneous (compartmentalized) (bio)systems we meet some restrictions: susceptibility inhomogeneity,  $T_1$  and  $T_2$  values differing for different environments/compartments, and walls, restricting or conducting the motion, which are not inert for magnetization and/or are (partly) permeable.

Susceptibility inhomogeneity will result in local field gradients, especially at higher magnetic field strength ( $>1$  T). In PFG-SE and PFG-STE the echo amplitude as a function of  $q$  ( $E_q$ ) is affected by local field gradients, resulting in a deformation of the actual  $P_S$ . This effect is minimized by using a PFG-CPMG sequence, which in addition results in a much higher S/N ratio (3).

The differences in  $T_1$  and  $T_2$  for protons in different environments or compartments result in a contribution of the different spins weighed by their  $T_2$  (PFG-SE and PFG-CPMG), or their  $T_1$  and  $T_2$  (PFG-STE). The PFG-CPMG method allows the discrimination of the spins with different  $T_2$ 's, without altering the  $T_2$  weighing when varying  $\Delta$  (4). This will result in  $P_S$ 's as a function of  $T_2$ , and allows for zooming in on data originating from different environments.

Loss of magnetization at the walls, e.g. due to wall relaxation or permeation of spins through the wall, largely affect  $E_q$  (5). When this rate of loss increases, the coherence peak in  $E_q$ , observed when  $\Delta > a^2/2D$ , shifts to higher  $q$  values. At high values (e.g. fully absorbing walls) the modulation in  $E_q$  is totally lost. This results in a  $P_S$  reflecting the structure in which the fluid moves and the rate of magnetization loss within that structure. The rate of magnetization loss at the wall (defined by the wall sink strength parameter  $H$  (5)) is a  $T_2$  (PFG-SE and CPMG experiment) or a  $T_1$  (PFG-STE experiment) process, which in general are not equal. Therefore, that experiment has to be chosen that results in the lowest  $H$  in the actual (bio)system under consideration.

We conclude that the resolution in q-space imaging is not only limited by the available magnitude of  $q$ , but also by the wall relaxation characteristics. Flowing fluid, travelling over larger distances in the same time with respect to diffusing fluid, will give a better competition between displacement and wall relaxation, resulting in a better resolution for q-space imaging.

1. Callaghan P.T., A. Coy, D. MacGowan, K.J. Packer and F.O. Zelaya, *Nature* **351**, 467 (1991)
2. Palstra W.D. and H. van As, One dimensional q-space imaging of transversal dispersive flow, this conference.
3. Van Dusschoten D., H. Van As, P.A. de Jager, A NMR method improving the measurement of diffusion/perfusion in the presence of *in situ* magnetic field gradients, 10th SMRM, San Francisco 1991, in press.
4. Van Dusschoten D., H. Van As, A multi component diffusion analysis using the  $T_2$ s of distinguishable compartments, 10th SMRM, San Francisco 1991, in press.
5. Snaar J.E.M., H. Van As, The effect of "absorbing" walls on NMR diffusion measurements, this conference.

APPLICATIONS OF CHEMICAL SHIFT MICROSCOPY TO NON-INVASIVE  
HISTOCHEMISTRY OF PLANT MATERIALS

J.M. Pope

Dept. of Biophysics, School of Physics, The University of New South Wales,  
P.O. Box 1, Kensington NSW 2033, Australia

Over the past 10 years,  $^1\text{H}$  magnetic resonance imaging has become the method of choice in clinical radiology for generating high resolution images of internal anatomy, particularly in the brain and spinal cord. While a variety of fruits and vegetables were used extensively as test objects in the early development of clinical MRI, renewed interest in the imaging of plant materials has been generated by the availability of micro-imaging attachments for conventional high resolution NMR spectrometers [1-4]. In general, however, although soft tissue contrast has been extensively investigated in human patients and animals, together with the effects of tissue injury, disease, oedema, necrosis and neoplasm, there is to date very little comparable information for the case of plant materials. Recently therefore a number of groups have turned their attention to a more detailed study of plant materials by MRI, with potential applications in agriculture and food processing.

An important potential advantage of MRI in the study of plant materials is its ability to distinguish different chemical constituents based on the chemical shift difference between them. In this talk some applications of chemical shift imaging (CSI) to plant materials will be reviewed. It will be shown that it is possible to image, at microscopic resolution, the distribution of aromatics and carbohydrates (sugars) in suitable samples as well as that of water and fat or oil. An advantage of plant materials in this respect is their immobility and stability, which facilitates signal averaging to improve the signal to noise ratio and hence map the distribution of relatively minor constituents. Thus we have been able to image sugar and oil distribution in a grape berry. Recently we have also combined 3D CSI with water suppression techniques to image the distribution of an aromatic component (anethole), as well as reserve oil, in a fresh fruit of fennel.

References

- [1] P.E. Pfeffer and W.V. Gerasmoqicz (Eds), 'Nuclear Magnetic Resonance in Agriculture', CRC Press (1989).
- [2] W. Kuhn, *Angewandte Chemie* 29, 1-19, (1990).
- [3] J.M. Pope and V. Sarafis, *Chemistry in Australia* 57, 221-224 (1990).
- [4] V. Sarafis, H. Rumpel, J.M. Pope and W. Kuhn, *Protoplasma* 159, 70-73, (1990).

SOME ASPECTS OF NMR MICROSCOPY APPLICATIONS IN  
PLANT SCIENCE AND AGRICULTURE

Mr. V. Sarafis  
Department of Science  
University of Western Sydney, Hawkesbury  
Richmond, New South Wales, Australia

NMR microscopy is an emergent technique in Plant Sciences and Agriculture. Applying the technique to plants is advantageous due to their dimensional stability permitting the long averaging periods needed to make high resolution high quality images.

Plant NMR microscopy has utilised proton distribution and chemical shift selective techniques.

Non-invasive anatomical study of plants, in particular the distribution of vascular structure has benefited from NMR microscopy. This avoids serial sectioning techniques hitherto used. Multislice imaging offers an appropriate solution and the possibility of three dimensional image acquisition would allow three dimensional reconstructions of whole vasculatures.

Dynamic studies of plant growth, in particular leaf morphogenesis at the apex are difficult to perform often requiring surgery can These may now be approached directly through NMR proton imaging. Thus there is a new approach to phyllotactic patterning and ontogenetic studies of flowering, fertilization and fruiting are now possible.

Seed swelling and germination can be followed and the influence of environmental factors such as light and heat can be followed.

NMR Microscopy by flow imaging techniques has been used to follow the dynamics of water flow in the plant body and has applications in plant physiology for monitoring the path and control of both xylem and phloem flow.

Chemical shift microscopy has been used for examining the composition and spatial distribution of fat and water in plants e.g. tubers of the tiger nut. Other applications of chemical shift imaging such as sugar distribution in fruit, essential oil distribution in spices and tanning localisation are now possible.

NMR mini-imaging applications are possible with other chemical species such as  $C^{13}$  but with considerably lower resolution.

Non-invasive monitoring of pathogens, their spread and distribution has been attempted and could be extended.

Applications of mini-imaging to whole plant communities such as grass turfs or moss cushions could be expected to yield results showing the patterns of growth in these complex communities without disruption to their activity.

NMR microscopy has been used for following drying and wetting of agricultural products such as cereal grains, and may have value in observing processes attendant upon cooking e.g. in pasta.

## The ripening of red raspberry fruits studied by NMR microscopy

Brian Williamson<sup>a</sup>, Bernard A. Goodman<sup>a</sup>, John A. Chudek<sup>b</sup> and Shelagh N. Scrimgeour<sup>b</sup>

<sup>a</sup> Scottish Crop Research Institute, Invergowrie, Dundee DD2 5DA, UK

<sup>b</sup> Department of Chemistry, University of Dundee, Dundee DD1 4HN, UK

The changes in spatial distributions of mobile protons in red raspberry (*Rubus idaeus*) fruits during a 3-day ripening period have been studied by NMR microscopy. Measurements were made with the fruit attached to the receptacle and of the receptacle with the fruit removed. All images were acquired using the protons from a single absorption peak at 4.6 ppm, which corresponds to water, and the data were collected using a standard Bruker spin-echo pulse sequence.

The major histological features of the raspberry fruit are clearly seen in the NMR images. The highest mobile proton densities are found at the lines of contact between drupelets, on the surface of the receptacle, and within its central vascular cylinder. The mesocarp tissues of the drupelets showed intermediate grey tones with some evidence of radial striations, whilst the seeds appeared black in all images, indicative of either low mobile proton densities or long relaxation times.

After 3 days the proximal ring of drupelets separated from the receptacle, the spaces between the drupelets enlarged and the boundaries between drupelets were less pronounced. The brightness of the images from the vascular bundles in the receptacle diminished, indicating a decrease in mobile protons in the receptacle after abscission of drupelets.

## Study Of Chilled And Nonchilled Zucchini Squash By NMR Imaging

Paul C. Wang<sup>1</sup> and Chien Yi Wang<sup>2</sup>

1. Department of Radiology, Howard University, Washington, DC 20060
2. Horticultural Corps Quality Lab, USDA, Beltsville, MD 20705

NMR imaging technique is used for detecting changes in the internal structure of zucchini squash (*Cucurbita pepo* L., Ambassador) during chilling exposure. Zucchini squash exposed to chilling temperature 2.5 C causes cellular breakdown and loss of membrane integrity. These effects result in the increase of membrane permeability, electrolyte leakage, and exudation of cellular fluid into the intercellular spaces. The injury further develops into water-soaking appearance and collapse of the tissues.

Zucchini squash used for this study were 18-22 cm in length freshly harvested from a local farm in Maryland, USA. The experimental group was placed at 2.5 C and the control group at 12.5 C. Samples were taken for NMR imaging at harvest and 3 days after storage. A 4.7 T 33 cm bore NMR scanner was used. The sample was positioned at the center of a saddle shaped RF coil. A spin echo imaging technique was used to obtain high resolution images. The spatial resolution was 107  $\mu\text{m}$  x 117  $\mu\text{m}$ . The slice thickness was 1.5 mm. A 6 points inversion recovery technique was used to measure the T1 relaxation times. The T2 relaxation times were measured using five spin-echo images taken by different echo times.

In the healthy nonchilled squash, there was a well defined high intensity layer in the epidermal region. However, in the chilled squash, the high intensity layer was thicker and was not well defined. The high intensity area extended into the flesh and vascular bundles. This indicates that the epidermal region and adjacent areas have higher water mobility and diffusion in the chilled squash than in the nonchilled samples. This high water mobility was apparently caused by increased membrane permeability and possibly the breakdown of compartment in the chilled squash as a result of chilling injury. Measurement of T1 and T2 relaxation times revealed that the chilled squash had a shorter T1 relaxation time and a longer T2 relaxation time than the nonchilled squash. These data indicate that the chilled squash would have a greater mobility of water than the nonchilled tissue which is consistent with the results obtained with NMR imaging.

Table 1. T1 and T2 relaxation times of zucchini squash.

Treatment	T1 (second)	T2 (second)
Nonchilled (12.5 C)	1.413	0.031
Chilled (5 C)	0.993	0.046

1st International Conference on  
NMR Microscopy – Heidelberg  
(September 16–19, 1991)

–ABSTRACT–

Deuterium NMR: Current and Future Uses *In Vivo*

J.J.H. Ackerman<sup>†</sup>, C.S. Bosch<sup>†</sup>, J.L. Evelhoch\*,  
J.J. Neil<sup>‡</sup>, R.S. Hotchkiss<sup>‡</sup>, and S.-K. Song<sup>†</sup>

<sup>†</sup>Washington University, Dept. of Chemistry, St. Louis, MO 63130

\*Washington University School of Medicine, St. Louis, MO 63110

<sup>‡</sup>Wayne State University School of Medicine, Detroit, MI 48201

The deuterium isotope of hydrogen provides a stable, readily available NMR-active nuclide (the deuteron) whose uses in NMR studies *in vivo* are only now being explored. As a metabolic tracer, deuterium presents a chemistry nearly equivalent to that of hydrogen and, thus, can be used to follow metabolic transformations *in vivo*. For example, rates of glucose utilization and lactate formation can be determined via [6,6-<sup>2</sup>H<sub>2</sub>]glucose. Heavy water, <sup>2</sup>H<sub>2</sub>O, can be used to provide a high biological concentration of deuterium in the form of a freely diffusible tracer of aqueous spaces. Using deuterium NMR as an external monitor of *in vivo* tracer concentration in concert with H<sub>2</sub>-residue washin/washout compartmental modeling allows determination of volumetric blood flow rates [ml blood/(min. • wt. tissue)] at the capillary level, i.e., perfusion. Because of the high concentrations of <sup>2</sup>H<sub>2</sub>O achievable *in vivo*, deuterium imaging is feasible and has been demonstrated. The quadrupole nature of the spin 3/2 nuclide may provide contrast distinct from <sup>1</sup>H imaging. Volumetric blood flow images may also be possible.

## OXYGEN-17 MRS AND MRI: THEORETICAL AND EXPERIMENTAL ASPECTS

Gheorghe D. Mateescu, Department of Chemistry

Case Western Reserve University, Cleveland, Ohio 44106, USA

After a brief comparison between  $^1\text{H}$ ,  $^2\text{H}$ , and  $^{17}\text{O}$  microimaging and spectroscopy, this lecture will concentrate on the properties of  $^{17}\text{O}$  and their reflection in the experimental setup for "high resolution - high sensitivity" measurements. Practical examples will be given, mainly with phantoms illustrating the potential and limitations of the method. The performance of a  $^1\text{H}/^{17}\text{O}$  double resonance probe will be discussed.

## Heteronuclear Solid State MRI of Biological and Nonbiological Ceramics

Jerome L. Ackerman, James R. Moore, Bettina Pfeleiderer

Yaotang Wu and Leoncio Garrido

NMR Center

Massachusetts General Hospital

Charlestown, Massachusetts, USA

The overwhelming majority of applications of magnetic resonance imaging (MRI) to solids involve the measurement of proton signals with  $T_2$ 's in the intermediate to fluid state range. However, just as conventional heteronuclear and solid state spectroscopy have enhanced the utility of NMR in the analysis of materials, we expect that the corresponding application of solid state and heteronuclear measurements will prove enormously useful for magnetic resonance imaging analysis of solid specimens. In this presentation, we describe our methods for the imaging of nuclei other than protons in rigid materials. Most of our examples are taken from bioceramic materials including bone. Additionally, we present our initial results on the materials science equivalent of *in vivo* spectroscopy, which we call "*in situ* spectroscopy" in reference to the fact that the volume in which spectroscopy is performed is not removed from the larger specimen, ground into a powder, or prepared in any other manner.

The phase encoding domain of an image acquisition which employs a  $180^\circ$  pulse to elicit a spin echo is intrinsically free of any anisotropic or isotropic chemical shift broadening. Using phase encoding methods for all spatial dimensions of an image therefore removes all chemical shift effects. We have demonstrated this approach both for back projection methods in  $^{31}\text{P}$  imaging of hydroxyapatite (a biologically important calcium phosphate ceramic). Essentially, each projection is obtained by a series of phase encoded echoes. The method works well also for more conventional Fourier transform proton acquisitions in the imaging of polymeric binders in green ceramic materials.

Alternatively, if the chemical shift broadening is not too severe, we may simply use a strong gradient to overcome this intrinsic spectral broadening, and still produce satisfactory images. We will demonstrate this approach for a number of nuclei, including  $^{31}\text{P}$ ,  $^{11}\text{B}$ , and  $^{27}\text{Al}$  in materials with linewidths (of the central transitions in the case of quadrupolar nuclei) of up to 15 kHz, employing gradients as large as  $230 \text{ G cm}^{-1}$  and echo times as short as  $200 \mu\text{s}$ .

We may also create rather subtle levels of chemical contrast in images by employing pairs of imaging pulse sequences which are designed to discriminate, for example, between nuclei with or without nearby protons (using solid state cross polarization), or with differing values of the quadrupole coupling. Again, we will demonstrate with examples of  $^{31}\text{P}$  in calcium phosphates, and  $^{27}\text{Al}$  in alumina-based ceramics.

Finally, we are venturing into the exciting new area of *in situ* spectroscopy, in which we use surface coils for localized spectroscopy of small regions in large objects. Our examples are taken from bone mineral studies, and include specimens as large as humans. The results demonstrate that a large repertoire of conventional solid state techniques, such as cross polarization, measurements of proton and heteronuclear  $T_{1\rho}$ 's, differential cross polarization, etc., are all amenable to surface coil spectroscopy. This suggests future applications to large objects such as composite structural panels, whole tires, logs and milled lumber, ceramic rotors, nozzles and other parts.

## BORON-11 MRI AND MRS

G. W. Kabalka<sup>\*</sup>, G.-Q. Cheng<sup>\*</sup>, P. Bendel<sup>§</sup>

<sup>\*</sup>Departments of Radiology and Chemistry, University of Tennessee Biomedical Imaging Center, Knoxville, Tennessee 37920, USA and

<sup>§</sup>Department of Isotope Research, Weizmann Institute of Science, Rehovot, 76100, Israel

Nuclear magnetic resonance has developed into a powerful tool for the noninvasive and nondestructive anatomical and physiological investigation of living systems. We have been developing boron-11 NMR (MRI and MRS) for use in boron neutron capture therapy (BNCT) for noninvasive quantification and localization of BNCT agents [1,2]. An obstacle to imaging boron *in vivo* is its very short transverse relaxation time ( $t_2 < 1$  ms), which is shorter than the minimal available time-to-echo (TE) in the standard spin-echo and gradient-echo imaging protocols. In boron MRI, the signal normally decays before it can be sampled.

We recently implemented an optimal method previously suggested for the imaging of solid samples [3]. In essence, the free induction decay (FID), rather than the echo signal, is used to generate images. We wish to report the use of this technique for *in vivo* boron-11 MRI of a live rat infused with a boron neutron capture agent.

The results demonstrate that the BNCT agent is excreted from the animal with a half-life on the order of one day which supports the results obtained in earlier, invasive studies. Thus, boron-11 MRI and MRS are potentially valuable techniques for the study of biodistribution and pharmacokinetics of BNCT agents noninvasively, and could prove superior and simpler to implement than BNC radiography.

### Acknowledgements:

We thank the U.S. Department of Energy for support.

### References:

1. Bendel, P.; Davis, M.; Berman, E.; Kabalka, G.W. *J. Magn. Res.* 88, 369-375, 1990.
2. Kabalka, G.W.; Davis, M.; Bendel, P. *Magn. Reson. Med.* 8, 231-237, 1988.
3. Corey, D.G.; Veeman, W.S., *J. Magn. Reson.* 84, 392-397, 1989.

# Spectroscopic $^{13}\text{C}$ and $^2\text{H}$ NMR Imaging in Solids

E. Günther, B. Blümich, H. W. Spiess

Max-Planck-Institut für Polymerforschung,  
Postfach 3148, D-6500 Mainz

For the detection of spatial variations of structure, order, or mobility in solid materials several new methods for the spatially resolved measurement of deuterium and  $^{13}\text{C}$  spectra have been developed. Concepts of multi-dimensional NMR spectroscopy are applied for the separation of spatial and spectral information.

For recording spatially resolved deuterium wide-line spectra in static samples a double-quantum<sup>1</sup> and an alignment echo<sup>2,3</sup> technique is presented. The principle order-imaging is demonstrated on a phantom with different oriented drawn polyethylene. How spatial variations of molecular dynamics can be characterized is shown by an image of polycarbonate and polystyrene, both deuterated at the phenylring, where the different correlation times of the ring motion lead to spectral contrast. Similarly, additives in polycarbonate hamper the flip motion of the phenylring and lead to significant changes in the corresponding wide-line spectrum. Regions without and with 10% additive can clearly be discriminated. Thus, investigation of slow particle diffusion in solids becomes feasible with spectroscopic imaging of the matrix.

For static samples the spatial resolution is 250  $\mu\text{m}$ . Here the limitation is the loss of coherence during spatial encoding in the evolution period caused by direct dipole-dipole couplings. These can be removed in first order by magic angle spinning (MAS) which has only minor effects to the wide-line spectrum containing the desired spectroscopic information. In combination with MAS, a simple one pulse technique is sufficient for performing spectroscopic imaging with high sensitivity and a spatial resolution of 50  $\mu\text{m}$ . This is demonstrated with static and MAS experiments on a deuterated phantom (dimethylsulfone- $\text{d}_6$ )<sup>4</sup>.

For spectroscopic imaging of nuclei in natural abundance (e.g.  $^{13}\text{C}$ ,  $^{29}\text{Si}$ ,  $^{31}\text{P}$ ) a commercial static double resonance probe has been equipped with a gradient system. Existing methods<sup>5</sup> which eliminate the chemical shift in the evolution period have been modified. First  $^{13}\text{C}$  experiments on polyethylene show the potential of the method for applications in material science.

## References:

- 1) E. Günther, B. Blümich, H. W. Spiess, *Mol. Phys.* **71** (1990) 477.
- 2) B. Blümich, P. Blümmler, E. Günther, G. Schauss, *Bruker Report* **2** (1990) 22.
- 3) E. Rommel, S. Hafner, and R. Kimmich, *J. Magn. Reson.* **86** (1990) 264.
- 4) E. Günther, B. Blümich, H. W. Spiess, submitted to *Chem. Phys. Lett.*
- 5) C. G. Fry, A. C. Lind, M. F. Davis, D. W. Duff, and G. E. Maciel, *J. Magn. Reson.* **83** (1989) 656.

Posters:  
Abstracts



## Methods

**MET 9: Designing and Building Screened Gradient Coils.**

*P.J. Back, A. Coy, R. Dykstra, and P.T. Callaghan*  
Palmerston North (New Zealand)

**MET 10: Transverse Quadrupolar Coil Field Profiles**

*C.J. Rofe, and P.T. Callaghan*  
Palmerston North (New Zealand)

**MET 11: An Actively-Shielded Micro-Imaging Probe for High-Field Narrow-Bore Magnets.**

*N. Schuff, I.-J. Feng, and X. Ni*  
Palo Alto, California (USA)

**MET 12: Surface Gradient Coil for MRI and MRS of Small, Moving Objects.**

*A. Jasinski\*, P. Kozlowski\*, J.K. Saunders, and A. Urbanski\**  
Ottawa (Canada) / \*Krakow (Poland)

**MET 13: High Resolution MRI Using a Three Channel Surface Gradient Coil System.**

*J. Link, K. Lüscher, and P. Brunner*  
Fällanden (Switzerland)

**MET 14: Sensitivity and Resolution of NMR Microscopy Using Surface Coils.**

*X. Zhou, and P.C. Lauterbur*  
Urbana, Illinois (USA)

**MET 15: Diffusion Limited Resolution for Different Pulse Sequences in NMR Microscopy.**

*X. Zhou, and P.C. Lauterbur*  
Urbana, Illinois (USA)

**MET 16: Probing below 1000 Å with PGSE-MASSEY.**

*A. Coy, and P.T. Callaghan*  
Palmerston North (New Zealand)

**MET 17: Fast 3D Projection Reconstruction.**

*M. Staemmler, R.Brill, and W. Kuhn*  
St. Ingbert (Germany)

**MET 18: Canceling Quadrature Artifacts Using Hermitian Symmetry of the Spin Echo.**

*F. Hennel*  
Krakow (Poland)

**MET 19: Spectroscopic Imaging with Stochastic Excitation.***J. Jansen, P. Konstanczak\*, and B. Blümich*

Mainz (Germany) / \*Berlin (Germany)

**MET 20: MAS NMR Imaging.***G. Schauß, M. Hehn, H. Raich, B. Blümich, and H.W. Spiess*

Mainz (Germany)

**MET 21: Micro-Imaging Measurements of  $T_1$  Relaxation.***S.J. Doran, T.A. Carpenter, and L.D. Hall*

Cambridge (United Kingdom)

**MET 22: Methodology for High-Field NMR Microscopy of Tumor-Bearing Mice.***K.-P. Fichtner, and W.E. Hull*

Heidelberg (Germany)

**MET 23: Spatial Mapping of Magnetic Fields Induced by Electric Currents.***P. Bendel*

Rehovot (Israel)

**EPR-Imaging****EPI 5: Biological Applications of Low-Field EPR Imaging and in vivo EPR.***H. Fujii, K. Kakinuma, and L.J. Berliner\**

Tokyo (Japan) / \*Columbus, Ohio (USA)

**Materials****MAT 10: Swelling Behavior, and Solubility of Drug Tablets Studied by NMR Microscopy.***E. Koeller, G. Koeller\*, W. Kuhn, and F. Moll\**

St. Ingbert (Germany) / \*Mainz (Germany)

**MAT 11: Study of the Permeability of Polyacrylamide Gel Beads for HLAD by NMR Microimaging.***M. Spanoghe, C. Gorrebeeck, D. Lanens, R. Domnisse, G. Lemiere, J. Lepoivre, F. van de Vyver, A. van der Linden, and F. Alderweireldt*

Antwerp (Belgium)

**MAT 12: Investigation of the Diffusion Process in Crosslinked Polystyrenes by  $^1\text{H}$  and  $^{19}\text{F}$  NMR Microscopy.**

*M. Ilg, B. Pfeleiderer\**, *K. Albert, W. Rapp, and E. Bayer*  
Tübingen (Germany) / \*Charlestown, Massachusetts (USA)

**MAT 13: NMR Imaging of Elastomers: Stress Distribution, Thermal, and Mechanical Aging.**

*P. Blümler, and B. Blümich*  
Mainz (Germany)

**MAT 14: Shear Thinning in High Polymer Solution Using Dynamic NMR Microscopy.**

*Y. Xia, and P.T. Callaghan*  
Palmerston North (New Zealand)

**MAT 15: Fluid Displacement in Porous Media Using NMR Microscopy.**

*G.J. Nesbitt, T.W. Fens\**, *J.S. van den Brink, and N. Roberts\**  
Amsterdam (Netherlands) / \*Liverpool (United Kingdom)

**MAT 16: SEEING-NMR Applied to Conductors and Superconductors.**

*U. Skibbe, and G. Neue*  
Dortmund (Germany)

**MAT 17: NMR Microimaging of some Polymeric Materials with Medical and Dental Applications.**

*S.N. Scrimgeour, C.H. Lloyd, G. Hunter, J.A. Chudek, and R.L. Mackay*  
Dundee, Scotland (United Kingdom)

**MAT 18: Kinetics of Water Phase Transition and Freezing-Thawing Phenomena Validated in a Porous Medium by NMR Microscopy.**

*S. Crestana, A. Posadas, \*D.R. Nielsen, R. Kauten\**, and *J. Brown#*  
São Carlos-São Paulo (Brazil) / \*Davis, California (USA) / #Columbia, Missouri (USA)

**MAT 19: Implementation of Online Parameter Selective MR-Image Analysis for Materials Research.**

*R. Brill, J. Stahl, M. Staemmler, and W. Kuhn*  
St. Ingbert (Germany)

**MAT 20: Spatially and Time Resolved Observation of the Water Uptake in Polyamid**

*M. Staemmler, and W. Kuhn*  
St. Ingbert (Germany)

**Diffusion**

**DIF 6: Effects of Bounded Diffusion on MR Microscopy.**

*W.B. Hyslop, and P.C. Lauterbur*  
Urbana-Champaign, Illinois (USA)

**DIF 7: The Effect of "Absorbing" Walls on NMR Diffusion Measurements.**

*A. Snaar, and H. van As*  
Wageningen (Netherlands)

**DIF 8: One Dimensional Q-Space Imaging of Transversal Dispersive Flow.**

*W. Palstra, and H. van As*  
Wageningen (Netherlands)

**DIF 10: 'One-shot' NMR Velocity Microscopy, Imaging of Motion Using a Single Phase-Encoding Step.**

*Y. Xia, and P.T. Callaghan*  
Palmerston North (New Zealand)

**DIF 11: Rotational Shearing of a Polymer Solution.**

*C.J. Rofe, Y. Xia, and P.T. Callaghan*  
Palmerston North (New Zealand)

**DIF 12: Imaging Plant Vascular Flow in vivo at a Velocity Resolution of  $6 \mu\text{m s}^{-1}$ .**

*Y. Xia, K.R. Jeffrey\*, W. Köckenberger#, and P.T. Callaghan*  
Palmerston North (New Zealand) / \*Guelph, Ontario (Canada) / #Bayreuth (Germany)

**DIF 13: Q-Space Imaging of Homogenous, Porous Structures.**

*A. Coy, P.T. Callaghan, D. MacGowan\*, K.J. Packer\*, and F.O. Zelaya\**  
Palmerston North (New Zealand) / \*Sunbury-on-Thames, Middlesex (United Kingdom)

**DIF 14: Velocity-Selective Pulse Sequences.***J.M. Pope, and S. Yao*

Kensington, New South Wales (Australia)

**Biomedicine****BIO 10: Parameter Selective NMR Microscopy - A New Tool in Atherosclerosis Research -***W. Kuhn, and M. Soma\**

St. Ingbert (Germany) / \*Milano (Italy)

**BIO 11: Atherosclerotic Lesions: ex vivo Characterization by 3D NMR Microscopy and Quantitative 3D-Data Processing.***G. Rohr, M. Heine, D. Gross\*, V. Lehmann\*, W. Ruhm\*, and U. Wark\**

Heidelberg / Mannheim (Germany) / \*Rheinstetten (Germany)

**BIO 12: Three-Dimensional Visualization in NMR-Microscopy Applied to an Anatomical Setting.***A. Kriete, and K.-P. Valerius*

Gießen (Germany)

**BIO 13: Characterization of Human Skin Tumors in-vitro by High Resolution Proton NMR Microimaging at 9.4 Tesla.***S. Aygen, S. el Gammal\*, T. Bauermann, R. Hartwig\*, and P. Altmeyer\**

Witten (Germany) / \*Bochum (Germany)

**BIO 14: NMR Microscopy of Lepidoptera pupae.***J.A.T. Woodford, S.C. Gordon, B.A. Goodman, J.A. Chudek\*, and S.N. Scrimgeour\**

Invergowrie, Dundee (United Kingdom) / \*Dundee (United Kingdom)

**BIO 15: Some Applications of NMR Microscopy on Insects.***D. Fresneau, P. Gonord, and S. Kan*

Paris (France)

**BIO 16: 3D NMR Microscopy: Imaging and 3D Image Presentation of Insects.***D. Gross, V. Lehmann, W. Ruhm, U. Wark, and G. Rohr\**

Rheinstetten (Germany) / \*Heidelberg / Mannheim (Germany)

**BIO 17: A Comparison of 3D NMR Microscopy and Subsequent Optical Microscopy of Thin Sections of Fixed Human Brain Tissue.**

*X. Zhou, C.S. Potter, and P.C. Lauterbur*  
Urbana, Illinois (USA)

**BIO 19: The Aging of the Human Lens as Studied by NMR Microscopic Imaging.**

*W. Kuhn, and A. Daxer\**  
St. Ingbert (Germany) / \*Innsbruck (Austria)

**BIO 20: NMR Microimaging at 7.0 T of the entire Spinal Cord of Chronic Recurrent Experimental Allergic Encephalomyelitis (EAE) Rats.**

*D. Lanens, #D. Groß, M. Spanoghe, A. van der Linden, \*E.J. 's-Gravenmade, \*M. Brekelmans, \*P.O. Gerrits, \*G. Holstege, F. van de Vyver, and R. Dommissie*  
Antwerp (Belgium) / \*Groningen (Netherlands) / #Rheinstetten (Germany)

**BIO 21: Test of the Membrane Permeability of Paramagnetic Metal Complexes of Derivatives of 3-Acetyltetramic Acid by NMR Microscopy.**

*C. Mügge, S. Päuser, A. Zschunke*  
Berlin (Germany)

**Plants & Agriculture**

**PLA 5: Real-Time Imaging of Acute Cadmium Toxicity in Cherrystone Clams (*Mercenaria mercenaria*) by NMR.**

*P.C. Wang, and L.-S. Kan\**  
Washington, DC (USA) / \*Baltimore, Maryland (USA)

**PLA 6: Three Dimensional NMR Microscopy of Corn Kernels Using Fast Interleaved Projection Reconstruction.**

*R. Ruan, X. Zhou, J.B. Litchfield, and P.C. Lauterbur*  
Urbana-Champaign, Illinois (USA)

**PLA 7: In vivo Magnetic Resonance Microscopy for Non-destructively Investigating Plants, Fruits, Vegetables, and Small Animals.**

*S. Crestana, R. Kauten\*, and D.R. Nielsen\**  
São Carlos, São Paulo (Brazil) / \*Davis, California (USA)

**PLA 8: Structural Studies of the Stems of Flax (*Linum usitatissimum*) by NMR Microscopy and Conventional Histological Techniques.**

*G.J. McDougall, B.A. Goodman, J.A. Chudek\*,  
S.N. Scrimgeour\**

Invergowrie, Dundee (United Kingdom) / Dundee (United Kingdom)

**PLA 9:  $^{17}\text{O}$  /  $^1\text{H}$  MR Microscopy Studies of Plant Anatomy and Physiology.**

*G.D. Mateescu*

Cleveland, Ohio (USA)

## *Designing and Building Screened Gradient Coils*

P J Back, A Coy, R Dykstra and P T Callaghan

Department of Physics and Biophysics, Massey University  
Palmerston North, New Zealand

### **Abstract**

The theory of gradient coil screening is well described in the literature although the numerical methods used in calculating actual wire paths are not so apparent. We describe here some techniques which we have used in designing NMR Microscopy gradient coils for superconducting magnets. We have designed coils using both standard primary geometry as well as target field methods. Final field profiles both inside and outside the gradient coils are calculated numerically via the Biot-Savart law. By this means the chosen coil winding design can be checked for the quality of internal gradient uniformity and external field screening.

The Massey University software generates wire path files which can be transferred directly to a specially developed milling machine controller. The mill controller uses stepping motors with both azimuthal and longitudinal drive to move the coil-former mandrill. Thus the wire paths are cut automatically.

## *Transverse Quadrupolar Coil Field Profiles*

C J Rofe and P T Callaghan

Department of Physics and Biophysics, Massey University  
Palmerston North, New Zealand

### **Abstract**

With the desire for higher resolution NMR images, larger gradient fields across the sample are required. Especially high gradients are obtainable using quadrupolar coils wound on a cylindrical surface. In the superconducting magnet geometry a transverse cylindrical current surface can incorporate two quadrupolar coils,  $G_x$  and  $G_z$ . The transverse orientation associated with the use of quadrupolar gradient coils in superconducting magnets raises some interesting questions regarding screening. Use of a coaxial active screen enables cancellation at all points outside the screen radius but not along the cylindrical axis. Consequently stray field will reach the wall of the magnet bore.

The solution to the axial screening problem remains unsolved, and leads us to examine the size of the field as a function of distance along the coil axis. Numerical solutions using Biot-Savart calculation are graphically displayed and we address the question as to whether axial screening is necessary.

## An Actively-Shielded Micro-Imaging Probe for High-Field Narrow-Bore Magnets

N. Schuff, I-J. Feng and X. Ni  
Varian Associates, Palo Alto CA 94304, U.S.A

### Purpose

For sensitivity reasons it is desirable to perform microimaging experiments at the highest magnetic field strength available today on commercial superconducting magnets providing 11.7T and 14.1T. While a 14.1T magnet version is only available with a bore size of 51mm, in general this bore diameter might be economically more justifiable for experiments on small objects than using magnets with larger bore sizes.

Our goal was to design and to build an actively-shielded gradient coil set for 51mm bore magnets which provides enough room to fit in NMR high resolution probes. Active shielding of the gradient coils was essential to obtain static conditions as soon as  $1 \times 10^{-4}$ s after a gradient pulse was switched and to minimize stress to the high-field superconducting magnets.

### Design of gradient coils

The gradient coils are mounted on a Varian high-resolution RF probe assembly within the RF shield in a 51mm narrow-bore magnet. The coil clearance inner diameter is 20mm with a ratio for the radius of the primary and shielding coils of 1: 1.25. The wire patterns were found from the calculation of the current distribution in continuous conductive media by solving Laplace equation and then approximated by discrete wires. We obtained a magnitude of the gradient field of 3G/cm/A for the z-gradient coil and 2G/cm/A for the transverse coils. Deviations from linearity were calculated to be below 1% over +/- 4mm along the transverse and +/- 5mm along the longitudinal directions. The residual field outside of the gradient coils at the position of the RF faraday shield of the probe is less than 2% of the unshielded value.

### Design of the RF coil

While active shielding eliminates eddy currents induced external to the shielding coil, they still may be induced in conducting structures internal to the shielding coil such as the RF coil. By slotting the RF coil to prevent eddy currents from forming closed loops this effect can be minimized.  $B_1$  - field homogeneity mapping showed that a one-sided slot on the conducting strip of the one-turn saddle coil does not degrade the  $B_1$  homogeneity nor does it cause a balancing problem which is usually common in the case of symmetrical slots.

### Experimental

Experiments to test the shielding effect were performed on a 51mm bore magnet manufactured by Oxford Instruments and assembled with a Varian Unity spectrometer console. The gradient settling time was monitored by measuring the phase evolution of the NMR signal from a spherical microsample filled with water. We found that active shielding reduced the eddy current amplitude to less than 0.3% of the unshielded value  $1 \times 10^{-4}$ s after a gradient pulse was applied. Results from high-resolution microimaging experiments on biological samples will be shown.

## Surface Gradient Coil for MRI and MRS of Small, Moving Objects.

A. Jasinski\*, P. Kozlowski\* , J. K. Saunders and A. Urbanski\*

National Research Council, Ottawa, Canada.

### Introduction.

Imaging and spatially resolved spectroscopy of moving objects is interesting challenge for MR scientists. Problem is, how to avoid motion artefacts in cross-sectional images or spectra. There are many methods of imaging of moving objects and/or removing influence of movement. One of them is to mount coil onto the surface of objects we are looking to. We describe a surface gradient coil, which can be fixed on moving object together with rf coil. This indeed new method was applied to get spectra from the beating heart wall.

### Methods.

One needs gradient coil for localized spectroscopy. It should:

- generate gradient, which:
  - linear over area of interest,
  - is insensitive to changes of coil orientation,
  - have the zero of the field at certain point.
- have no mechanical torque due to interaction with magnetic field  $B_0$ .
- be light, to avoid object and its movement distortions.

The hexagonal surface gradient coil consists of two layers of current paths. Each layer consists of two opposing pairs of half hexagons with current flowing in opposite direction. Currents in both layers are opposite, either. A computer code was written to optimize the dimensions and vary the shape of current paths.

The surface gradient coil was made of copper enamel wire glued with cyanoacrylic glue to a plastic former. A surface rf coil of 23 mm in diameter doubly tuned for  $^1\text{H}$  and  $^{31}\text{P}$  was incorporated into the former giving a small integrated surface probe.

1D CSI spectra were obtained by implanting the surface probe on a dog heart wall in an open chest preparation.

### Results.

The gradient coil with 50 mm longest dimension gave the best compromise between the homogeneous gradient volume and coil size. It yields a linear gradient (<15%) over distance of 10 mm, which corresponds to the rf surface coil volume of sensitivity, with 2 mT/m/A efficiency. Good correlation between calculated and measured gradient strength and distribution were achieved. Zero of the field given by gradient coil is being outside of area of interest, however, this can be corrected by a first order phase correction in the time domain.

$^{31}\text{P}$  spectra were obtained within 20, 10 and even 5 minutes with good S/N ratio. Layer thickness was about 1 mm. One can easily distinguish differences among spectra taken from different depths of heart wall. Number of obtained  $^{31}\text{P}$  spectra shows, this method is promising tool for removing undesired influence of movements.

---

\* on leave from Institute of Nuclear Physics, Cracow, Poland.

**HIGH RESOLUTION MRI USING A  
THREE CHANNEL SURFACE GRADIENT COIL SYSTEM**

J.Link, K.Lüscher, P.Brunner  
Spectrospin AG, Medical Instruments, Fällanden CH

Medical MR imaging currently shows great interest in high resolution anatomical imaging (joints, skin...), and in real-time imaging applications. Both fields are not accessible to standard scanners due to the strong requirements for the gradient system: High resolution imaging demands extremely high currents on whole body gradient systems; fast imaging requires very high voltages and low inductivity gradients. In both cases induced eddy currents strongly deteriorate the expected results.

To circumvent these problems, the surface coil concept was generalized to include a local gradient system. This approach allows very strong gradients at very fast switching times and minimized eddy current induction. On the other hand, due to the reduced symmetry, characteristic geometry distortions are introduced. We present our results on design, optimisation, and specification of such a planar integrated system, as well as several applications.

**Design:**

Modification of the geometry introduced by Yi and Cho (SMRM 1989, Book of Abstracts, 201).

Multiturn distributed current paths, numerically optimized.

**Specifications:**

FOV max. 5cm in all dimensions.

Gradient strength 70kHz/cm at 60A.

Preemphasis identical zero in all channels.

**Applications (on Biospec 47/30 and Tomikon S200):**

Multislice applications on capillary phantoms to evaluate geometry distortions.

Standard imaging on human hand joints.

Snapshot imaging movie of the moving finger.

Imaging of skin structure : animals/humans.

## Sensitivity And Resolution of NMR Microscopy Using Surface Coils

Xiaohong Zhou and Paul C. Lauterbur

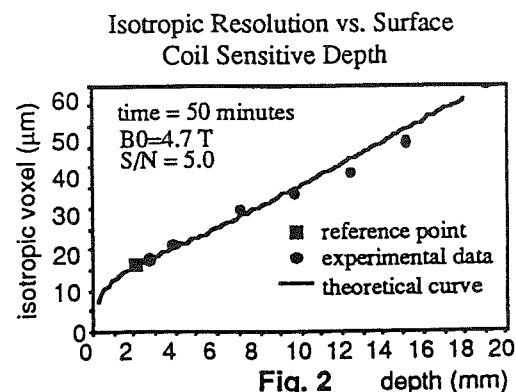
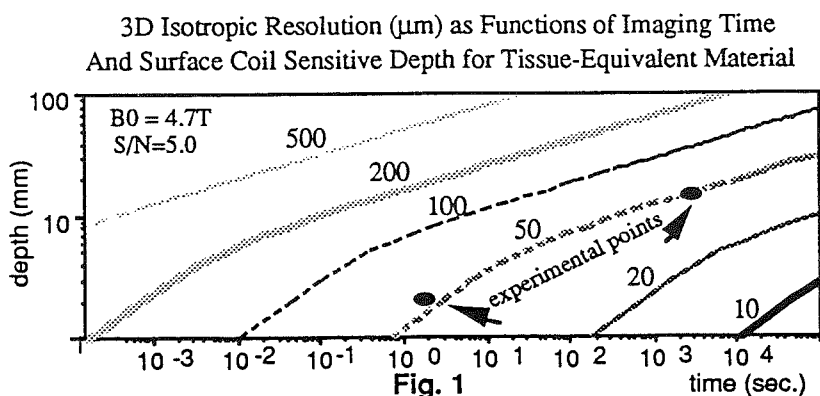
Biomedical Magnetic Resonance Laboratory, University of Illinois at Urbana-Champaign  
1307 West Park Street, Urbana, Illinois 61801, USA

Surface coils are useful in magnetic resonance imaging because they can improve signal-to-noise ratios by increasing the filling factor and decreasing the loading and noise caused by conducting samples. They also permit increased resolution by limiting the field of view spanned by a given number of voxels. In NMR microscopy, small surface coils will be relatively unaffected by sample conductivity, but larger ones will behave much like standard imaging coils. We have calculated theoretically the performance of surface coils over a range of sizes spanning this transition region, and have compared the predictions with the measured performance of a set of seven coils with diameters ranging from 6 to 43 mm.

The seven coils with diameters of 6, 7.5, 11, 20, 27.5, 35, and 43 mm, were constructed from copper wire and the coil inductances were measured at 200 MHz.  $Q$  values for these coils were obtained using a sweep generator under three different conditions, unloaded, loaded with human fingers, and loaded with a saline solution. Based on these measurements, the coil loss resistance and the sample loss resistance were calculated. According to the principle of reciprocity, the coil sensitivity at a point in a sample can be evaluated by calculating the  $B_1$  field generated by the coil at that point. In our study, the  $B_1$  field strengths were calculated for measurements of the  $90^\circ$  pulse width for a tiny sample ( $\sim 800 \mu\text{m}$ ) located at a distance of  $0.707r$  from the surface coil plane (For a given depth, the S/N is maximal for an unloaded surface coil with a radius 1.4 times that depth). A signal-to-noise ratio factor defined as

$\frac{B_1}{\sqrt{R_{coil} + R_{sample}}}$  was calculated for each coil with different loading conditions. We then used the 6 mm surface coil as a reference coil to determine the coefficient which relates S/N to isotropic resolution achieved at a given imaging time. This coefficient was used to predict the performance of larger surface coils under the same loading condition. Several proton imaging experiments were performed on phantoms using a 3D projection reconstruction method to verify these predictions (1). The signal-to-noise ratio factors were also calculated theoretically for the coils, based on the scaling laws and taking into account sample conductivity and skin depth of the coils.

The results, which relate isotropic voxel size to distance from the surface coil and to imaging time at S/N of 5.0, are summarized in Fig. 1. The relationship between depth and voxel size obtained both theoretically and experimentally is shown in Fig. 2. In both of these figures, good agreement between experiment and theory is demonstrated. These results suggest that 3D isotropic resolution of the order of  $(50 \mu\text{m})^3$  can be achieved with surface coils at depths of the order of a centimeter in a reasonable amount of data acquisition time.



Acknowledgements: This work was supported by the Servants United Foundation and grants from NIH (PHS1P41RR5964-01) and NSF (BNS88-09490). The National Center for Supercomputing Applications is gratefully acknowledged for providing computing facilities.

Reference: (1) X. Zhou and P.C. Lauterbur, "Abstracts of the 10th SMRM", San Francisco, 1991 (in press).

## Diffusion Limited Resolution for Different Pulse Sequences in NMR Microscopy

Xiaohong Zhou and Paul C. Lauterbur

Biomedical Magnetic Resonance Laboratory, University of Illinois at Urbana-Champaign  
1307 West Park Street, Urbana, Illinois 61801, USA

Many NMR microscopists realize that diffusion limited spatial resolution is pulse sequence dependent (1-3). However, few quantitative discussions of this phenomenon have been published, although it must be understood in order to design optimal pulse sequences for NMR microscopy, especially as the spatial resolution approaches the diffusion limit. In this study, we compare diffusion resolution limits as well as signal attenuation effects for three commonly used pulse sequences, projection reconstruction using FIDs, projection reconstruction using spin echoes, and Fourier imaging using the spin-warp sequence. Only unbounded diffusion is discussed here; new phenomena appear in the presence of barriers (4, 5).

Unbounded diffusion has three major effects in NMR microscopy, signal loss, line broadening, and phase misregistration, all of which can be attributed to the loss of phase coherence in the transverse magnetization. In the presence of a linear magnetic field gradient, a generalized expression for the diffusion related phase is given as (2),

$$\phi_d = -\gamma^2 D \int_0^t \left[ \int_{t'}^t G(\tau'') d\tau'' \right]^2 dt' \quad [1]$$

This expression can be applied to both FID and echo signals, depending on the time variables in the integral limits. Assuming the distribution of the phase is Gaussian, it can be shown that the root-mean-square phase is  $\sigma = 2|\phi_d|$ . Using this relationship, the signal attenuation factor,  $1 - \exp(-\sigma^2/2)$ , can be calculated for different pulse sequences and Fourier transformed to obtain the line broadening in the frequency domain. It should be noted that this resolution limit is applicable only to frequency encoding directions. In phase-encoding directions, phase misregistration, instead of line broadening, is introduced by diffusion and the amount of phase shift can be directly obtained from Eq. [1].

We have evaluated the signal attenuation factors and the resolution limits for several pulse sequences based on a set of parameters used in our experimental studies on NMR microscopy (e.g.,  $G \approx 10$  Gauss/cm,  $TE_{\text{proj. recon.}} = 4$  ms, etc.) (6). The results, summarized in the following table, indicate that the diffusion resolution limit in the projection reconstruction pulse sequences is always isotropic and that the single FID acquisition gives both higher resolution and smaller signal attenuation. For Fourier imaging, the diffusion limited resolution is anisotropic, with the phase-encoding direction giving a higher resolution. On the average, projection reconstruction pulse sequences have a higher resolution and smaller signal attenuation as compared to the Fourier imaging pulse sequences under normal experimental conditions.

Method	Resolution	Attenuation Factor
Proj. Recon. -- FID:	5.20 $\mu\text{m}$	0.00
Proj. Recon. -- Spin Echo:	6.15 $\mu\text{m}$	0.01
Fourier Imag. -- Read-Out:	8.08 $\mu\text{m}$	0.07
Fourier Imag. -- Phase-Encoding:	3.16 $\mu\text{m}$	

- (1) P.T. Callaghan and C.D. Eccles, *J. Magn. Reson.*, **78**, 1 (1988).
- (2) C.B. Ahn and Z.H. Cho, *Med. Phys.*, **15**, 22 (1989).
- (3) E.W. McFarland and A. Mortara, *Proc. of the 32nd ENC*, p.55, St. Louis, Mo. (1991).
- (4) W.B. Hyslop and P.C. Lauterbur, "Abstracts of the 9th SMRM", pp. 393 (1990), and *J. Magn. Reson.*, (in press).
- (5) B.P. Hills, K.M. Wright, and P.S. Belton, *Magn. Reson. Imaging* **8**, 755, (1990).
- (6) X. Zhou, C.S. Potter, P.C. Lauterbur, and B. Voth, "Abstracts of the 8th SMRM", pp. 286, Amsterdam, 1989.

Acknowledgements: This work was partially supported by Servants United Foundation, an NIH grant (PHS1P41RR5964-01) and an NSF grant (BNS88-09490).

# *Probing below 1000 Å with PGSE-MASSEY*

A Coy and P T Callaghan

Department of Physics and Biophysics, Massey University  
Palmerston North, New Zealand

## Abstract

The pulsed gradient spin-echo (PGSE) NMR experiment has traditionally been limited by the ability to match the areas of the two gradient pulses. Any pulse mismatch will leave a phase twist along the sample causing additional attenuation to the NMR signal and leading to 'enhanced diffusion' in the normal experiment. Presented here is an experimental test of a pulse sequence to overcome this problem, along with any net phase shifts due to sample movement.

The MASSEY sequence<sup>(1)</sup> involves acquiring the spin echo in the presence of a standard imaging read gradient. This gradient has the effect of imaging out the phase twist left by any pulse mismatch which can then be removed by co-adding the squared modulus of the spectra of successive accumulations.

The implementation of this sequence involves the application of two gradients of different size to one coil, and computer analysis of each individual spin echo acquisition. Although the sequence suffers from weaker signal to noise ratios, on most samples of interest this is not too much of a problem. We have investigated the diffusion of polymers in the melt and in semi-dilute solution where the mean-squared distance diffused is below 1000 Å over the time scale of our experiment ( $D_s < 10^{-14} \text{ m}^2 \text{ s}^{-1}$ ). Using this technique the use of gradients sufficiently large to probe down to 100 Å was made possible ( $D$  of order  $10^{-16} \text{ m}^2 \text{ s}^{-1}$ ).

1. P T Callaghan, *J. Magn. Reson.* **88**, 493-500 (1990).

## Fast 3D Projection Reconstruction

M. Staemmler, R. Brill, W. Kuhn

Fraunhofer Institute for Nondestructive Testing, D 6670 St. Ingbert, Germany

### Introduction

Currently the application of 3D backprojection is limited to small image matrices due to long reconstruction times. Several approaches have taken place to shorten reconstruction time by dedicated expensive hardware. In this poster three steps for changing the reconstruction algorithm are shown, which allow sufficiently fast reconstruction using programming language C.

### Methods

Usually  $n_\vartheta \cdot n_\phi$  projections are taken in the spherical coordinate system ( $r, \phi, \vartheta$ ). Marr et al. report on two approaches for 3D-backprojection [1]. The true 3D approach needs  $n_\vartheta \cdot n_\phi$  loops for the reconstruction of the 3D volume, whereas the cascaded approach 2D-2DBP of two subsequent backprojections over  $n_\vartheta + n_\phi$  projections needs  $n_\vartheta + n_\phi$  loops for the volume, thus reducing the order of the computing effort by one. Both approaches employ filtered or convoluted backprojection.

Since filtering needs one order less computing effort compared to convolution, only filtered backprojection leads to acceptable reconstruction times. The step of linear interpolation suffers from multiplications, even if a fractional notation is used. Thus, we combined the fractional notation with a two-staged table oriented approach, which is free from multiplications. Furthermore, the inner loop was speed up using some parallelism. The effect of this discrete approach on the achievable resolution is discussed in the results. For accessing the run-time requirements of the final algorithm different implementations were done: (i) high-level implementation ('C' on a SUN 4/260), (ii) a company specific microcode programmable pipeline processor and (iii) a high-level programmable parallel processor architecture (transputer T800, 16 nodes).

### Results

Table 1 shows computing time requirements for the different implementations.

	linear interpolation			
	with multiplication		using tables	
	true 3DBP	cascaded 2D-2DBP	true 3DBP	cascaded 2D-2DBP
high-level SUN 4/260	317,0	12,5	-, -*	7,4
pipeline processor	40,1	1,5	-, **	-, **
high-level parallel	63,1	2,3	-, -*	1,3

Tab.1: Reconstruction times in hours for a  $256^3$  object using  $n_\vartheta = n_\phi = 128$  projections (\* not evaluated, \*\*not applicable due to limited memory).

The performance of the discrete linear interpolation using tables was verified with simulated projection data. The quantification of reconstruction quality with modulation transfer functions proved that the fast interpolation is as good as the slow version. The different implementations were verified and compared by distance measurements.

### Conclusion

The new fast approach for 3D backprojection reconstruction allows its application in NMR microscopy. The cascaded algorithm is the basis for on-line reconstruction during image acquisition. Furthermore, the high-level language implementation on commercial systems needs no special processors.

### References

- 1 Marr, .R.B., Chen, C., Lauterbur, P.C., in Mathematical Aspects of Computed Tomography vol. 8, G.T.Herman and F.Natterer, Eds., New York, Springer Verlag, 1981, pp.225-240

## Canceling Quadrature Artifacts using Hermitian Symmetry of the Spin Echo

Franciszek Hennel

Institute of Physics, Jagiellonian University, 30-059 Krakow, Poland

In MNR experiments with realspectra, like imaging, where the spectrum corresponds a real function of spin density, the complex envelope of the spin echo has *Hermitian symmetry*:

$$S(t) = S^*(-t) \quad [1]$$

where  $t = 0$  is the middle of the echo. Thus, on a symmetrically sampled signal, the following operation can be done:

$$S_1(t) = S(t) + S^*(-t) \quad [2]$$

which does not affect the true signal and cancels some of the spurious contributions. **Figure 1** shows real and imaginary part of a spin echo before and after the operation.

The operation of "*Hermitian filtering*", Eq.[2], provides a simple way of correcting imperfections of a quadrature detector. If the phase of the reference is shifted by  $\alpha$  and the channels are not orthogonal ( $\varphi$  is the deviation from 90deg), we obtain the effective signal:

$$\begin{aligned} \text{Re} [S^{eff}(t)] &= \text{Re}[S(t)] \cos(\alpha) - \text{Im}[S(t)] \sin(\alpha) \\ \text{Im} [S^{eff}(t)] &= \text{Im}[S(t)] \cos(\alpha+\varphi) + \text{Re}[S(t)] \sin(\alpha+\varphi), \end{aligned} \quad [3]$$

the Fourier transform of which is dephased and contains symmetrical ghosts. Applying Hermitian filter to  $S^{eff}$  gives, to first order in  $\alpha$  and  $\varphi$ , the original function  $S(t)$ . **Figure 2** shows a 1D NMR image (projection) of a water filled cylinder. The ghost (on the left side of  $\omega$  axis), caused by  $\varphi$ -deviation, disappears after the Hermitian filtering.

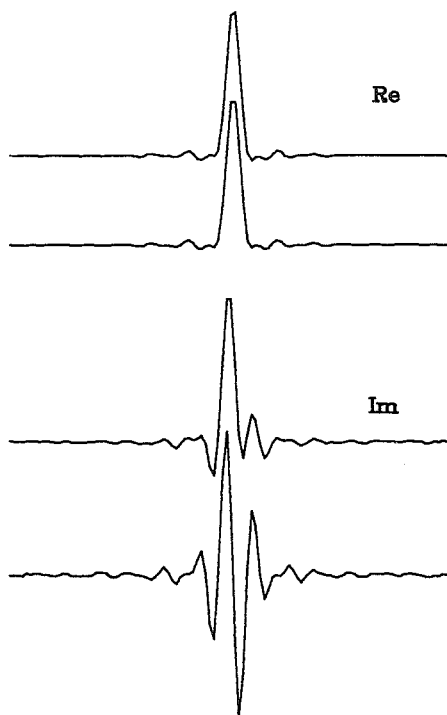


*Fig.1*

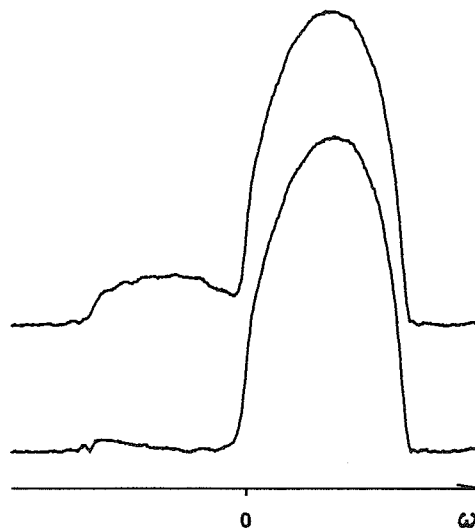


*Fig.2*

## SPECTROSCOPIC IMAGING WITH STOCHASTIC EXCITATION

J. Jansen,<sup>a</sup> P. Konstanczak,<sup>b</sup> B. Blümich<sup>a</sup><sup>a</sup> Max-Planck-Institut für Polymerforschung, Postfach 3148, D-6500 Mainz,<sup>b</sup> Iwan-N.-Stranski-Institut, Straße des 17. Juni 112, D-1000 Berlin 12.

Noise as well as pulse excitation are associated with the multiplex advantage. However, the input power is lower for noise excitation by a factor of  $T_1/t_p$ , where  $T_1$  is the spin-lattice relaxation time and  $t_p$  is the duration of a  $90^\circ$  pulse. Noise excitation is considered for medical high field imaging of large volumes, because the maximum excitation power which may be applied to humans is limited by law.

Imaging with noise excitation has been proposed several years ago.<sup>1</sup> The theory has recently been extended to incorporate spectroscopic resolution,<sup>2</sup> and first experiments were performed on a phantom of water and oil.<sup>2,3</sup> When considering the nonlinear sample response, even 2D spectroscopic resolution can be achieved.<sup>4</sup> To explore the experimental conditions for stochastic imaging with 2D spectroscopic resolution, a Bruker Biospec imaging spectrometer was modified for stochastic 4-phase<sup>5</sup> excitation, and imaging experiments with 1D spectral resolution were carried out on phantoms using the back-projection technique.<sup>6</sup> The features of the method and experimental results are summarized. It is anticipated, that the technique will be of use not only for medical applications, but also for investigations of large heterogeneous objects in materials science.

## References:

- 1) B. Blümich, *J. Magn. Reson.* **60** (1984) 37.
- 2) M. S. Roos, S. T. S. Wong, *J. Magn. Reson.* **87** (1990) 554.
- 3) M. S. Roos, S. T. S. Wong, B. deB. Frederick, *Proc. SMRM New York*, p. 135 (1990).
- 4) B. Blümich, *J. Magn. Reson.* **90** (1990) 535.
- 5) S. T. S. Wong, M. S. Roos, R. D. Newmark, T. F. Budinger, *J. Magn. Reson.* **87** (1990) 242 and 265.
- 6) D. G. Cory, J. B. Miller, A. N. Garroway, W. S. Veeman, *J. Magn. Reson.* **85** (1989) 219.

# MAS NMR IMAGING

G. Schauß, M. Hehn, H. Raich, B. Blümich, H. W. Spiess

Max-Planck-Institut für Polymerforschung, Postfach 3148, D-6500 Mainz

The highest resolution in solid state NMR imaging is obtained with magic angle spinning (MAS).<sup>1</sup> Here the magnetic field gradients required for space encoding are applied in a coordinate frame, where the z-axis is along the spinner axis and the xy-plane is perpendicular to it. In this frame the effective x and y gradients must rotate at the spinner frequency, so that the gradients appear static in the rotating sample.

This simple approach encounters severe difficulties in practice, since a current applied to the z gradient coils invokes a z gradient as well as x and y gradients. This complication is inherently related to the fact, that applying the gradients in the sample frame requires rotation of a tensor and not a vector of gradient components. As a consequence of neglecting this relation, 3D spatial resolution and slice selection could not be achieved in the past. However, high spatial resolution was achieved by imaging thin slices of material.<sup>2</sup>

We have built a probe and accessories for MAS imaging, which permit simultaneous application of currents to x, y and z gradient coils. In this way disturbing gradient terms can be cancelled and clean x, y and z gradients can be achieved over the rotating sample. This is demonstrated by slice selection on a phantom. The physics of MAS imaging is described,<sup>3</sup> and the construction principle of the probe is given.<sup>4</sup>

## References:

- 1) W. S. Veeman, D. G. Cory, *Adv. Magn. Reson.* **13** (1989) 43.
- 2) D. G. Cory, J. C. de Boer, W. S. Veeman, *Macromolecules* **22** (1989) 1618.
- 3) G. Schauß, B. Blümich, H. W. Spiess, to be published.
- 4) G. Schauß, M. Hehn, H. Raich, B. Blümich, H. W. Spiess, to be published.

## MICRO-IMAGING MEASUREMENTS OF $T_1$ RELAXATION

S. J. Doran, T. A. Carpenter and L. D. Hall

Herchel Smith Laboratory for Medicinal Chemistry, University of  
Cambridge School of Clinical Medicine, Robinson Way,  
Cambridge. CB2 2PZ UK

Measurements of NMR relaxation parameters have long been used, to provide information about a variety of physical, chemical and biological systems. Since most real systems consist of a number of different physical and chemical environments for the NMR-active nucleus, a method is needed of distinguishing the different relaxation times which result. This need is as important in NMR Microscopy as in more conventional spectroscopic and imaging studies.

Previous work has tended to concentrate on "whole-sample" measurements, in which a single relaxation curve is plotted for the entire sample volume. By fitting the curve to a variety of models, one hopes to recover a "spectrum" of relaxation times. However, this approach does not always recover successfully all the  $T_1$  components which are present. More seriously, the solutions are not unique — a number of different sets  $\{ (M_{0i}, T_{1i}) \}$  can often give equally good fits to the observed data. The reason for this failure is not due to inadequate experiment or poor data analysis but rather a mathematical property (non-orthogonality) of the exponential decay function itself.

We study the potential of a different approach : spatially-localized  $T_1$  measurements. With a micro-imaging spectrometer, it is possible to obtain an inversion- or saturation-recovery curve for each individual pixel of an image at very high resolution. Suitable software can produce "pure"- $T_1$  images, which are an accurate representation of the relaxation at the level of the individual pixel. We believe that this technique makes it possible to acquire information, which is unobtainable by conventional NMR microscopy or relaxometric measurement procedures.

## Methodology for High-Field NMR Microscopy of Tumor-Bearing Mice

Klaus-Peter Fichtner & William E. Hull  
Central Spectroscopy Dept., German Cancer Research Center,  
Neuenheimer Feld 280, W-6900 Heidelberg, FRG

High-field NMR microscopy of small irregular objects requires that special care be taken in dealing with the problems of eddy currents, local object-induced inhomogeneities in the RF and magnetic fields, and chemical shift effects, all of which can have a severe influence on image quality. For our studies of human tumors implanted in the hind legs of nude mice, we have developed methodologies for dealing with these effects. A variety of imaging sequences have been tested and a number of convenient setup routines have been developed for our system (Bruker AM-300 super-wide-bore with 15 cm vertical magnet and Bruker wide-bore microscopy probehead with max. 25 mm diam. resonator and *unshielded* gradient coil insert).

Eddy current effects are minimized by using a 9 cm glass-epoxy shim system and by *removing* the sample spinner turbine and upper bore tube (made of aluminum). Without gradient pre-emphasis this results in eddy currents that decay completely in ca. 30 ms. To simplify the adjustment of pre-emphasis, we have developed a setup program which generates 7 sequential FIDs in a single display. The recovery time following the test gradient is increased for each successive FID; pairs of FIDs are assigned to each of the three pre-emphasis time constant/amplitude functions and the final FID serves as a reference to check the shim settings. The continuous display of all FIDs makes interactive adjustment of all pre-emphasis settings relatively easy. Complete recovery of the field homogeneity within 0.2 - 0.3 ms can be routinely obtained for gradients as large as 30 G/cm. The short switching times achieved facilitate gradient-echo imaging with very short  $t_e$  values.

The tumors we are studying have an irregular shape and a high surface/volume ratio with large susceptibility effects distorting the  $B_0$  field. Although the tumor is roughly centered in the resonator, a major portion of the NMR signal obtained with a hard pulse comes from the mouse's body, i.e. conventional shimming using the bulk signal will often give poor results. This problem can be solved by using a volume-selective shim procedure based on a slice-selective spin-echo sequence to generate an FID only from the desired ROI, e.g. the region to be examined by a multi-slice procedure. The result is a dramatic improvement in lineshape and the assurance that  $B_0$  and chemical shift frequencies are constant for each slice to be imaged. The quality of  $B_0$  over the ROI can be readily visualized using the SENEX technique [1] and is particularly important for chemical-shift-selective techniques and any gradient-echo applications. At 7 T the chemical shift of subcutaneous fat represents several pixels; we use a fat-selective presaturation pulse as preparation period to allow efficient multi-slice water imaging. The slice-selective shim procedure is also convenient for localized spectroscopy and can be further refined by the application of OSIRIS-type noise pulses [2].

Efficient and accurate measurement of  $T_1$  is important for tissue characterization. We have found that a progressive-saturation (variable  $T_1$ ) spin-echo technique with *hard* 90° excitation gives excellent image quality and precise localized  $T_1$  values equivalent to those obtained with the time-consuming inversion-recovery method. The possibilities of using the even more efficient "snapshot" inversion-recovery techniques [3] are also being examined.

[1] M.Braun, W.J.Jung, O.Lutz, R.Oeschey, Z.Naturforsch. 43a, 291-296 (1988).

[2] A.Connelly, C.Counsell, J.A.B.Lohman, R.J.Ordidge, J. Magn. Reson. 78, 519-525 (1988).

[3] A.Haase, Magn. Reson. Med. 13, 77-89 (1990).

## Spatial mapping of magnetic fields induced by electric currents.

Peter Bendel

Dept. of Chemical Physics, Weizmann Institute, Rehovot, Israel.

The idea that magnetic fields induced by electric currents could be mapped using chemical shift imaging was proposed several years ago (1). A more efficient and sensitive realization of this concept consists of using phase images to detect and map the magnetic fields of electric currents passing through the sample (2). When a current is transiently active during evolution of the spin system, the resulting z-component of the current-induced magnetic field will induce a local phase shift at the time of signal detection (the echo). Other contributions to such phase shifts caused by intrinsic field inhomogeneities and bulk susceptibility distortions can be eliminated by subtracting data obtained under identical conditions, but in the absence of the current. In principle, both gradient echo and spin echo imaging sequences can be used to map the current induced phase shifts. If spin-echo detection is used, the current should occur either before or after the 180° pulse, or in any case be nonsymmetric around it. Thus, the effect of a bipolar current pattern can be maximized by having the refocusing pulse coincide with the current reversal.

In this contribution, current localization was extended to finer spatial resolution (0.12 mm in-plane, 0.6 mm slice thickness) and weaker applied currents (about  $10^{-5}$  Ampere) compared to previous reports (2). Examples of current-induced field distributions were obtained in phantoms on a Bruker Biospec 47/30 spectrometer, operating at 200.2 MHz for protons. The examples include currents in both electronic and ionic conductors, mapping the field outside the conductor for the former, and both inside and outside for the latter. The results are in excellent quantitative agreement with the field dependence derived from exact solutions of the Biot-Savart integrals. The sensitivity of detection is limited by the integral over  $Bdt$ , where  $B$  is the z-component of the current-induced magnetic field. It depends upon instrumental stability and signal-to-noise (in the magnitude image), and was about  $10^{-10}$  Tesla-sec on our instrument, for a S/N of 100:1. The definition of sensitivity in terms of the currents themselves depend upon the spatial resolution vis-a-vis the cross section area of the current source.

1. Y. Manassen, E. Shalev, and G. Navon, *J. Magn. Reson.* 76, 371, 1988.
2. M. Joy, G. Scott, and M. Henkelmann, *Magn. Reson. Imag.* 7, 89, 1989.

Biological Applications of Low-Field EPR Imaging and In Vivo EPR.  
– Significance of Nitroxide Spin-labels and Nitroso Compounds

Hirotsada Fujii<sup>1</sup>, Katsuko Kakinuma<sup>1</sup> and Lawrence J. Berliner<sup>2</sup>

<sup>1</sup> Department of Inflammatory Research, The Tokyo Metropolitan Institute of Medical Science, Tokyo 113, <sup>2</sup> Department of Chemistry, The Ohio State University, Ohio 43210

EPR imaging carries information somewhat different from that of MRI, that is, the spacial distribution of paramagnetic centers. When we challenge *in vivo* EPR and EPR imaging works, conventional EPR spectrometers operating at X band (8 to 12 GHz) are very limited, since the dielectric losses at X band are huge in living samples containing large amounts of water. Therefore, we employed the flat loop coils operating at 1 - 2 GHz and we have measured EPR image from *in vivo* field gradient spectra of a living murine tumor (Cloudman S-91 melanoma in the tail of a DBA-2J mouse) using the paramagnetic nitroxide imaging agent, 2,2,5,5-tetramethyl-pyrrolidine-1-oxyl-3-carboxamide or CTPO (1). This image demonstrated not only the feasibility of imaging a tumor by EPR, but also usefulness of nitroxide spin-labels as the paramagnetic imaging agent: (i) The concentrations of nitroxide in different parts of tissue are based on the metabolism of the nitroxide, i.e. the redox metabolism in the tissue, and thus the image reflects in part the difference in nitroxide spin label reduction/reoxidation rates in the tissue. (ii) Visualization of diffusion and transport phenomena of nitroxide is possible as monitored by nitroxide distribution with time.

Another candidates for the paramagnetic imaging agent beside nitroxide are paramagnetic metal ions and naturally occurring free radicals. Recently we observed naturally occurring free radicals were generated *in vitro*, when some nitroso compounds were reacted with reducing agents in blood. Several nitroso compounds tested were converted to the corresponding hydronitroxide radicals. We also observed that upon mixing blood with nitroso compounds, oxygen is consumed, followed by the production of superoxide anions. Hydronitroxide radicals are very autoxidizable and seem to transfer one electron to electron acceptors such as oxygen and quinone. Since nitroso compounds are recognized in general as potential reactive carcinogenic materials, an EPR image using nitroso compounds as the paramagnetic imaging agent should be important to monitor "the effect" of carcinogenic materials *in vivo*.

1. Berliner, L.J., Fujii, H., Wan, X. and Lukiewicz, S.J. (1987) *Magn. Reson. Med.* 4, 380-384.

## SWELLING BEHAVIOR AND SOLUBILITY OF DRUG TABLETS STUDIED BY NMR MICROSCOPY

E. Koeller<sup>1</sup>, G. Koeller<sup>2</sup>, W. Kuhn<sup>1</sup>, F. Moll<sup>2</sup>

<sup>1</sup> Fraunhofer-Institute for Nondestructive Testing, Ensheimer Straße 48, D-6670 St. Ingbert, Germany

<sup>2</sup> Institute for Pharmacy, University of Mainz, Saarstraße, D-6500 Mainz, Germany

Biodegradable polymers like L- and DL- polylactic acid are widely used in pharmaceutical technology as matrix material in drug delivery systems for peroral and parenteral application.

Tablets containing theophylline as a model drug and low molecular weight polylactic acid as matrix material gave pH dependent release profiles accompanied by swelling and erosion phenomena of these tablets.

L-poly-lactic acid tablets erode slowly due to polymer hydrolysis. Drug release could be described with a diffusion dependent release kinetic. Using spin echo images of water protons a correlation between drug release and diffusion of buffer solution in the tablets has been established which allows investigations of drug release on these tablets.

DL-poly-lactic acid tablets showed changes in tablet structures correlating with drug release.

At pH values < 6.5 the porous matrix structure changed to a homogeneous matrix without pores leading to less than 10% drug release. At pH values > 6.5 a swelling of the tablets up to 40% occurred with faster drug release. So far no explanations have been published for this release behavior.

These changes have been investigated with spin echo images of water protons of the buffer solutions. The images showed only at pH > 6.5 a diffusion of water into the tablets, which explains the pH dependent drug release from low molecular weight DL-poly-lactic acid tablets.

The observed changes in tablet morphology were accompanied by a loss of tablet hardness, the tablets became a viscous and amorphous mass. Parameter-selective T<sub>1</sub>-images of the tablets demonstrated correlating changes in T<sub>1</sub>-relaxation time according to water uptake and swelling of the DL-poly-lactic acid polymer.

STUDY OF THE PERMEABILITY OF POLYACRYLAMIDE GEL BEADS  
FOR HLAD BY NMR MICROIMAGING.

Mark Spanoghe<sup>1,2</sup>, Carine Gorrebeeck<sup>2</sup>, Dirk Lanens<sup>1,2</sup>, Roger Donnizze<sup>1,2</sup>, Guy Lemiere<sup>2</sup>, Jozef Lepoivre<sup>2</sup>, Frank Van de Vyver<sup>1</sup>, Annemie Van der Linden<sup>1</sup>, Frank Alderweireldt<sup>2</sup>

<sup>1</sup>Research Group for Biomedical NMR, <sup>2</sup>Dept. of Organic Chemistry, University of Antwerp, Antwerp, Belgium.

We studied the penetration of enzyme molecules into polyacrylamide gel beads which are used to immobilize the enzyme in preparative enzymatic reactions.

The enzyme, Horse Liver Alcohol Dehydrogenase (HLAD MW=70000) catalyzes the stereospecific conversion of ketones into S-alcohols<sup>1</sup>. The  $\epsilon$ -amino groups of the lysine residues of HLAD were labeled with Gd-DTPA, using the N-hydroxy-succinimide active ester method<sup>2,3</sup>. The HLAD-(DTPA-Gd)<sub>x</sub> has a 3.7-fold greater longitudinal (R1) and a 14-fold larger transversal relaxivity (R2) (at 2.4 T) than the free Gd-DTPA. A series of dry polyacrylamide gel beads ( $\pm$ 5 mm diameter), with different ratio of cross linking (5/5, 10/5, 15/5, 20/5, 25/5 and 30/5) were synthesized. The permeability of these gels depends on the total monomer concentration<sup>4</sup>: the lower the monomer concentration the higher the permeability. The beads were swollen in a 3-(N-morfoline)propanesulfonic acid-buffered (MOPS) solution of HLAD-(DTPA-Gd)<sub>x</sub> (1 mg HLAD/ml) and subsequently examined with high resolution NMR-imaging. A standard 3D spin echo sequence was used and the TE/TR of the T1- and T2-weighted images was 24/100 and 60/1000 ms respectively. The T1 and T2 images reveal that the different gel beads show different permeability for the labeled HLAD. The 5/5 gel was entirely penetrated, the 10/5 and 15/5 gels showed the HLAD-(DTPA-Gd)<sub>x</sub> only in the outer layer, while in the 20/5, 25/5 and 30/5 gels no penetration of the labeled HLAD was detected.

Simultaneously with the NMRI experiments, in-vitro enzyme activity measurements were performed on enzyme fractions immobilized on the investigated gel beads. The results show that the enzymatic activity decreases from the 5/5 gel (100 % activity) to the 15/5 gel (35 % activity), the 20/5, 25/5 and 30/5 gels showed a constant residual enzyme activity of 20 %.

The correlation between the NMRI results and the enzymatic activities demonstrate that Gd-labeled products can be used to monitor the diffusion of diluted, water soluble products in a to solid matrix.

1. Lemiere G. Enzymes as catalyst in organic synthesis ed. An P. Schneider, NATO ASI (178, p13) Dordrecht Reidel Publishing Company.
2. Buckley R. G. and Searle F. FEBS lett. 166(1), p202, 1984
3. Paxton R. J., Jakowatz J. G., Beatty J. D. et al. Cancer Res. 45, p5694, 1985
4. Thomas W. Encyclopedia of polymer science and technology, 1, p177

INVESTIGATION OF THE DIFFUSION PROCESS IN CROSSLINKED  
POLYSTYRENES BY  $^1\text{H}$  AND  $^{19}\text{F}$  NMR MICROSCOPY

Martin Ilg<sup>+</sup>, Bettina Pflöiderer<sup>\*</sup>, Klaus Albert, Wolfgang Rapp and Ernst Bayer

Institute of Organic Chemistry, D-7400 Tübingen, FRG

present address:

+ BRUKER MEDIZINTECHNIK GmbH, D-7512 Rheinstetten 4, FRG

\* MGH-NMR Center, 149, 13th Street, Charlestown, MA 02129, USA

NMR microscopy has been used to monitor the diffusion of dioxane of 1 %, 2.5 % and 5 % cross-linked polystyrene. These materials are used as stationary phases in chromatography, for extraction and separation processes, and as supports for a variety of reactions in solid-phase syntheses. In these applications surface interactions and diffusion are the most important processes for mass transport and exchange phenomena and are heavily dependent upon matrix parameters such as cross-linking.

Analyzing spin-density weighted FLASH-images we were able to distinguish different types of diffusion by comparison of the intensity profiles: Fig. 1 is a stacked plot of the signal intensity of semiprofiles stretching from the center of the cylinder to bulk dioxane in the test tube. The figures indicate the time (in minutes) elapsed after exposure to dioxane. The plateau to the right is the signal of bulk dioxane, the inverted spike is due to a susceptibility change at the surface of the polymer. The diffusion gradient is to the left of the high plateau. The low plateau of untouched polystyrene is to the extreme left. The stacked plots demonstrate the consequences of crosslinking: the material with 1% cross-links sports a steep gradient advancing with time but keeping its slope throughout the process and followed by a zone of constant concentration. (Fig. 1a). This can be correlated to a type of diffusion which is referred to as CASE II. 5% cross-linked polystyrene in the beginning shows a steep gradient starting at the surface of the sample, gradually flattening with time, which is the normal fickian way of diffusion (Fig. 1c). The behaviour of the 2.5% cross linked polymer lies between these two extremes, showing elements of both types (Fig. 1b).

With  $^{19}\text{F}$ -NMR-microscopy we were able to get more insight into the liquid-liquid displacement process of preswollen polymer beads. Moreover, the adsorption and desorption of a fluorinated amino acid in a column packed with such polystyrene beads was monitored. The images show for the first time that the amino acid is capable of unhindered diffusion in the bead pores and therefore does not remain within the beads.

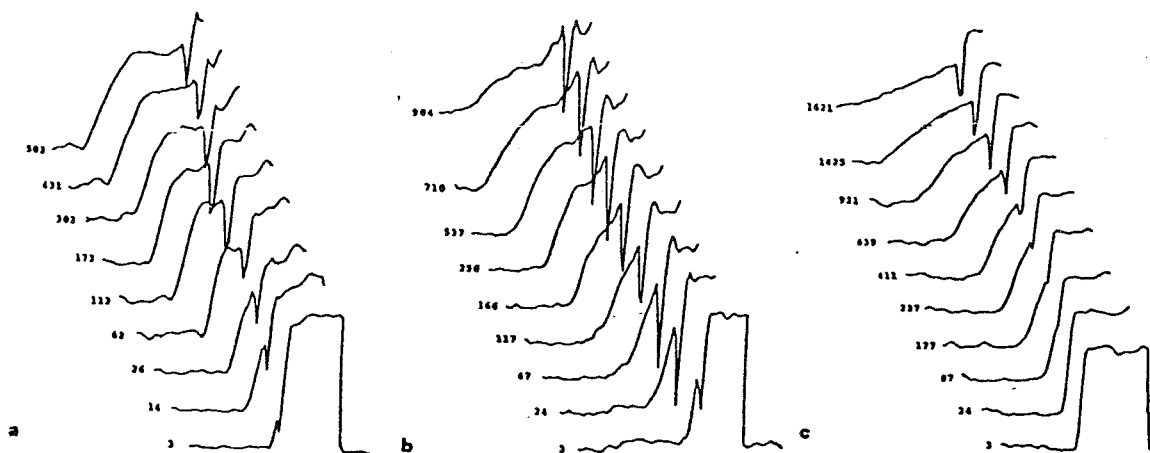


Fig. 1: Stacked plot of the intensity profiles. a) 1.5 %, b) 2.5 % and c) 5 % cross-links

# NMR Imaging of Elastomers: Stress Distribution, Thermal and Mechanical Aging

P. Blümmler and B. Blümich

Max-Planck-Institut für Polymerforschung,  
Postfach 3148, D-6500 Mainz

From the point of NMR elastomers can be considered as materials in between a solid and a liquid. Therefore they are suitable for conventional NMR imaging. Inhomogeneities are easy to detect,<sup>1</sup> and in some cases it is possible to characterize them.

Proton spin-echo imaging was applied to investigations of thermal aging in elastomeric materials. Vulcanized natural rubber filled with carbon black was aged in air at elevated temperature. A diffusion controlled hardening of the surface layer was observed. Its radial growth was studied, and the local kinetics of the aging reaction were followed by the amplitudes of the spin-echoes. It could be shown that the growth of the surface layer proceeds twice as fast as the aging reaction takes place<sup>2</sup>.

Furthermore, for contrast enhancement different magnetization filter methods were applied to thermally and mechanically aged synthetic rubber samples (SBR). It was demonstrated that the dipolar filter<sup>3</sup> combined with an imaging sequence is most suitable for elastomeric systems with regions of different molecular mobility and displays better contrast in comparison to other filter methods ( $T_1$ ,  $T_2$ ,  $T_{1\rho}$ ). In addition to that, the multipulse sequence used for dipolar filtering results in a line narrowing (here factor 2) and better spatial resolution<sup>4</sup>.

Another important question is the distribution of stress in stretched elastomers. As a result of stress induced crystallization the  $T_2$ -relaxation time is often a measure of the molecular mobility. Varying stress inside the sample can be detected by  $T_2$ -images. We have investigated a stretched silicon rubber with a small cut on one side. The calibration of  $T_2$  versus the elongation allows one to calculate a stress map from  $T_2$ -image<sup>5</sup>.

## References:

- 1) C. Chang, R. A. Komoroski, *Macromolecules* **22** (1989) 600.
- 2) P. Blümmler, B. Blümich, *Macromolecules* **24** (1991) 2183.
- 3) K. Schmidt-Rohr, *Diploma Thesis* (1989).
- 4) P. Blümmler, B. Blümich, to be published.
- 5) P. Blümmler, B. Blümich, to be published.

*Shear Thinning in High Polymer Solution*  
*using Dynamic NMR Microscopy*

Y Xia and P T Callaghan

Department of Physics and Biophysics, Massey University  
Palmerston North, New Zealand

**Abstract**

High molar mass polymer melts and solutions exhibit unusual rheological properties. Among the non-linear viscoelastic properties of such complex liquids is the non-Newtonian dependence of the shear stress on shear rate, commonly known as shear-thinning. Dynamic NMR Micro-imaging has been used to measure velocity profiles for water solutions of WSR301 poly(ethylene oxide) in laminar flow through a 700  $\mu\text{m}$  i.d. capillary as a function of concentration and pressure gradient. A transition from Poiseuille flow to power law shear-thinning is apparent as the concentration is increased above  $c^*$ .

Equilibrium self-diffusion coefficients have been measured as a function of concentration for WSR301 and as a function of molar mass for monodisperse poly(ethylene oxide) standards in  $\text{D}_2\text{O}$  and it is apparent that the data are consistent with the usual reptative scaling behaviour. A measurement of self-diffusion in the presence of the flow field indicates that shear thinning is associated with significant enhancement of the polymer Brownian motion along the axis of shear. In particular we show that it is possible to measure self-diffusion rates some 4 orders of magnitude slower than that of the free water molecule in a flow field where the velocity spread in a single pixel greatly exceeds the spread due to Brownian motion. The experimental data are interpreted using a simple adaptation of the entanglement/blob model.

Abstract of a paper to be presented at the International Conference on NMR Microscopy to be held at Heidelberg, Germany, 16-19 September 1991.

FLUID DISPLACEMENT IN POROUS MEDIA USING NMR MICROSCOPY

by

G.J. Nesbitt, T.W. Fens\* J.S. van den Brink and N. Roberts\*

KONINKLIJKE/SHELL-LABORATORIUM, AMSTERDAM  
(Shell Research B.V.), Amsterdam, The Netherlands  
KONINKLIJKE/SHELL EXPLORATIE EN PRODUKTIE LABORATORIUM  
(Shell Research B.V.), Rijswijk, The Netherlands  
UNIVERSITY OF LIVERPOOL, Liverpool

We have previously reported NMR imaging data of fluid flowing through porous-media models, and discussed methods through which the data<sup>1</sup> can be quantified. New methods giving higher resolution are now shown, which employ the gradient direction to differentiate between transverse and longitudinal displacement components. Combining these methods with image analysis methods yields a fuller understanding of fluid behaviour in porous media.

Applications are demonstrated of single- and multi-phase fluid conditions in silica and glass models.

1. G.J. Nesbitt, A. de Groot, T.W. Fens, J.M. Bonnie, 1st International Meeting, Recent Advances in NMR Applications to Porous Media, Bologna, Italy, 14-16 November 1990, to be published in Magnetic Resonance Imaging.

## SEEING-NMR Applied to Conductors and Superconductors

U. Skibbe, G. Neue,

Physical Chemistry, University of Dortmund, W-4600 Dortmund 50, F.R.G.

SEEING-NMR provides extremely high spatial resolution ( $< 1 \mu\text{m}$ ) in highly conductive solid samples. It uses the passive  $B_1$ -field gradient produced by the skin effect. In many cases theory and practice is very simple and straightforward [ 1 ].

This paper is aimed to discuss less trivial things, like off-resonance irradiation, the presence of strong quadrupolar couplings etc. to show the applicability as well as the limits of this new technique. The various effects are illustrated by experimental SEEING-NMR spectra of classical conductors as well as of single crystals of high temperature superconductors.

[ 1 ] G. Neue, Bruker Report 2 (1990), 25

## NMR MICROIMAGING OF SOME POLYMERIC MATERIALS WITH MEDICAL AND DENTAL APPLICATIONS

S.N. SCRIMGEOUR<sup>a</sup>, C.H. LLOYD<sup>b</sup>, G. HUNTER<sup>a</sup>, J.A. CHUDEK<sup>a</sup> and R.L. MACKAY<sup>a</sup>.

<sup>a</sup>Chemistry Department and <sup>b</sup>Dental Sciences, University of Dundee, DUNDEE, DD1 4HN, Scotland, UK.

A range of polymeric materials are used in both orthopaedic and dental surgery for restoration. Prefabricated prostheses are available for implants and materials which can be moulded and set *in vivo* are increasingly used for filling and impression taking.

### Silicone elastomers

(i) The biocompatibility and elastomeric properties of silicone polymers have led to their widespread use in tendon grafting, specific joint replacement and soft tissue augmentation. Good quality images have been obtained of the mobile methyl protons of silastic artificial tendon. Stretching the tendon causes an increase in the crystallinity of the polymer material. The observed reduction in image intensity after stretching is interpreted as a decrease in methyl group mobility.

(ii) Addition reaction silicones produce accurate and stable impressions of tooth preparations. A satisfactory impression requires a homogeneous mix of two components. The component pastes and set elastomer show contrasting image intensities. Microimaging has revealed the presence of heterogeneities and the transient nature of these in the impression.

### Light cured dental materials

Command setting filling materials and periodontal dressings are acrylic resins whose polymerisation is initiated by intense blue light. The progress and effective depth of the curing can be followed by nmr microimaging of the monomer.

### Dental cements

Dental polyalkenoate glass cements have been developed both as adhesive aesthetic filling materials and luting cements. Polyalkenoic acids react with amphoteric glass powder to create a solid ionomeric matrix around the superficially reacted glass. Nmr microimaging is ideally suited to examining the setting characteristics of such material. These cements are usually hand mixed which can produce undesirable heterogeneity. Examination of these polyalkenoate cement mixes has shown setting progressing at different rates within the sample.

**KINETICS OF WATER PHASE TRANSITION AND FREEZING-THAWING PHENOMENA VALIDATED IN A POROUS MEDIUM BY NMR MICROSCOPY.**

**S. Crestana** (NPDIA-EMBRAPA, P.O. Box 741, 13560 São Carlos-São Paulo-Brazil); **Posadas, A.** (DFCM-USP-São Carlos-SP), **Nielsen, D.R., Kauten, R.** (University of California-Davis-Ca-USA) and **Brown, J.** (University of Missouri-Columbia-Mi-USA)

The transport of heat and mass within a porous medium is a relevant and not well understood research problem. Nowadays, one of the main challenges to be overcome is the lack of experimental techniques capable of non-destructively measuring the related processes occurring in such media, principally under unsaturated conditions. Recently, NMR microscopy was successfully employed to observe water phase transition and to measure freezing-thawing cycles taking place in the interior of an unsaturated sand column submitted to a variable temperature gradient simulating, in the laboratory, the correspondent cycles usually occurring in soils under natural conditions. Also, a one-dimensional model was proposed to explain the kinetics of the freezing-thawing processes happened in the sand column. NMR images which some of them presenting pixel resolution better than 50 microns permitted to validate the proposed model. The images were obtained by a non-medical NMR scanner (2T magnetic field) commercially designed for imaging small objects. Coils were employed allowing the obtention of high-resolution images. The results to be presented demonstrated the appropriateness of magnetic resonance imaging to observe and to follow the position of the freezing or thawing front in the interior of the unsaturated sand column. Moreover, the NMR signal at the interface solid-liquid is markedly higher than in the solid or liquid region. Due to the loss of the NMR signal in the frozen region and its enlargement at the interface of transition both water phase transition and frozen-unfrozen water kinetics could be observed and quantified. Consequently, NMR imaging particularly at high resolution constitutes a novel methodology already achievable to investigate and to validate models related to transport of mass and water phase transition occurring in the interior of porous media.

## Implementation of online parameter selective MR-image analysis for materials research

R. Brill, J. Stahl, M. Staemmler, W. Kuhn  
Fraunhofer Institute for Nondestructive Testing, D6670 St. Ingbert,  
Germany

### Introduction

Parameter selective image analysis on basis of relaxation times  $T_1$ ,  $T_2$ ,  $T_{1\rho}$  and spin density  $\rho$  is a new method for examination of elastomers and polymers. Aged and non aged areas are characterized by different molecular mobilities and net densities. Visualisation of relaxation times and spin densities by colour coded display enables easy differentiation of these areas. Short response times of the parameter selection software allowing for online display of the colour coded image is crucial for effective usage of this new method.

### Method

Measurement of the probe is done by acquireing several echo images on an MR-machine. From these an intermediate data file is computed, containing information about all  $T_{1i}$ ,  $T_{2i}$ ,  $T_{2\rho i}$ , and  $\rho$  values for each pixel ( $0 < i \leq$  number of components found for that specific pixel). Since computational effort is enormous for the multiexponential data analysis, it is done prior to the clustering step of the parameter selective analysis. Clustering for the online display exploits a fast array processor available as subsystem for a UNIX based computer (Aspect X32, Bruker Rheinstetten, Germany). After verification of the algorithm on the machine's main processor using 'C'-code, implementation was done in assembler for the array processor to get maximum computing speed.

### Results

Processing time for the clustering of the precomputed intermediate data file is typically  $6.5 \mu\text{s}/\text{pixel}$  (including data averaging for two components found for this pixel [1]). This amounts to 430 ms for a full  $256 \times 256$  pixel image. Most times smaller images are sufficient for parameter analysis, further speeding up online selection.

False colour display showed very helpful for determination of small changes in the parameters of the measured samples.

Our graphical user interface, Specially designed for this time critical application, keeps handling of the program easy and fast at the same time.

### Conclusion

The fast parameter selective image analysis allows for easy evaluation of aged elastomer and polymer samples. Online display of the clustered image is very helpful in determination of specific parameters for aged areas in the samples.

### References

- 1 Th. Tolxdorff, Systemanalyse bei der Verarbeitung NMR-Spektroskopischer Daten in der diagnostischen Medizin und Realisierung des RWTH Aachen Magnetic resonance Software Systems (RAMSES), PhD thesis RWTH Aachen, 1985 pp. 74-79

## Spatially and Time resolved Observation of the Water Uptake in Polyamid

M. Staemmler, W.Kuhn

Fraunhofer Institute for Nondestructive Testing, D6670 St. Ingbert, Germany

### Introduction:

The water uptake of polyamid degrades the strength and the hardness of polyamid. Conventional measurement of the water uptake is based on the weight of the probe and thus does not allow to resolve the spatial distribution. NMR microimaging, however, reveals the spatial distribution of the water uptake.

### Probe preparation:

The water uptake was investigated for two polyamid samples PA66 (A3K and A3EG5). Probe 2 is the same as probe 1, except an additive of GFRP. Stripes ( $6 * 4 * 40\text{mm}^3$ ) of both probes were prepared by exposing them to water for times of 1, 2, 4, 6, 8, 12, 18 and 24 hours at  $80^\circ\text{C}$ . Prior to the NMR measurements the water uptake was measured by increase in weight.

### Methods:

On first inspection the probes showed a linewidth of about 2kHz corresponding to a  $T_2$  of 160  $\mu\text{s}$ . Standard Fourier imaging using phase encoding gradients is not applicable, because gradient switching and settling times require at least 50 $\mu\text{s}$ . To avoid this problem, backprojection imaging was used, which is free from gradient switching after the observation pulse. However, the observation pulse has to be given in the presence of gradients. Test measurements with given gradients and hard, nonselective rf-pulses have shown, that the influence of this bandlimited rf-pulse is negligible compared to the influence due to  $T_2$ . Due to the short  $T_2$  all images were done without slice selection and represent a projection along the long axis of the probe. Backprojection was performed using the FID signal and 120 projections. To increase the signal to noise ratio four scans were averaged. Each image took 8 min of acquisition.

After reconstruction the images were imported in the software SUNRISE [1]. The images were subjected to a normalization, because (i) eight probes were used for the different exposure times and (ii) the non reproducible positioning of a probe in the probehead of the MSL 400. The normalization is based on the measured weight during probe preparation and image integral intensity. The water uptake is displayed in a colour coded representation using the features of SUNRISE. Furthermore the spatial distribution of the water uptake and the time dependency is shown for each pixel.

### Results:

NMR microimaging using backprojection provides a tool for measuring the water uptake of polyamid nondestructively. The measurement is performed in less than 10 minutes and results in a quantitative spatially and time resolved determination of the water uptake.

### References:

- (1) M. Staemmler, R. Brill, K. Becker, K.H. Folkerts, K. Gersonde, "SUNRISE - A Software System for Medical Imaging Analysis", Proceedings of the International Symposium CAR '89, Springer Verlag, Berlin, pp 671-677, (1989).

## Effects of Bounded Diffusion on MR Microscopy

W. Brian Hyslop and Paul C. Lauterbur  
University of Illinois at Urbana-Champaign

Diffusional effects on image resolution in MR microscopy are spatially invariant for free diffusion<sup>1</sup>, but not for bounded diffusion. Computer simulations were used to study the effects of bounded molecular diffusion on microscopic imaging as a function of the gyromagnetic ratio  $\gamma$ , gradient strength  $G$ , diffusion coefficient  $D$ , and length  $L$  of the object.

**Methods:** Both random walk and Fourier-Laplace inversion techniques<sup>2</sup> were used to calculate the absorption spectrum  $I(\omega)$  corresponding to the Fourier transform of the solution of Torrey's equation

$$\frac{\partial M}{\partial t} = (-i\gamma Gr + DV^2 - T_2^{-1})M = AM \quad (1)$$

where  $M$  is the complex transverse magnetization following an rf pulse and  $G$  is time-invariant. Both techniques showed excellent agreement in 1D simulations. The random walk technique was used for 2D- and 3D-simulations.

**Results:** Figure 1 shows normalized spectra for the case of diffusion in a 1D-box with edges at  $\pm 0.5$ ,  $D$  that of water at 25C ( $D_w$ ),  $G = .05$  T/m,  $\gamma$  of the proton ( $\gamma_p$ ),  $1/T_2=0$ , and box lengths  $L$  of 10, 20, and 80  $\mu\text{m}$ . For large  $L$ , spectral intensity is displaced inward near the edges of the box. As  $L$  decreases, the spectral peaks broaden and shift towards the center of the spectrum, eventually coalescing into a single motionally-narrowed spectral line.

The spectral lineshape displayed on a normalized frequency scale  $\omega/\gamma GL$  is uniquely determined by the dimensionless scaling factor  $d = 4\pi D/(\gamma GL^3)$ . Figure 2 allows diffusional-induced changes in linewidth to be estimated as a function of experimental parameters.  $W$  is defined as the full spectral width at half the intensity of the spectral center divided by  $\gamma GL$ . Plots of  $W$  vs.  $G$  for non-zero  $1/T_2$  will also be shown.

The shift  $\Delta x$  of the spectral peak from the edge of the box for the  $L=80$   $\mu\text{m}$  case shown in Figure 1 is 5.8  $\mu\text{m}$ . Neglecting intrinsic relaxation effects,

$$\Delta x = 10 \sqrt[3]{D\gamma_p / (D_w \gamma G)} \mu\text{m} \quad (2)$$

where  $G$  is in gauss/cm. An impermeable barrier with equal spin density on either side would have a peak-to-peak splitting of 11.7  $\mu\text{m}$ , as shown in Figure 3. Simulations as a function of  $G$  and barrier permeability will be presented.

Simulations of 2D images of discs with diameters ranging from 10 to 80  $\mu\text{m}$  will be presented. The predicted effects increase somewhat from 1 to 2 dimensions.

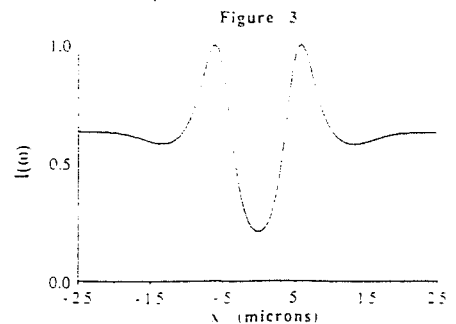
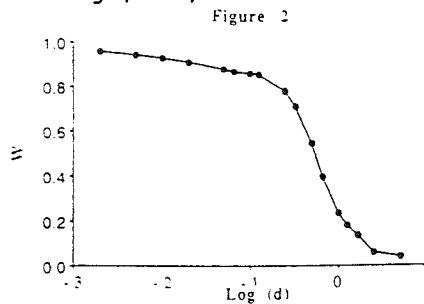
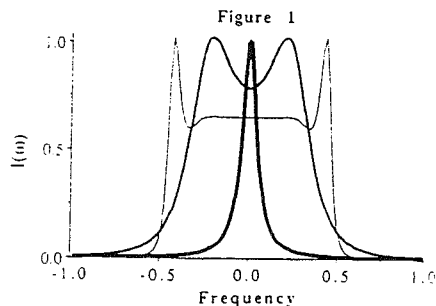
Experimental work is in progress to illustrate diffusional effects in both EPRI and NMRI using gas phase imaging. Such effects can be readily confounded with those due to processing artifacts (i.e., Gibbs oscillations), surface relaxation effects, and susceptibility differences near diffusional barriers.

**Conclusions:** Experimental NMR microscopy has attained isotropic image resolution on the order of (10  $\mu\text{m}$ )<sup>3</sup>. In this size regime, restricted diffusion can alter the image appearance and may be exploited to detect permeability barriers.

**Acknowledgements:** We thank the National Center for Supercomputing Applications for computational resources, Clint Potter for the viewit software, Klaus Schulten for suggesting Ref. 2, and Servants United Foundation for financial support.

**References:**

1. Callaghan, P.T. and Eccles, C.D., *J. Magn. Reson.*, 78, 1, 1988.
2. Kubo, R., *Fluctuation, Relaxation and Resonance in Magnetic Systems*, D. ter Haar, Ed., Oliver & Boyd, Edinburgh, 23, 1962.



## The effect of "absorbing" walls on NMR diffusion measurements

Angeliën Snaar and Henk Van As  
 Lab. of Molecular Physics  
 Wageningen Agricultural University  
 Wageningen, the Netherlands

Pulsed field gradient (PFG) NMR diffusion measurements of fluid in bounded regions permit restricted diffusion to be characterized. This results in the measurement of the diffusion coefficient ( $D$ ) and the distance between the barriers. Fourier transformation of the echo amplitude as a function of  $\gamma\delta G$ , the gradient pulse area, results in the diffusion displacement profile (1,2,3). The theory for the interpretation of the results assumes fully inert and reflecting walls. However, in most realistic (e.g. biological) systems these walls (membranes) are partially permeable and/or contain magnetization sinks.

We have investigated the effect of 'absorbing' walls, by deriving analytical solutions for the echo attenuation ( $R$ ) in PFG NMR experiments for some geometries (planar, cylindrical, and spherical) with the loss of magnetization at the walls as a variable parameter. The rate of magnetization loss at the walls is given by a parameter  $H$  ( $\text{m s}^{-1}$ ), and is the same as has been used for the description of the relaxation behaviour of a confined fluid by Brownstein and Tarr (4). Only the planar geometry resulted in a closed analytical equation.

For a planar geometry (planes at distance  $a$ ; infinite fast relaxation outside the planes, so all spins permeating the walls are lost for observation) computer simulations of the echo amplitude as a function of  $\gamma\delta G$  and  $\Delta$  (time between the gradient pulses) have been performed as a function of the parameter  $aH/D$ . It turns out that for  $H=0$  (fully reflecting walls) at  $\Delta > a^2/2D$  phase coherence is observed for the echo amplitude as a function of  $\gamma\delta G$ , with a local minimum at  $a^{-1} = (2\pi)^{-1}\gamma\delta G$ . Increasing  $H$  results in a shift of that local minimum to higher  $\gamma\delta G$  values. As  $H \rightarrow \infty$  the local minimum disappears. The envelope of the echo amplitude in general is non exponential w.r.t  $(\gamma\delta G)^2$ , as is the case for unrestricted diffusion. The initial slope and the curvature strongly depends on the value of  $aH/D$ .

Based on these computer simulations we conclude that absorbing walls limits  $q$ -space imaging (1), and lead to wrong conclusions for  $a$ ,  $D$ , and distributions of  $a$ , when these wall effect are not taken into account. By measuring  $D_{\text{observed}}$  from the initial slope of a  $\ln R$  versus  $(\gamma\delta G)^2$  plot at four different values of  $\Delta$  the actual values of  $a$ ,  $D$ , and  $H$  can be calculated iteratively from a theoretical plot of  $D_{\text{obs}}/D$  versus  $D_{\text{obs}}\Delta/a^2$  as a function of  $aH/D$  for the actual geometry (cf.5).

1. Callaghan P.T., A. Coy, D. MacGowan, K.J. Packer and F.O. Zelaya, Nature **351**, 467 (1991)
2. Kärgler J., W. Heink, J. Magn. Reson. **51**, 1 (1983)
3. Cory D., A. Garraway, Magn. Reson. Medicine **14**, 435 (1990)
4. Brownstein K.R., C.E. Tarr, Phys. Rev. A **19**, 2446 (1979)
5. Frey S., J. Kärgler, H. Pfeifer, P. Walther, J. Magn. Reson. **79**, 336 (1988)

## One Dimensional Q-Space Imaging of Transversal Dispersive Flow.

Wybo Palstra and Henk Van As  
Lab. of Molecular Physics  
Wageningen Agricultural University  
Wageningen The Netherlands.

Kärger et al [1] and Callaghan et al [2] showed in publications that the conditional probability function for diffusing molecules in zeolite's and loosely packed polymer sphere systems could be found by using the PFG-SE technique. We performed the same type of experiment using the PFG-STE technique in large pore glass bead systems with flowing water. Perpendicular to the flow direction we found that the conditional probability function contains two Gaussian curves upon analysis for displacements smaller than the pore radius. The obtained relative amplitudes and dispersion/diffusion coefficients show that as a function of  $D$  one dispersion coefficient is constant with a value a few times larger than the spin self-diffusion coefficient, while the other dispersion coefficient increases until the molecules have travelled through one pore and levels off for travel distances larger than a pore radius. This is in agreement with [3]. For small displacements the relative amplitude corresponding to the small dispersion coefficient is large while for larger displacements this relative amplitude decreases. For large displacements the conditional probability function, obtained from Fourier transformation of the echo amplitude to  $\gamma\delta G$ , the pulse gradient area, shows minima, the position of which are related to the average pore diameter.

- 1 Kärger J. and Heink W., "The propagator representation of molecular transport in microporous crystallites.", *J. Mag. Res.*, **51**, 1-7 (1983)
- 2 Callaghan P.T., Coy A., MacGowan D., Packer K.J. and Zelaya F.O., " Diffraction-like effects in NMR diffusion studies of fluids in porous solids." *Nature* **351** 467-469 1991.
- 3 Palstra W.D., Van As H. and Brink van den J., "The time dependence of the transversal hydrodynamic dispersion coefficient in glass bead phantoms as observed by NMR." submitted to *J. Appl. Phys.*

***'One-shot' NMR Velocity Microscopy,  
Imaging of Motion using a Single Phase-encoding Step***

Y Xia and P T Callaghan

Department of Physics and Biophysics, Massey University  
Palmerston North, New Zealand

**Abstract**

The single-step phase-encoding method reported here combines gradient phase alternation with the use of a final  $90_x$  'z-storage' rf pulse. This method is capable of producing a velocity image in 'one-shot' by nulling the signal from stationary spins. In our application of this method to NMR Microscopy, we measure the water velocity distribution in a 700  $\mu\text{m}$  i.d. capillary at 12  $\mu\text{m}$  transverse pixel resolution, compare the results with those obtained using the more comprehensive Dynamic NMR Microscopy, and extend the velocity detecting range by employing a four-quadrant analysis method. We also use the method to measure the spatial distribution of vascular water flow in a living plant. The *in vivo* plant flow experiment has shown that a velocity down to 45  $\mu\text{m s}^{-1}$  can be measured by the single-step phase-encoding technique.

## *Rotational Shearing of a Polymer Solution*

C J Rofe, Y Xia and P T Callaghan

Department of Physics and Biophysics, Massey University  
Palmerston North, New Zealand

### **Abstract**

Velocity profiles in capillary flow have previously been obtained<sup>(1,2,3)</sup> for water and polyethylene oxide solutions using Dynamic NMR Microscopy. In the case of the polymer study these measurements demonstrated the non-Newtonian properties of the fluid associated with shear-thinning. In steady-state capillary flow experiments a large quantity of solution is required since enough fluid must be supplied from the header tank to last several hours of measurement. A more elegant method of inspecting non-Newtonian behaviour is achieved by using a concentric rotating cylinder geometry. This method requires only a small amount of sample and also lends itself to rheological studies in melts. Some preliminary Dynamic NMR Imaging results using a rotating cylinder rheometer in an electromagnet are presented.

1. P T Callaghan, C D Eccles and Y Xia, *J. Phys. E* **21**, 820 (1988).
2. P T Callaghan and Y Xia, *J. Magn. Reson.* **91**, 326 (1991).
3. Y Xia and P T Callaghan, *Macromolecules*, in press (1991).

*Imaging Plant Vascular Flow in vivo at a  
Velocity Resolution of 6  $\mu\text{m s}^{-1}$*

Y Xia, K R Jeffrey\*, W Köckenberger† and P T Callaghan

Department of Physics and Biophysics, Massey University, Palmerston North, New Zealand

\*Department of Physics, University of Guelph, Ontario, Canada

†Botanisches Institut der Universität Bayreuth, D-8580 Bayreuth, Germany

**Abstract**

The non-invasive measurement of plant water and nutrient flow *in vivo* represents one of the major challenges of plant physiology. Knowledge of such flow is important to any explanation of growth regulation and the response of plants to environmental stress. Here we demonstrate the remarkable potential of Dynamic NMR Microscopy in such measurement. Dynamic NMR Microscopy utilizes Pulsed Gradient Spin Echo contrast to provide motion-dependent phase encoding. Complex (*ie* real and imaginary) images are obtained sequentially using PGSE gradient pulses of increasing magnitude and the resulting set is Fourier analysed to yield dynamic displacement profiles for each pixel of the image. These Gaussian profiles have peak centres whose position depends upon the molecular velocity and whose widths depend upon the self-diffusion coefficient. Profile analysis therefore yields both velocity and diffusion maps.

Dynamic NMR Microscopy experiments on plants *in vivo* require the maintenance of viable environmental conditions for the specimen over a timescale of several hours. In this work an imaging probe was constructed especially for the study of vascular flow in Castor Bean stems. The probe incorporates two water baths and facility for nutrient addition and water aeration. Rather than threading the plant through the r.f. coil, the coil is individually wound around each specimen. The magnetic field shim coils, the gradient coils, the r.f. coils and the water baths are all mounted within the 32 mm gap between the electromagnet pole faces.

We have measured xylem flow from the root to the cotyledon in Castor Bean seedlings and observed vascular flow asymmetry which results when one cotyledon is removed. In experiments using plants with developed green leaves we have simultaneously measured both xylem and phloem transport. Velocity measurements in the vicinity of 6  $\mu\text{m s}^{-1}$  reported here are the lowest yet recorded using NMR.

# *Q-Space Imaging of Homogenous, Porous Structures*

A Coy and P T Callaghan

Department of Physics and Biophysics, Massey University  
Palmerston North, New Zealand

D MacGowan, K J Packer and F O Zelaya

BP Research, Chertsey Road, Sunbury-on-Thames  
Middlesex TW16 7LN, UK

## Abstract

In pulsed gradient spin-echo (PGSE) NMR a Fourier relationship exists between the dynamic displacement space  $P_s(\mathbf{r}; \mathbf{r}', \Delta)$  and the gradient wavevector  $\mathbf{q}$ , where  $\mathbf{q} = (2\pi)^{-1} \gamma \mathbf{g} \Delta$ . In a homogenous, porous sample containing a diffusing liquid (in this case water), the distribution of displacements of the water molecules will be influenced by the structure of the porous sample<sup>(1,2)</sup>. In particular, structure will be seen in the  $\mathbf{q}$ -space data when  $\mathbf{q}$  is of order  $b^{-1}$ , where  $b$  is the inter-pore spacing and  $\Delta$  is the mean time for a water molecule to diffuse from one pore to a neighbouring pore.

In this report, we show PGSE data obtained for proton NMR of water diffusing in an orientationally disordered, loosely packed array of monodisperse polystyrene spheres. A first-order coherence peak is seen, by analogy with X-ray diffraction from a glass, when  $q \sim (16 \mu\text{m})^{-1}$  which matches well the pore spacing  $b$  which is roughly equal to the sphere diameter of  $15.8 \mu\text{m}$ .

PGSE is a form of imaging in its own right, with resolution limited only by the available magnitude of  $q$ . An inverse (3D) fourier transform can be performed to reveal a spherically averaged 'image' of the pores in the sample.

1. P T Callaghan, A Coy, D MacGowan, K J Packer and F O Zelaya, *Nature(London)* **351**, 467-469 (1991).
2. P T Callaghan, D MacGowan, K J Packer and F O Zelaya, *J. Magn. Reson.* **90**, 177-182 (1990).

## VELOCITY-SELECTIVE PULSE SEQUENCES

J.M. Pope and S. Yao

Dept. of Biophysics, School of Physics, The University of New South Wales,  
P.O. Box 1, Kensington NSW 2033, Australia

We have developed a series of flow imaging techniques which combine flow velocity measurement with stationary signal suppression in a single sequence. The methods employ the concept of flow-selective pulses (1) which excite signals from flowing material only. We describe a family of such pulses based on the binomial selective excitation sequences commonly employed for solvent suppression in NMR spectroscopy (2). Simple adaptation of these methods to incorporate bipolar flow encoding gradients (3) results in a set of pulse sequences which can be employed to selectively excite signals only from flowing spins. These include, in the notation of Hore (2):

$$\begin{aligned} & 1 - G \overline{G} - \overline{1} \\ & 1 - G \overline{G} - \overline{2} - G \overline{G} - 1 \\ & 1 - G \overline{G} - \overline{3} - G \overline{G} - 3 - G \overline{G} - 1 \quad \text{etc.} \end{aligned}$$

where  $G \overline{G}$  denotes a bipolar flow-encoding gradient (3).

In practice the effectiveness of these basic pulse sequences for stationary signal suppression in MRI is rather poor, because magnetic field inhomogeneity over the sample volume causes dephasing of both stationary and flowing spins. However the performance can be dramatically improved by incorporation of  $180^\circ$  pulses to re-focus these off resonance effects, as well as chemical shift differences, to yield for example

$$\begin{aligned} & 1 - G - 180^\circ - G - 1 \\ & 1 - G - 180^\circ - G - 2 - G - 180^\circ - G - 1 \quad \text{etc.} \end{aligned}$$

The calculated signal response for such sequences, plotted as transverse magnetisation  $M_{xy}$  versus flow-induced phase shift  $\phi$  (in units of  $\pi$ ) is shown in figure 1. In practice the latter is proportional to the velocity of flow in the gradient direction  $v$  since

$$\phi = -\gamma G \Delta \delta v$$

where  $\Delta$  is the separation of the gradient pulses, each of duration  $\delta$ .

These velocity-selective excitation pulse sequences can be readily combined with conventional Fourier or back-projection imaging techniques to yield images of flowing spins, with excellent suppression of signals from static material. This is achieved in a single sequence without the need to employ subtraction methods. In addition the signal intensity in a magnitude image gives a direct measure of flow velocity.

In our case the imaging sequences have been implemented on a Bruker 4.7 T micro-imaging system based around a cryomagnet with 15 cm horizontal room temperature bore and standard MSL 200 imaging/spectroscopy console. Results for flow

phantoms demonstrate static signal suppression approaching 100-fold combined with quantitative measurement of flow velocity at an in-plane resolution down to 60  $\mu\text{m}$ .

Since the methods do not rely on signal subtraction or difference methods for suppression of static signals they are inherently relatively insensitive to sample or patient motion. The sequences can also be tailored to suppress contributions from slow-moving as well as stationary spins. While the 1-G-180-G-1 sequence yields images in which the relationship between signal intensity and flow velocity is simplest, the more complex sequences are better in suppressing stationary signal.

#### References

- [1] Nishimura, D.G., Macovski, A. and Pauly, J.M., IEEE Transactions on Medical Imaging MI5, 140, 1986.
- [2] Hore, P.J., J. Magn. Reson. 55, 283, 1983.
- [3] Dumoulin, C., Souza, S.P., Walker, M.F. and Wagle, W. Magn. Reson. Med. 9, 139, 1989.

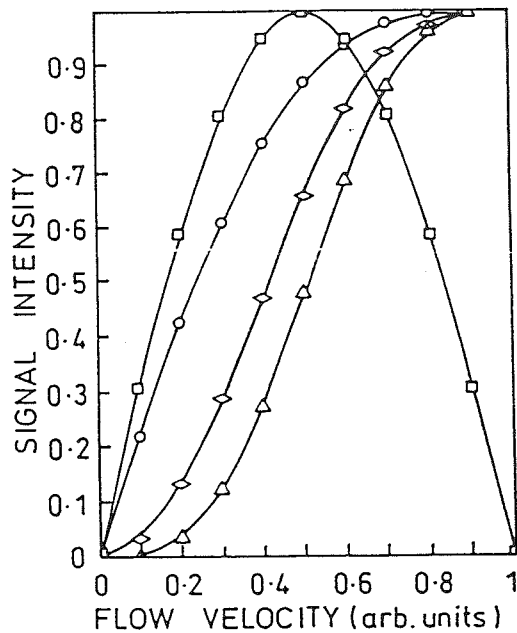


Figure 1: Signal intensity  $M_{xy} = \sqrt{M_x^2 + M_y^2}$  versus flow velocity  $v$  for  $1 - G \overline{G} - \overline{1}$  with pulse flip angle  $\theta = 90^\circ$  (Ref. 1);  $O$   $1 - G \overline{G} - \overline{1}$  with  $\theta = 45^\circ$ ;  $\square$   $1 - G \overline{G} - \overline{2} - G \overline{G} - 1$ ,  $\theta = 22.5^\circ$ ;  $\Delta$   $1 - G \overline{G} - \overline{3} - G \overline{G} - 3 - G \overline{G} - 1$ ,  $\theta = 11.25^\circ$ .

## **Parameter Selective NMR Microscopy - A New Tool in Atherosclerosis Research -**

W. Kuhn\*, M. Asdente \*\*, T. Beringhelli\*\*, M. Soma\*\*

\* Fraunhofer Institute for Biomedical Engineering, D-6670 St. Ingbert, Germany

\*\* University of Milano, Dept. of Pharmacology, Milano

Atherosclerosis is a degenerative process of the arterial wall characterized by an accumulation of lipids, smooth muscle cells, various types of collagen, elastin, necrotic tissue and minerals. This process may eventually result in the development of plaques with irregular narrowing of the arterial lumen. Magnetic resonance imaging (MRI) has been evaluated as a potential tool in cardiovascular diagnosis. NMR angiography can be performed and indicates alterations in the vessel lumen, but provides no information on the state of the atherosclerotic lesion. It could be shown that NMR microscopy and NMR spectroscopy on in vitro samples allow the characterization of atherosclerotic lesions by the investigation of their morphology and chemical composition (1). The combination of spin preparation sequences prior to imaging sequences provide additional information on the state of an atherosclerotic lesion. Moreover by application of chemical shift selective  $T_1$ - and  $T_2$  imaging and parameter selective image analysis lesions in different states such as an advanced plaque, fatty streak or calcified plaque can be clearly distinguished and characterized. The experiments were performed on Bruker AM 300 and MSL 400 spectrometers equipped with a microimaging accessory. The data evaluation and parameter selective image analysis were performed with a software package developed for mono- and multiexponential data analysis and written in C. For  $T_1$  image analysis an iterative algorithm (2) for monoexponential fits was used. For  $T_2$  image analysis four different algorithms for mono- and multiexponential data evaluation were applied. The according relaxation times, which could be chemical shift selectively determined, were obtained for voxel sizes of  $30 \times 30 \times 500 \mu\text{m}^3$ . The results are applicable as  $T_1$ - and  $T_2$ - values as well as chemical shift selective  $T_1$  and  $T_2$  water and fat images. It could be shown that parameter selective image analysis with respect to the relaxation times and chemical shifts is a very valuable tool in the characterization of plaques and lesion as well the investigation of plaque progression.

### **References:**

- (1) **M. Asdente, L. Pavesi, P.L. Oreste, A. Colombo, W. Kuhn, E. Tremoli**  
Evaluation of Atherosclerotic Lesions Using NMR Microimaging  
*Atherosclerosis* 80:3, 245 (1990)
- (2) **R. Gerhards, W. Dietrich**, *Journal of Magnetic Resonance* 23, 21 (1976)

Atherosclerotic Lesions: ex vivo Characterization  
by 3D NMR Microscopy and Quantitative 3D-Data Processing

G. Rohr, M. Heine. Medical Clinic IV and Institute for Pathology, Klinikum Mannheim  
University of Heidelberg  
D. Gross, V. Lehmann, W. Ruhm, U. Wark. Bruker Analytische Meßtechnik, Rheinstetten,  
FRG

Background:

Atherosclerosis is a chronic disease of the arterial vessels which starts with an accumulation of lipids at the epithelium of the arterial wall, giving rise to "fatty streaks". This is followed by proliferation of cells of the vessel wall, associated with an accumulation of extracellular connective tissue. Atherosclerotic plaques particularly involve the intimal layer of the artery wall. These plaques may grow, leading to disturbances and interruption in blood flow, formation of thrombi or calcifications, occlusion of the vessel, resulting in ischemia or necrosis.

Introduction:

Until now, distribution of the lesions in the arterial wall, especially lipid distribution, are followed on a histological level by light microscopy. There are few reports that document characterization of atherosclerotic lesions by NMR microscopy. But especially morphological quantification of those lesions for either the pathology departments' routine or for scientific reasons is mainly done by quantitative histomorphometry. After development of a new 3D data processing software we applied this software to 3D NMR microscopy data sets to quantify atherosclerotic lesions on autoptic arteries and compare those data with quantitative histomorphometry of the same specimens.

Materials and methods

Normal or atherosclerotic autoptic specimens of iliacal or femoral human arteries were used either unfixed or fixed with formalin. After 3D-NMR-measurements the samples were processed for conventional histology and histomorphometry and the data were compared.

The nmr experiments were performed on a Bruker AMX 300 spectrometer supplied with microscopy hardware and a 7 Tesla vertical superwidebore magnet (150 mm). A maximum gradient strength of about 1T/m is available with the gradient coils of the microimaging system. A chemical shift selective 3D gradient echo method was used to aquire  $128^3$  voxel data sets. The resonance signal from the water as well as from the lipid protons was excited alternatively in the same experiment, which resulted in two data sets for the water and the lipid distributions. The experiment time can thus be shortend by a factor of two. There is no chemical shift artifact as in the case of non selective measurements. This improves the quality of quantitaive data interpretation.

The data were processed on a Bruker Aspect X32 workstation by means of the 3D image processing and analysis package, which enables to reconstruct sectional 2D-images in oblique

planes as well as to present a spatial reconstruction of either the surface of the specimen or single isolated clusters of water or lipid signals. As the size of the voxels are known - the resolution was  $40 \times 40 \times 80 \text{ um}^3/\text{voxel}$  from a 5mm sample - an exact volume calculation of single clusters is possible.

#### Results and discussion:

Chemical shift imaging separates lipid images and water images - the lipid content in the arterial wall or in atherosclerotic plaques of artery specimens can be 3D-reconstructed and calculated. Spatial presentation of single clusters improves interpretation. From the 3D data sets a quantitative morphological analysis and volume calculation of lipid deposits as well as their distribution in the different layers of the arterial wall was made. The intimal thickening as well as the lipid infiltration with its physicochemical properties in atherosclerotic vessels could be analyzed. The 3D-NMR-Microscopy data were in good agreement when compared to the data from conventional histomorphometry.

Our results indicate that 3D-Microscopy is a valid method for morphological quantification and physicochemical analysis of atherosclerotic lesions in autoptic arteries.

## Three-dimensional Visualization in NMR-Microscopy Applied to an Anatomical Setting

A.Kriete and K.-P.Valerius

Institut für Anatomie und Zytobiologie  
Aulweg 123, 6300 Giessen, FRG

For morphological studies it is of great practical importance to assemble three-dimensional models of anatomical structures. In light- and electron microscopy it is necessary to dissect small organisms and organs mechanically into multi-planar series. The computer aided reconstruction of such sections is biased by distortions arising from the mechanical sectioning process and by laborious alignment procedures. We therefore set out to use NMR-microscopy to assemble and visualize 3-D data sets of small organisms.

Tomography was done with a NMR-microscope (Bruker) at a magnetic field strength of 7 Tesla. Series of up to 128 spin-echo images (TE = 15 msec) of fixed rat embryos (1-2 cm of length) were acquired and transferred to an image processing workstation (Kontron). For a direct reconstruction of the complete data-volumes we used volume rendering instead of conventional geometric graphics. The algorithms included ray-casting and front-to-back (FTB). Hereby rays were traced throughout the data volume following a user defined geometry. The different possible ways to sum up the greyvalues of the volume-elements (voxel) were tested to allow surface-displays, transparent views or animated sequences of thresholded intensities.

Special care was taken to visualize volumetric sub-structures (organs) after extensive pre-processing and segmentation. As we are especially interested in the quantitative description of growth processes, this is an important prerequisite to analyse the spatio-temporal changes of volume, surface and form of anatomical structures.

The results were compared, verified and will be discussed with findings from conventional reconstructions of histological serial sections.

### Acknowledgement:

We would like to thank Dr.Groß (Bruker, Karlsruhe) for the kind support during the data-acquisition phase. This work was supported in part by funds of the EC-project 'Advanced Informatics in Medicine' (AIM).

S. Aygen<sup>1</sup>, S. el Gammal<sup>2</sup>, T. Bauermann<sup>1</sup>, R. Hartwig<sup>2</sup>, P. Altmeyer<sup>2</sup>

<sup>1</sup>Institut für biomedizinische Analytik und NMR-Imaging an Universität Witten/Herdecke, D-5810 Witten, FRG.

<sup>2</sup>Dermatologische Klinik der Ruhr Universität Bochum, D-4630 Bochum, FRG

### Introduction

Upto now, high resolution ultrasound was one of the few non-invasive methods available in Dermatology [1]. Recently has been reported in-vivo NMR-Imaging of the human skin [2]. We present new applications of high resolution proton NMR microimaging from different human skin tumors in-vitro. Different measurements setups were used: multislice spin-echo, T1 and T2 imaging and chemical shift selective water and fat imaging. The skin layers (epidermis, dermis, subcutaneous fatty tissue) and different pathological conditions (corneal cysts, tumorous tissue) were quantified and characterized in comparison with correlated histology.

### Materials and methods

12 basal cell carcinomas, 5 seborrheic verrucae, 5 papillomatous nevus and 2 psoriasis vulgaris plaques from different patients - freshly excised - were shortly dipped in 5% buffered formalin for 30 seconds and entered into the NMR-microscope for examination.

The experiments were performed on an BRUKER AM400 WB NMR spectrometer equipped with a advanced microimaging accessory. Initial images were obtained using an image matrix of 128x128 pixels. We performed 16 spin-echo images on selected slice planes of the human skin. The tissue specimen was placed for this purpose in the center of a 5 or 10 mm proton-RF coil. A vertical 50 mm diameter gradient coil was used to generate gradients between 5.7 and 11.7 G cm<sup>-1</sup>. The spatial resolution was in range of 20-39  $\mu$ m and slice thickness was between 300 and 500  $\mu$ m. The T1 images were recorded using an aperiodic saturation sequence, by applying 90° hard pulses and a slice selective 180° hermitian shaped pulse (TE 20 ms, TR from 100 to 5000 ms). For T2 images CPMG pulse sequences were used. To attain an acceptable signal/noise ratio in the images, the total data acquisition time for 16 slice images amounted approximately one hour.

To plot the relaxation curves and determine the tissue-specific T1 and T2-relaxation times corresponding points in 16 consecutive images were analyzed.

After NMR-microscopy, the tissue specimen was further fixed in formalin, dehydrated in ascending concentrations of ethanol and embedded in paraffin. To achieve good correlations with histology, special precautions are necessary to be sure the tissue is oriented in the same way NMR-multislice took place: During serial sectioning always 6 sections (7 $\mu$ m) were mounted on glass slides and 70 sections (about 500  $\mu$ m) were rejected. The sections were numbered, stained with haematoxylin-eosine and examined with an Axiophot microscope (Zeiss, FRG).

### Results and Discussion

Papillomatous nevus	T <sub>2</sub> -values	T <sub>1</sub> -values range
epidermis	18.6 - 20,1	930 - 1020
dermis normal	12.7 - 13.6	830 - 910
fat	43 - 51	370 - 430
nevus cell nests	19.7 - 20,1	1250 -1320
<i>basal cell carcinoma</i>		
dermis	13.5 - 16.4	810 - 880
fat	42 - 48	360 - 410
basal cell tumor nests	19.3 - 20.4	1520 - 1600

Tab 1: T1 and T2 relaxation times range in skin tumors (5 Panillomatous Nevus and 4 basal cell carcinome.

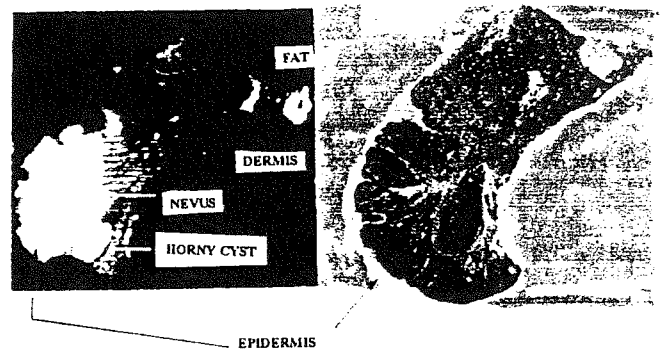


Fig. 1: (a) High resolution spin-echo NMR-image of a papillomatous nevus cell nevus, resolution 39x39x400  $\mu$ m, regions of interest are labeled. (b) Correlating histology.

Fig. 1a shows a simple spin-echo NMR-image of an papillomatous nevus cell with an horny cyst. The comparison with histology (Fig 1b) from exactly the same region reveals, that different layers of the skin are well correlated. Although the epidermis of the normal skin is often difficult to discern, the dermis and the subcutaneous fatty tissue showed significantly different T1 and T2 relaxation times (Tab 1). T1 and T2 of the subcutaneous fat were very similar in different body regions (eg. back, breast) and can be used as reference value (Tab1).

In the papillomatous nevus, the nevus cell nests in the upper dermis were well delineated to the surrounding dermis. (Fig. 1a) The basal cell carcinoma buds could be observed as small round structures, having often direct contact with the epidermis. T1 values is significantly longer as normal epidermis(Tab.1).

The normal skin layers were clearly distinguished from tumor tissue (e.g. nevus cell nevus, basal cell carcinoma) in T1 and T2 weighted images. The contrast between the skin layers and tumor tissue was excellent. Chemical shift selective NMR microimaging give additional information for the physical-chemical characterization of skin layers.

Our results indicate, that the T1 and T2 measurements of different skin layers and tumours in-vitro differ sufficiently to allow clinically relevant tissue differentiation, thus promoting further developments of NMR-Imaging of the human skin in-vivo [2].

### References

1. el Gammal S, et al. New concepts and developments in high resolution ultrasound. In: Altmeyer, P, el Gammal S, Hoffmann K, ed., "Ultrasound in Dermatology". Springer Verlag, Heidelberg 1991, in press.
2. Bittoun J, et al. "Radiology" 176, 457, 1990.

## NMR microscopy of Lepidoptera pupae

J. A. T. Woodford<sup>a</sup>, S. C. Gordon<sup>a</sup>, B. A. Goodman<sup>a</sup>, J. A. Chudek<sup>b</sup> and S. N. Scrimgeour<sup>b</sup>

<sup>a</sup>Scottish Crop Research Institute, Invergowrie, Dundee DD2 5DA, UK

<sup>b</sup>Department of Chemistry, University of Dundee, Dundee DD1 4HN, UK

NMR microscopy has been used to investigate two stages of pupal development in Lepidoptera. Specimens of a fully developed pupa of a noctuid moth (*Graphiphora augur*) and an immature pupa (3 days after pupation) of a butterfly (*Pieris brassicae*) were used. For NMR microscopic imaging they were anaesthetised and placed in glass NMR tubes (10 mm o.d.).

The <sup>1</sup>H NMR spectrum of the noctuid moth pupa showed one broad line, centred at 4.6 ppm, from water. The pierid butterfly gave 2 lines, a strong absorption at 4.6 ppm and a weak absorption at 1.0 ppm, from water and lipid respectively. Images of both pupae were accumulated using standard Bruker spin-echo pulse sequences. The sequence XYIMAGE used for images of the moth pupa excites all of the protons in the region of interest, whilst the sequence XYSIMAGE that was used for the butterfly pupa allows chemical shift selectivity. Separate images were generated for both the water and lipid resonances.

Images of the mature moth pupa show that tissues with high water content, e.g. the gut, wings and heart, can be clearly distinguished in a longitudinal section. Cross sectional images produce greater detail with many features of the adult moth, e.g. proboscis, legs, antennae and flight muscles. The images of the immature butterfly pupa show no clear organisation within the head, thorax or reproductive organs, but the gut is clearly visible (high water, low lipid). Differences in the distributions of water and lipid are apparent in other parts of the body, but these have not yet been correlated with known histological features.

## Some applications of NMR microscopy on insects

D. Fresneau\*, P Gonord, and S. Kan

\*Laboratoire d'Ethologie et Sociobiologie, Université de Paris XIII, F.  
Institut d'Electronique Fondamentale, CNRS URA22, Université de Paris XI, F.

The non destructive nmr method to gather information regarding the internal physiological state of insects is interesting as it requires no dissection. This is particularly appreciated in the case where the type of insect belongs to a rare species or is difficult to rear in laboratory. The *Dinoponera quadriceps* ant of Brasil belongs to the family of primitive queenless society where certain female workers can be fecundated and thus regenerate the colony's population. The absence of a queen ant is the cause of agressivity among female workers, either fecundated or not, and leads to incessant rituel aggression among them[1]. Biologists working in this field are therefore interested in studying the ants' ovarian development in the course of their life in order to distinguish the distribution of the main function between the reproductive workers and those remaining sterile.

**Experimental:** Over a hundred 3D images were obtained using a dead specimen. Image resolution was typically  $47 \mu \times 47 \mu$  with a slice thickness of  $375 \mu$ , the choice being a compromise between image detail and signal to noise ratio. These images serve to identify the internal organs, hitherto unknown, of the ant, and will be compared ultimately with histological pictures. Nmr experiments were performed on a 8.5 T (360MHz) using a saddle-shape rf antenna for spin excitation and signal observation.

**Discussion:** The preliminary results obtained so far are encouraging. Nevertheless, supplementary effort is needed to improve the image contrast in order to discriminate more easily the tissue fat, in an attempt to visualize the ovaries and the ovocytes. Also, despite their physical dimension, the *Dinoponera* ant is rather fragile and cannot be subject to prolonged anaesthesia under nitrogen gas. Work is in progress to study live ants by a multislice-3D rather than the conventional 3D technique, as a means of reducing experimental time.

**REFERENCE:** [1] C.Z. Dantas de Araujo, J.P. Lachaud, and D. Fresneau  
Behav. Proc., 22 ,101-111(1990)

## 3D NMR Microscopy: Imaging and 3D Image Presentation of Insects

D.Gross, V.Lehmann, W.Ruhm, U.Wark, Bruker Analytisch Meßtechnik, Rheinstetten, FRG  
G.Rohr, Medical Clinic IV Klinikum Mannheim University of Heidelberg

### Introduction

Compared to other microscopic methods NMR microscopy has the advantage that image surface information is available along with structural details from the interior of biological samples or living animals without tissue destruction. Recently the spatial resolution of this method was improved to about  $7 \times 7 \times 40 \text{ } \mu\text{m}^3$  voxels. New hard- and software was developed for 3D image visualization of 3D data sets, allowing easier and improved interpretation of the microscopy data. In this work applications of 3D image processing from living insects are presented.

### Methods

Insects up to a size of  $8 \times 8 \times 12 \text{ mm}$  such as *Porcellio Scaber* or *Apis mellifica* (honey bee) have been investigated. They were cooled down alive to  $4^\circ\text{C}$  to prevent motion artifacts and kept in the probehead at the same temperature during the data acquisition. After the data acquisition the insects regained again room temperature and could be investigated in further experiments.

The experiments were performed on a Bruker AM 300 spectrometer supplied with microscopy hardware and a 7 Tesla vertical superwidebore magnet (150 mm). A maximum gradient strength of about 1 T/m is available with the gradient coils of the microimaging system. Various radiofrequency solenoid coils with diameters between 1 mm and 8 mm had been used, depending on the sizes of the insects.

A 3D spin echo sequence was chosen to acquire isotropic  $128^3$  data sets from the entire insect or from parts as the head. The pixel resolutions are  $(50 \text{ } \mu\text{m})^3$  down to  $(15 \text{ } \mu\text{m})^3$ . The echo time was  $TE = 4.56 \text{ ms}$ , the repetition time  $TR = 100 \text{ ms}$ .

The data were processed on a Bruker Aspect X32 workstation by means of the 3D image presentation and analysis package. After Fourier transformation the volume definitions were performed by interactive density thresholding or by interactive selection of individual volume clusters. The visualization is supported by fully free interactive selection of viewing angles, setting of rotation axis along the three cardinal axes, adjustment of shadowing and lighting parameters, three-dimensional cursor movement and quantitative 3D-measurements of distances, angles, mean values and volumes.

### Results and discussion

The spin echo method was preferred against the gradient echo method because often fine structures inside small objects result in strong field inhomogeneities from susceptibility effects which may destroy the theoretical achievable image resolution. Another advantage of the 3D method is the short possible echo time by using only hard rf pulses. This minimizes the signal

loss due to rather short  $T2_{eff}$  relaxation times often observed in small samples. The short repetition time results in strong T1 weighted images at high magnetic field strengths. This will enhance the image contrast.

The 3D visualization software enables to reconstruct sectional 2D images in oblique planes. Details of anatomic structures as eyes, parts of the gut, heart or genital organs were highly resolved. 3D image presentation has the advantage of spatial reconstruction of the insects' surface and interior, small surface organs as antennae, mandibulae or maxillae are presented in their spatial appearance as well as organs of the interior as gangliae, genital organs, heart or the distinct parts of the gut. Advanced features of the 3D image processing allow fast visualization under various orientations, measurements of distances and angles in the 3D space, volume calculations and mean values from the volumes e.g. from the gut or from parts of the ganglions. Presentation of single clusters improves interpretation. Postacquisition image processing as change in light versus shadow distribution enhances contrast. It is very difficult and time consuming to get the same informations out of 2D data.

As the insects are alive during microimaging, they can be imaged for several times and changes e.g. during the development of parasites as varroa in a living honey bee can be followed. Such studies are now in progress.

## A Comparison of 3D NMR Microscopy And Subsequent Optical Microscopy of Thin Sections of Fixed Human Brain Tissue

Xiaohong Zhou<sup>1</sup>, Clinton S. Potter<sup>1,2</sup>, and Paul C. Lauterbur<sup>1</sup>

Biomedical Magnetic Resonance Laboratory<sup>1</sup> and National Center for Supercomputing Applications<sup>2</sup>  
University of Illinois at Urbana-Champaign  
Urbana, Illinois 61801, USA

Recent developments in NMR microscopy have led to spatial resolution of the order of  $(10\ \mu\text{m})^3$  (1), suggesting new possibilities for applications of magnetic resonance imaging techniques to such areas of the biomedical sciences as histology, neurology, and pathology. These new opportunities make it necessary to investigate the appearance of microscopic tissue structures in NMR images and to study the natural contrast phenomena and mechanisms within tissue specimens at the microscopic level. Comparisons with conventional optical microscopy are needed because many structures may be difficult to identify because of the unfamiliar contrast relationships and lower resolution of NMR microscopy. This newer microscopic technique, however, has the advantages of being able to give 3D images within thick opaque objects without sectioning, and of being directly extendable to living tissues, organs and organisms.

Fixed human brain tissue from the putamen was used in this study. The putamen specimen, obtained from an elderly female who died of heart disease, was fixed in a formalin solution and punched out with an  $800\ \mu\text{m}$  glass tube for NMR microscopy. After the NMR imaging experiments, the sample was carefully taken out of the glass tube for sectioning and optical microscopy. Proton 3D microscopic NMR imaging experiments were carried out using a custom-built probe, incorporating both RF and gradient coils, in conjunction with a Spectroscopy Imaging Systems instrument operating at 4.7 Tesla. Technical details of the instrument have been described elsewhere (1). A 3D filtered back projection reconstruction algorithm was employed to obtain microscopic NMR images with isotropic resolution. A magnetic field gradient with a constant magnitude ( $0.0721\ \text{T/m}$ ) was reorientated to give 3542 projections evenly distributed in three dimensions.  $T_2$ -weighted images were obtained by a Hahn spin echo pulse sequence with the echo time (13 ms) close to the average  $T_2$  of the specimen. The  $T_2$ -weighted microscopic NMR image of the putamen was reconstructed as a  $(128)^3$  array on an  $(815\ \mu\text{m})^3$  field of view, resulting in an isotropic voxel size of  $(6.4\ \mu\text{m})^3$ . The specimen used for NMR microscopy was sectioned perpendicular to its axis over the region of interest at intervals of  $50\ \mu\text{m}$ . 2D sections with thickness comparable to NMR images ( $\sim 10\ \mu\text{m}$ ) were stained using haematoxylin and eosine. Optical micrographs were digitized and compared with the NMR images.

In the NMR image, well-resolved cylindrical dark and bright structures of  $50\text{-}100\ \mu\text{m}$  in diameter were found. In the corresponding optical micrographs, blood vessels and fiber tracts, as well as the nuclei of cells, were clearly visible. Comparison between the NMR image and the corresponding optical micrographs reveals that: (i) the bright cylindrical structures in the NMR image correspond to blood vessels in the optical micrographs, and (ii) the dark cylindrical structures in the NMR image correspond to fiber tracts in the optical micrographs, which suggests that the fiber tracts in the fixed putamen have a shorter  $T_2$  than the surrounding tissue. Results obtained from microscopic NMR images clearly demonstrate that tissue structures at microscopic level can be well resolved with natural contrast in fixed tissues. In addition, correlation of microscopic NMR images with optical micrographs can greatly assist in the interpretations of complicated biological structures, especially when NMR microscopy is still in its infancy.

**Acknowledgements:** This work was partially supported by the Servants United Foundation. We thank Dr. R. B. Wellman for providing the putamen sample, Dr. D. P. Lawrance for digitizing the optical sections, and the National Center for Supercomputing Applications for the computing facilities.

(1) X. Zhou, C.S. Potter, P.C. Lauterbur, and B. Voth, "Abstracts of the 8th SMRM", pp. 286, Amsterdam, 1989.

## The Aging of the Human Lens as studied by NMR Microscopic Imaging.

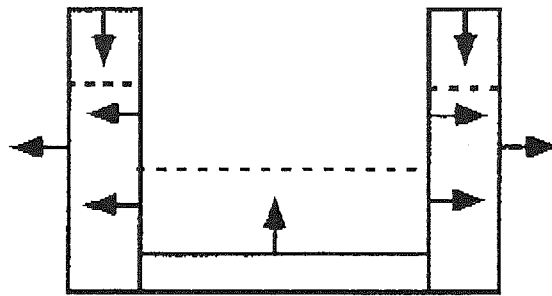
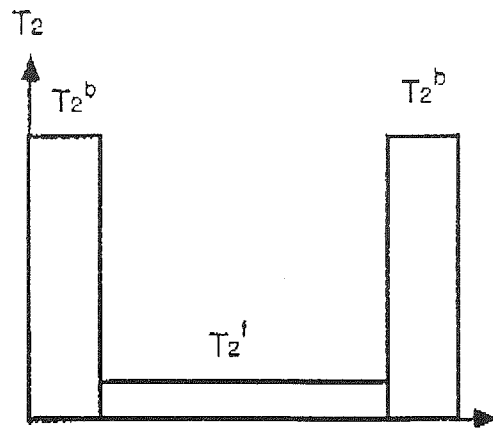
W. Kuhn (Fraunhoferinstitut für zerstörungsfreie Prüfverfahren, Ensheimerstr. 48, D - 6670 St. Ingbert, Germany) and  
A. Daxer (Universitätsklinik für Augenheilkunde, Anichstr. 35, A - 6020 Innsbruck, Austria).

From the clinical point of view two important changes in the behaviour of the human lens are diagnosed frequently throughout the aging process: Presbyopia and Cataract. Presbyopia is a progressive reduction of the accommodation ability, while cataract formation is characterized by the opacification of the lens. Both are believed to be interdependent. Experiments with different methods (NMR, Raman spectroscopy, etc) indicate, that the aging of the human lens leads to changes in its hydration state. A free water fraction may be distinguished from a protein bound water fraction.

We studied normal (young and clear) as well as cataractuous (old and opaque) human lenses by means of NMR Microscopy.  $T_2$  - weighted images showed high  $T_2$  values in the cortical region of the normal lenses, while low  $T_2$  values are found in its nucleus. Between these two extremes a relatively sharp drop can be found. The low  $T_2$  values ( $T_2^b$ ) are interpreted to result from the protein bound water fraction and the high  $T_2$  values ( $T_2^f$ ) from the free water fraction, respectively. So, these results show the validity of a two compartment model for normal lenses in a very impressive way.

During aging a homogenisation like effect with respect to the  $T_2$  distribution seems to take place. The  $T_2$  values are reduced in the cortex and elevated in the nucleus. These  $T_2$  specific changes may be interpreted to result from changes in the water binding capabilities of the aging human lens.

The behaviour of the  $T_1$  values were studied along the optical axis and it was found to show less impressive intraindividual variations. The aging of the human lenses leads to a uniform elevation in the  $T_1$  values along the optical axis.



NMR Microimaging at 7.0 T of the entire Spinal Cord of  
Chronic Recurrent Experimental Allergic Encephalomyelitis  
(EAE) Rats.

<sup>1</sup>Lanens D., <sup>2</sup>Groß D., <sup>1</sup>Spanoghe M., <sup>1</sup>Van der Linden A., <sup>2</sup>'s-Gravenmade  
E.J., <sup>2</sup>Brekelmans M., <sup>2</sup>Gerrits P.O., <sup>2</sup>Holstege G., <sup>1</sup>Van de Vyver F.,  
<sup>1</sup>Domnisse R.

<sup>1</sup>Univ. of Antwerp, Belgium. <sup>1</sup>Univ. of Groningen, The Netherlands.  
<sup>1</sup>Bruker Analytische Messtechnik, Rheinstetten, Germany.

In vitro NMR microscopy of the entire spinal cord was used to investigate the NMR characteristics of lesions in CR-EAE induced Lewis rats at different stages of the disease. The findings were correlated with the specific neuropathologic features of the lesions.

Two controls and 6 diseased animals with at least hindlimb paralysis were sacrificed during the first (2), second (2) and third (2) relapse. Following dissection the vertebral column was divided into cervical, thoracic and lumbar parts and postfixed in a 4% formalin solution for at least 10 days.

Imaging was performed at 300 MHz on a Bruker AM-300 spectrometer equipped with a vertical 7.0 T super wide bore magnet (15 cm) and a micro imaging probehead with actively shielded gradients. A standard spin echo multislice sequence was used to obtain transverse images (256 x 256 pixels) with an echo time (TE) of 12 ms and a repetition time (TR) of 3 s. The in-plane resolution was 40 x 40 µm while the slice thickness corresponded to 500 µm. Corresponding spinal cord segments were embedded in plastic and 2 µm sections were stained with cresyl violet, Soedan black and anti-myelin basic protein antibody staining.

Control NMR images show a clear delineation between the white and grey matter while anatomical features of both the spinal cord and vertebral bodies are clearly visualized in detail.

High resolution NMR imaging (40 x 40 µm in-plane resolution) at high field (7.0 T) of fixed spinal cords of EAE rats at different stages of the disease show different sharply delineated abnormalities in comparison with the spinal cords of healthy rats. These abnormalities correlate in a high degree with the neuropathological features.

---

 Abstract
 

---

 TEST OF THE MEMBRANE PERMEABILITY OF PARAMAGNETIC METAL COMPLEXES  
 OF DERIVATIVES OF 3-ACETYLTETRAMIC ACID BY NMR MICROSCOPY
 

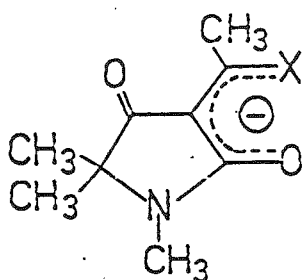
---

C.Mügge, S.Päuser, A.Zschunke

 Institute of Analytical Chemistry, Humboldt University of Berlin  
 Hessische Str. 1-2, D(0)-1040 Berlin

The membrane penetration of NMR contrast agents is important to imaging and spectroscopy of subcellular structures.

Metal complexes of 1,5,5-trimethyl-3-acetyltetramic acid derivatives



complex	X (ligand)	M
I	N-CH <sub>2</sub> -CH <sub>2</sub> -N	Cu <sup>2+</sup>
II	O	Fe <sup>3+</sup>
III	O	Gd <sup>3+</sup>

are soluble in water and should be able to penetrate biological membranes because of hydrophobic groups at the molecule.

3-Acetyltetramic acid is contained in some biological active natural products and is known as membrane permeably.

An appropriate test system to study membrane permeability by means of NMR microscopy is the oocyte of *Xenopus laevis*.

In connection with the relaxivities of different complexes in aqueous solution and in culture medium the changes of T<sub>1</sub>- and T<sub>2</sub>-values and contrasts indicate the membrane penetration.

Preliminary results show the Cu complex (I) is membrane permeably.

Real-Time Imaging of Acute Cadmium Toxicity in Cherrystone Clams  
(Mercenaria mercenaria) by NMR

Paul C. Wang<sup>1</sup> and Lou-sing Kan<sup>2</sup>

1. Howard University, Washington, DC 20060
2. Johns Hopkins University, Baltimore, MD 21205

The transition metal cadmium is widely used in industrial processes and constitutes one of the major environmental pollutants. Cadmium has been shown to be toxic to a variety of wildlife including shell fish. In this study, we used NMR imaging technique as a non-invasive procedure to monitor possible damages by cadmium to individual Cherrystone clams on a real time basis.

Cherrystone clams from Chesapeake Bay, Maryland, USA size ranging from six to eight cm in diameter were used. Clams were incubated in ten gallon tanks with instant sea water (North Carolina Biological) with or without 100  $\mu\text{m}$  CdCl<sub>2</sub> at 15°C for two to four weeks. A 4.7 T 33 cm bore size magnet was used with a 5 cm diameter saddle shaped coil for high resolution study. A spin echo imaging sequence with TR, 3 sec, and TE, 27 msec, was used. The slice thickness was 1.5 mm and the spatial resolution was 97  $\mu\text{m}$ . A 0.5 T scanner with a 10 cm diameter solenoidal coil was used for T1 relaxation time measurements. Cadmium content in different tissues of the clams was also measured by atomic absorption spectrometry for correlation.

A series of high resolution cross sectional images along the short and long axes of the clams were obtained. Detailed anatomical structures such as: foot, intestines, adductor muscles, stomach, gills and anus were clearly discerned. In T1 measurements, the T1 varies not only depending on the cadmium concentration in the tissues but also the types of tissues. The level of cadmium accumulation in various tissues of the clam upon exposure for various times was directly measured by atomic absorption spectroscopy. T1 values are significantly shortened particularly in the gill. The atomic absorption spectroscopy data is nicely correlated with T1 measurements.

Cadmium at as low as 0.2  $\mu\text{m}$  is rapidly (6 hours) lethal to cells in culture and 2 mg/Kg is lethal to whole animals such as mice. However, in clams at dosage 100  $\mu\text{m}$  used, no visible decoloration or necrosis was apparent visually but the difference in NMR images became increasingly obvious with time in a matter of hours. It is significant that the major structure change lies in the muscle instead of kidney even though the latter is expected to concentrate the highest amount of cadmium. It is possible that the differential distribution of metal in specific organs may reflect the homeostatic state and defense mechanism of an animal. That is in muscle myosin fibers are more sensitive to cadmium and the clumping of the muscles prevents further intakes of the toxic metals.

## Three Dimensional NMR Microscopy of Corn Kernels Using Fast Interleaved Projection Reconstruction

R. Ruan<sup>1</sup>, X. Zhou<sup>2</sup>, J. B. Litchfield<sup>1</sup>, and P. C. Lauterbur<sup>2</sup>

Department of Agricultural Engineering<sup>1</sup> and Biomedical Magnetic Resonance Laboratory<sup>2</sup>, University of Illinois at Urbana-Champaign

Studies of water distribution and structural changes inside corn kernels are of fundamental importance in many processes such as drying and steeping. Traditional techniques for these studies are generally invasive and destructive so that following these processes as they occur is impossible. Recently developed techniques using magnetic resonance imaging and microscopy, with their unique non-invasive and non-destructive nature, have great potential in studying moisture distribution and structural changes in the corn kernel(1), although spatial resolution and imaging time remain as two major obstacles. We have used a method based on interleaved projection acquisitions to optimize these two factors, allowing a full 3D data set with an isotropic voxel size of  $(74 \mu\text{m})^3$  to be acquired within three minutes (2).

The pulse sequence used in this method is diagramed below (Fig.1). The flip angle of the RF pulse is calculated by the Ernst formula. The orientations of the magnetic field gradient vector, synthesized from three orthogonal gradients, are divided into several subsets, each covering the full 3D space with a different initial angle. Although the angular sampling density of each subset may not be sufficient for high resolution image reconstruction, different subsets, which do not contain any redundant k-space vectors, can be combined to increase the angular sampling density for high resolution image reconstruction (Fig. 2). Since the total number of projections for each subset is relatively small (typically 2642 projections), the data acquisition can be accomplished within 2~3 minutes using the Ernst flip angles. Each sequential subset of projections is used to construct an image with low spatial resolution. Projections from those subsets where no spatial displacements are detected can be combined to reconstruct a high resolution image. Experimental studies were performed on a yellow dent corn kernel containing structures with a range of  $T_1$  values. The  $T_2$ 's within the kernel were relatively short (a few milliseconds) at 200 MHz, so that we employed an FID acquisition to avoid the signal attenuation which occurs in most of the echo sequences. Experiments were carried out on a SISCO instrument (4.7 T) using a custom-built microscope consisting of a 1 cm surface coil and a set of gradient coils giving a gradient strength of 5 Gauss/cm (2). Each subset contained 2642 projections collected in less than 3 minutes, and a total number of 4 such subsets was acquired.

In the four low resolution images reconstructed from each individual subset, germ, pericarp, and endosperm were identified, although some artifacts due to insufficient angular sampling appeared in these images. When the four subsets were combined, the resultant image clearly demonstrated internal structures and moisture distributions with an improved S/N and reduced artifacts. Using this fast and flexible acquisition method, studies of steeping processes of the corn kernel are being conducted to study quantitatively moisture movements and structural changes.

Acknowledgements: This work was partially supported by the Servants United Foundation. We thank C.S. Potter for the image reconstruction software and the National Center for Supercomputing Applications for the computing facilities.

- (1) R. Ruan and J.B. Litchfield, "ASAE Winter Meeting", Chicago, IL, 1990.
- (2) X. Zhou and P. C. Lauterbur, "Abstracts of the 10th SMRM", San Fransisco, CA, 1991.

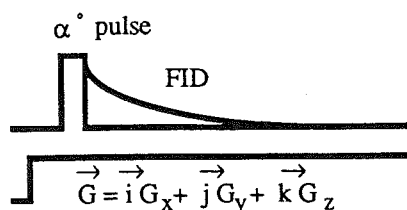


Fig. 1 3D fast acquisition pulse sequence

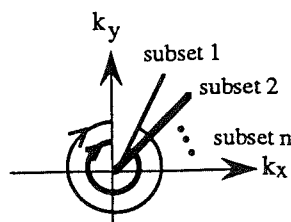


Fig. 2 Interleaved projections

**IN-VIVO MAGNETIC RESONANCE MICROSCOPY FOR NON-DESTRUCTIVELY INVESTIGATING PLANTS, FRUITS, VEGETABLES AND SMALL ANIMALS.**

**S. Crestana** (NPDIA-EMBRAPA, P.O. Box 741. 13560 São Carlos, S.P.-Brazil) ; **Kauten, R. and Nielsen, D. R.** (University of California. 95616 Davis-CA-USA)

Presently, the non-invasive and local evaluation of the internal structure of porous and biological systems consists of a real scientific and technological challenge. Particularly, in the areas related to Agriculture, Food Science, Plant Physiology, Veterinary Medicine and related ones non-destructive studies of biological, physical and chemical processes occurring in the interior of fruits, vegetables, plant tissues and small animals are of great interest. The internal quality evaluation of fruits and vegetables is an important factor in the production and marketing selection. Also, diagnosis of in-vivo animals is highly desirable in Veterinary Medicine research. The results to be shown are demonstrating that Magnetic Resonance Imaging (MRI) performed at micrometric resolution is already an achievable and novel opportunity for characterizing and quantifying those processes and problems. The images were obtained by employing a non-medical NMR spectrometer commercially designed for in-vivo imaging small objects and animals( up to 20 cm internal diameter). High-resolution coils were used and set up in the centre of the magnetic cavity aiming the obtention of microscopic images with pixel resolution better than 50 microns. With the goal of testing the appropriateness of high-resolution MRI in investigating the presence of bruises, voids, seeds, pits, stage of maturity, dry regions and worm damage of several fruits and vegetables such as tomatoes, peaches, nectarines, apples, oranges and a bean seedling in a soil column were imaged. In-vivo MRI of small animals such as small dogs and a macaw (parrot) permitted the observation and diagnosis of knee and ear infections, hydrocephalic anomalies and brain lesions. The principal constraints and possibilities of obtaining MR images of porous and biological materials such as those studied, at high-resolution, will be discussed.

## Structural studies of the stems of flax (*Linum usitatissimum*) by NMR microscopy and conventional histological techniques.

Gordon J. McDougall<sup>a</sup>, Bernard A. Goodman<sup>a</sup>, John A. Chudek<sup>b</sup> and Shelagh N. Scrimgeour<sup>b</sup>

<sup>a</sup> Scottish Crop Research Institute, Invergowrie, Dundee DD2 5DA, UK

<sup>b</sup> Department of Chemistry, University of Dundee, Dundee DD1 4HN, UK

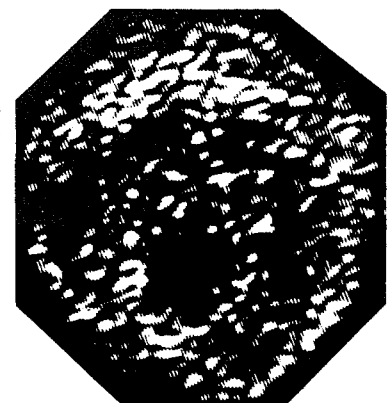
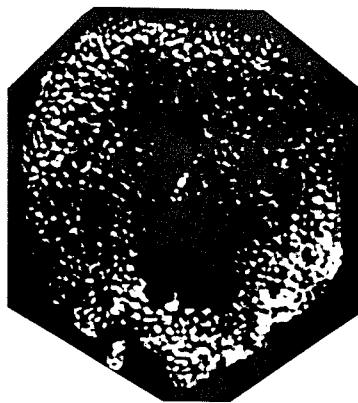
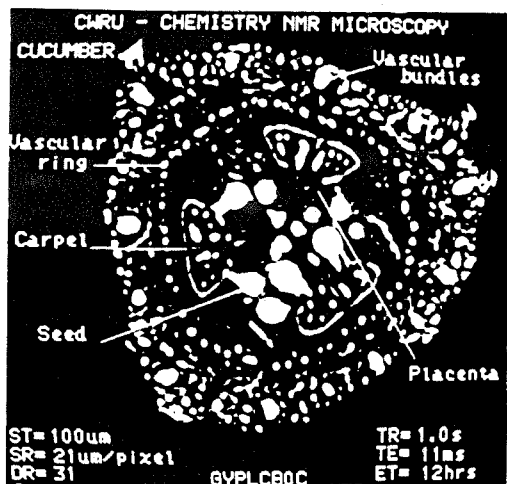
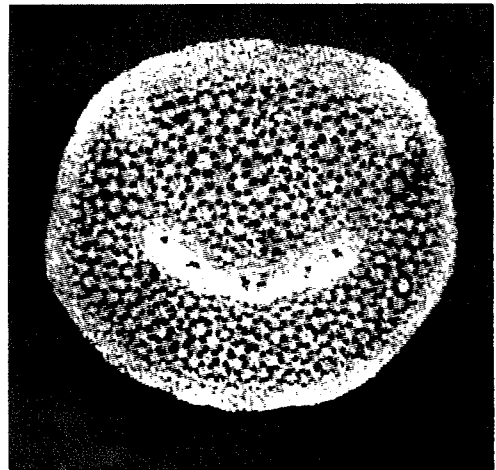
The spin echo pulse sequence has been employed to obtain NMR microscopic images of the spatial distribution of mobile protons around the cotyledonary node of flax (*Linum usitatissimum*) plants of two differing growth morphologies. The gross anatomy of the tissues of the stem is clearly discerned and excellent images are obtained of the complex changes in stem structure that occur at the point of emergence of the side shoots. Detailed structure can be visualised within the xylem and the presence of fibre bundles deduced as dark areas amongst tissues of higher mobile proton density.

As a result of the non-invasive and non-destructive nature of the NMR procedure, the images have been compared with micrographs obtained by conventional histological techniques on the same plant tissue. In general, there is good agreement between the two sets of results, but the NMR images are complicated by the presence of paramagnetic molecules. These produce enhanced relaxation rates of protons in their vicinity and an apparent increase in proton density when short delay times are used. Such images, therefore, can provide chemical information in addition to structural details.

$^{17}\text{O}/^1\text{H}$  MR MICROSCOPY STUDIES OF PLANT ANATOMY AND PHYSIOLOGY

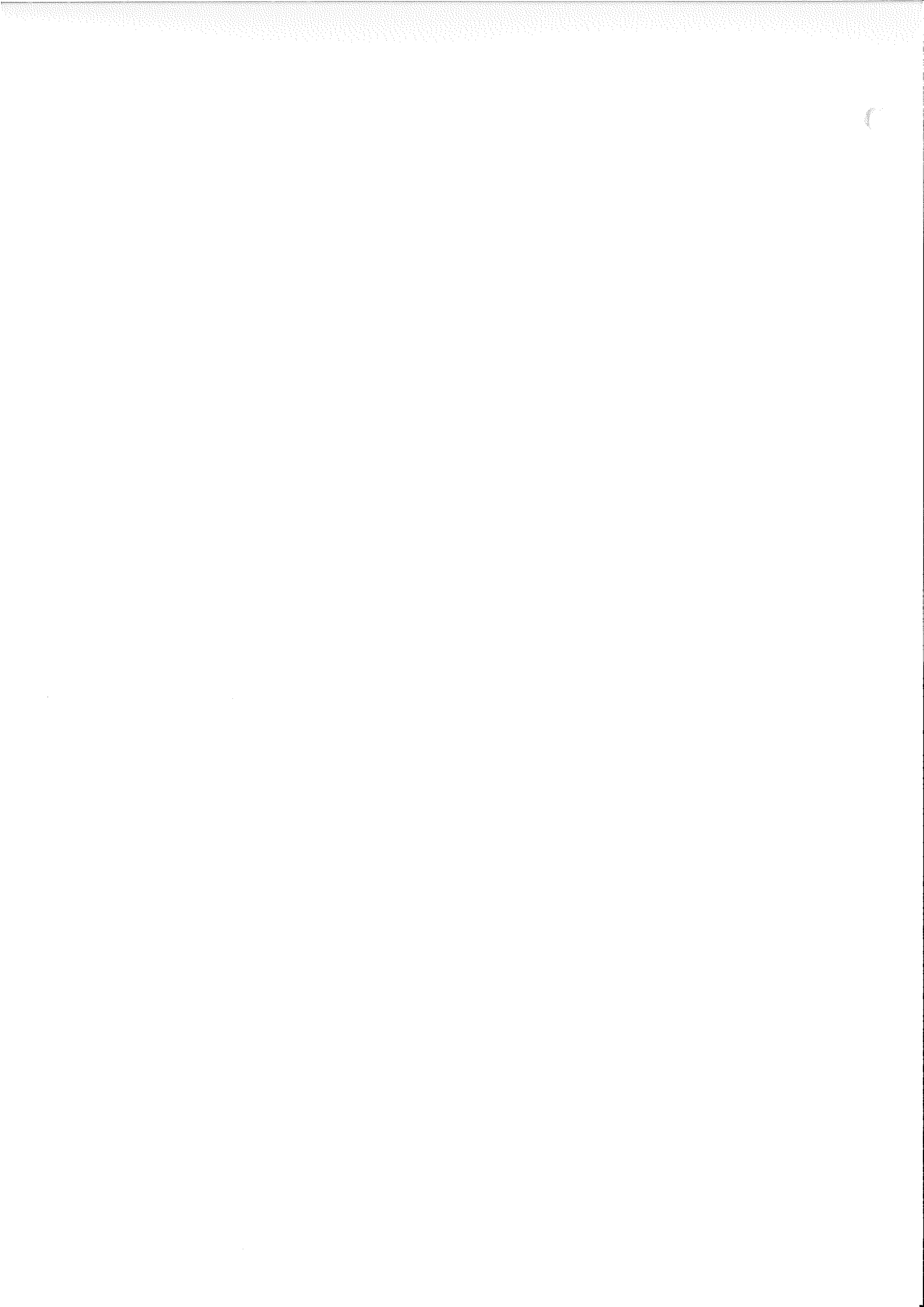
Gheorghe D. Mateescu, Department of Chemistry  
Case Western Reserve University, Cleveland, Ohio 44106, USA

Auspiciously, our first high resolution  $^1\text{H}$   $\mu$ -image of a plant (African Violet petiole, Fig. 1) yielded a smiling face. This was followed by an interesting occurrence: a small cucumber which had already been imaged was given to a botanist (1) to take a picture of the same site with an optical microscope. He said he was embarrassed because, while sectioning the cucumber, he had forced some seeds out of their placenta. But it amazed him seeing that the MR micrograph indicated the seeds were already displaced in the intact object (Figure 2). The possibility to register  $^{17}\text{O}$  images with  $^1\text{H}$  images without altering the plant position allowed us to initiate studies of water absorption and flow.  $^{17}\text{O}$  has been shown to be an excellent tracer for detection of water molecules in a pool of natural abundance water (2). This is illustrated in Figures 3 and 4. A tomato stem was imaged before and after immersion in a pool of  $\text{H}_2^{17}\text{O}$  (enriched to 45 atom %  $^{17}\text{O}$ ). Although the  $^{17}\text{O}$  resolution is worse than that of proton by a factor of 7.37 (the ratio of their magnetic moments) it is seen that it is possible to follow exogenous water distribution with a reasonable degree of accuracy. Another interesting application is the study of absorption and distribution of  $^{17}\text{O}$  labeled phosphate, sulphate and carbonate ions. We will discuss the potential and limitations of the oxygen-17 method for quantitative analysis.



1. This communication is dedicated to Norman A. Alldridge, the botanist, whose untimely death is much regretted by this colleague-friend.
2. G.D. Mateescu, G. Yvars, I. Pazara, N. Alldridge, J.C. LaManna, W.D. Lust, M. Mattingly & W. Kuhn, in *Synthesis and Applications of Isotopically Labeled Compounds*, eds. Baillie & Jones, Elsevier, Amsterdam (1989) 499-508.

# Authors



Ackerman, J.J.H. (RAI 1)	70
Ackerman, J.L. (RAI 3)	72
Aiken, N. (BIO 7)	62
Albert, K. (MAT 7)	42
Albert, K. (MAT 12)	100
Alderweireldt, F. (MAT 11)	99
Altmeyer, P. (BIO 13)	122
Altobelli, S.A. (MET 5)	26
Armstrong, R.L. (DIF 2)	46
As, H. van (BIO 9)	65
As, H. van (DIF 7)	110
As, H. van (DIF 8)	111
Aygen, S. (BIO 13)	122
Back, P.J. (MET 9)	82
Barrall, G.A. (DIF 4)	48
Bartuska, V.K. (CPI 3)	53
Bauermann, T. (BIO 13)	122
Bayer, E. (MAT 7)	42
Bayer, E. (MAT 12)	100
Bendel, P. (MET 23)	96
Bendel, P. (RAI 4)	73
Benveniste, H. (BIO 2)	56
Berliner, L.J.	20
Berliner, L.J. (EPI 2)	32
Berliner, L.J. (EPI 5)	97
Bernardo, M.L., Jr. (Opening Lecture)	
Bijl, G. (MET 8)	30
Black, R.R. (BIO 2)	57
Blackband, S.J. (BIO 7)	62
Blümich, B. (MAT 5)	40
Blümich, B. (RAI 5)	74
Blümich, B. (MET 19)	92
Blümich, B. (MET 20)	93
Blümich, B. (MAT 13)	101
Blümmler, P. (MAT 5)	40
Blümmler, P. (MAT 13)	101
Bolas, N. (CPI 4)	54
Bolt-Westerhoff, J.A. (MAT 8)	43
Bosch, C. S. (RAI 1)	70
Bowtell, R. (MET 1)	22
Brekelmans, M. (BIO 20)	130

Brereton, I. (BIO 5)	60
Brill, R. (MET 17)	90
Brill, R. (MAT 19)	107
Brink, J.S. van den (MAT 15)	103
Brown, G. (MET 1)	22
Brown, J. (MAT 18)	106
Brunner, P. (MET 13)	86
Bruynooghe, O. (MAT 9)	44
Callaghan, P.T. (DIF 3)	47
Callaghan, P.T. (DIF 9)	50
Callaghan, P.T. (MET 9)	82
Callaghan, P.T. (MET 10)	83
Callaghan, P.T. (MET 16)	89
Callaghan, P.T. (MAT 14)	102
Callaghan, P.T. (DIF 10)	112
Callaghan, P.T. (DIF 11)	113
Callaghan, P.T. (DIF 12)	114
Callaghan, P.T. (DIF 13)	115
Canet, D. (MET 7)	29
Carpenter, T.A. (MAT 4)	39
Carpenter, T.A. (MET 21)	94
Caprihan, A. (MET 5)	26
Chingas, G.C. (DIF 4)	48
Cheng, G.-Q. (RAI 4)	73
Chudek, J.A. (PLA 3)	68
Chudek, J.A. (MAT 17)	105
Chudek, J.A. (PLA 8)	135
Chudek, J.A. (BIO 14)	123
Clayden, N.J. (MAT 4)	39
Cory, D.G. (MET 2)	23
Cory, D.G. (MAT 3)	38
Cofer, G.P. (BIO 2)	56/57
Coy, A. (MET 9)	82
Coy, A. (MET 16)	89
Coy, A. (DIF 13)	115
Crestana, S. (MAT 18)	106
Crestana, S. (PLA 7)	134
Crozier, S. (BIO 5)	60
Dannhauer, K. (BIO 6)	61
Datema, K.P. (MAT 8)	43
Daxer, A. (BIO 19)	128/129

Doddrell, D.M. (BIO 5)	60
Dommissie, R. (MAT 11)	99
Dommissie, R. (BIO 20)	130
Doran, S.J. (MET 21)	94
Durand-Vidal, S. (MAT 9)	44
Dusschoten, D. van (BIO 9)	65
Dykstra, R. (MET 9)	82
Evelhoch, J. L. (RAI 1)	70
Ewert, U. (EPI 4)	35
Feng, I.-J. (MET 11)	84
Fens, T.W. (MAT 15)	103
Fichtner, K.-P. (BIO 1)	55
Fichtner, K.-P. (MET 22)	95
Fresneau, D. (BIO 15)	124
Freyer, J.P. (DIF 5)	49
Frydman, L. (DIF 4)	48
Fujii, H. (EPI 5)	97
Fujii, H. (EPI 2)	32
Fukushima, E. (MET 5)	26
Gammal, S. el (BIO 13)	122
Garroway, A.N. (MET 2)	23
Garrido, L. (RAI 3)	72
Gerrits, P.O. (BIO 20)	130
Gersonde, K. (BIO 6)	61
Gewalt, S.L. (BIO 2)	57
Goldie, F. (CPI 4)	54
Gonord, P. (BIO 15)	124
Gonord, P. (MAT 9)	44
Goodman, B.A. (PLA 3)	68
Goodman, B.A. (BIO 14)	123
Goodman, B.A. (PLA 8)	135
Gordon, S.C. (BIO 14)	123
Gorrebeeck, C. (MAT 11)	99
Gravenmade, E.J. 's- (BIO 20)	130
Gross, D. (BIO 11)	120
Gross, D. (BIO 16)	125
Groß, D. (BIO 20)	130
Grossa, M. (MAT 7)	42
Groth, N. (EPI 4)	35
Grucker, D. (EPI 3)	33/34
Gründer, W. (BIO 6)	61

Guillot, G. (MAT 9)	44
Günther, E. (RAI 5)	74
Günther, U. (MAT 7)	42
Hall, L.D. (MAT 4)	39
Hall, L.D. (MET 21)	94
Hartwig, R. (BIO 13)	122
Harwood, J.S. (DIF 4)	48
Hedges, L.K. (Opening Lecture)	
Hedlund, L.W. (BIO 2)	57
Hehn, M. (MET 20)	93
Heine, M. (BIO 11)	119
Hennel, F. (MET 18)	91
Herrling, T. (EPI 4)	35
Holstege, G. (BIO 20)	130
Hornung, P.A. (CPI 1)	51
Hotchkiss, R. S. (RAI 1)	70
Hsu, E. (BIO 7)	62
Hull, W. E. (BIO 1)	55
Hull, W.E. (MET 22)	95
Hunter, G. (MAT 17)	
Hyslop, W.B. (Opening Lecture)	
Hyslop, W.B. (DIF 6)	109
Ikeya, M. (EPI 1)	31
Ilg, M. (MAT 7)	42
Ilg, M. (MAT 12)	100
Jackson, P. (MAT 4)	39
Jansen, J. (MAT 5)	40
Jansen, J. (MET 19)	92
Jasinski, A. (MET 12)	85
Jeffrey, K.R. (DIF 9)	50
Jeffrey, K.R. (DIF 12)	114
Jelinski, L. W. (BIO 4)	59
Jezzard, P. (MAT 4)	39
Johnson, G.A. (BIO 2)	57
Kabalka, G.W. (RAI 4)	73
Kakinuma, K. (EPI 5)	97
Kan, L.-S. (PLA 5)	132
Kan, S. (MAT 9)	43
Kan, S. (BIO 15)	124
Kärger, J. (MAT 8)	43
Kärger, J. (DIF 1)	45

Kauten, R. (MAT 18)	106
Kauten, R. (PLA 7)	134
Kimmich, R. (MET 3)	24
Kirsch, C.F. (DIF 5)	49
Köckenberger, W. (DIF 12)	114
Koeller, E. (MAT 6)	41
Koeller, E. (MAT 10)	98
Koeller, G. (MAT 10)	98
Koenig, J.L. (MAT 1)	36
Komoroski, R.A. (MAT 2)	37
Konstanczak, P. (MET 19)	92
Kozlowski, P. (MET 12)	85
Kramann, B. (BIO 18)	128/129
Kriete, A. (BIO 12)	121
Kuhn, W. (MAT 6)	41
Kuhn, W. (MET 17)	90
Kuhn, W. (MAT 10)	98
Kuhn, W. (MAT 19)	107
Kuhn, W. (MAT 20)	108
Kuhn, W. (BIO 10)	118
Kuhn, W. (BIO 19)	128
Kusaka, Y. (BIO 6)	61
Kwiecinski, S. (BIO 8)	64
Lanens, D. (MAT 11)	99
Lanens, D. (BIO 20)	130
Lauterbur, P.C. (Opening Lecture)	
Lauterbur, P.C. (MET 14)	87
Lauterbur, P.C. (MET 15)	88
Lauterbur, P.C. (DIF 6)	109
Lauterbur, P.C. (BIO 17)	127
Lauterbur, P.C. (PLA 6)	133
Lehmann, V. (BIO 11)	120
Lehmann, V. (BIO 16)	125
Lemaire, C. (DIF 2)	46
Lemiere, G. (MAT 11)	99
Lepoivre, J. (MAT 11)	99
Linden, A. van der (MAT 11)	99
Linden, A. van der (BIO 20)	130
Link, J. (MET 13)	86
Litchfield, J.B. (PLA 6)	133
Lloyd, C.H. (MAT 17)	105

Lüscher, K. (MET 13)	86
MacGowan, D. (DIF 13)	115
Mackay, R.L. (MAT 17)	105
Maffei, P. (MET 7)	29
Majors, P.D. (MET 5)	26
Mansfield, P. (MET 1)	22
Maraviglia, B. (MET 4)	25
Maronpot, R.R. (BIO 2)	56/57
Mateescu, G.D. (BIO 3)	58
Mateescu, G.D. (RAI 2)	72
Mateescu, G.D. (PLA 9)	136
Mattingly, M. (CPI 2)	52
McDougall, G.J. (PLA 8)	135
McJury, M. (MET 1)	22
Menzinger, M. (DIF 2)	46
Miller, J.B. (MET 2)	23
Moll, F. (MAT 10)	98
Moore, J.R. (RAI 3)	72
Mügge, C. (BIO 21)	131
Neeman, M. (DIF 5)	49
Nesbitt, G.J. (MAT 15)	103
Neue, G. (MAT 16)	104
Ni, X. (MET 11)	84
Nielsen, D.R. (MAT 18)	106
Nielsen, D.R. (PLA 7)	134
Nil, J.J. (RAI 1)	70
Packer, K.J. (DIF 13)	115
Palstra, W.D. (BIO 9)	65
Palstra, W. (DIF 8)	111
Päuser, S. (BIO 21)	131
Pfeifer, H. (DIF 1)	45
Pfleiderer, B. (RAI 3)	72
Pfleiderer, B. (MAT 12)	100
Pines, A. (Special Lecture)	21
Pope, J.M. (PLA 1)	66
Pope, J.M. (DIF 14)	117
Posadas, A. (MAT 18)	106
Potter, C.S. (Opening Lecture)	
Potter, C.S. (BIO 17)	127
Raich, H. (MET 20)	93
Randell, C.F. (CPI 4)	54

Rapp, W. (MAT 12)	100
Roberts, N. (MAT 15)	103
Rofe, C.J. (MET 10)	83
Rofe, C.J. (DIF 11)	113
Rohr, G. (BIO 11)	119/120
Rohr, G. (BIO 16)	125/126
Ruan, R. (PLA 6)	133
Ruhm, W. (BIO 11)	119/120
Ruhm, W. (BIO 16)	125/126
Sagnowski, S. (BIO 8)	63/64
Samoilenko, A.A. (MET 6)	28
Sarafis, V. (PLA 2)	67
Sarkar, S.N. (MAT 2)	37
Saunders, J.K. (MET 12)	85
Schauß, G. (MAT 5)	40
Schauß, G. (MET 20)	93
Schoeniger, J.S. (BIO 7)	62
Schuff, N. (CPI 1)	51
Schuff, N. (MET 11)	84
Scrimgeour, S.N. (PLA 3)	68
Scrimgeour, S.N. (MAT 17)	105
Scrimgeour, S.N. (BIO 14)	123
Scrimgeour, S.N. (PLA 8)	135
Sharp, J. (MET 1)	22
Skibbe, U. (MAT 16)	104
Sillerud, L.O. (DIF 5)	49
Snaar, A. (DIF 7)	110
Snaar, J.E.M. (BIO 9)	65
Soma, M. (BIO 10)	118
Song, S.-K. (RAI 1)	70
Spanoghe, M. (MAT 11)	99
Spanoghe, M. (BIO 20)	130
Spiess, H.W. (MAT 5)	40
Spiess, H.W. (RAI 5)	74
Spiess, H.W. (MET 20)	93
Staemmler, M. (MET 17)	90
Staemmler, M. (MAT 19)	107
Staemmler, M. (MAT 20)	108
Stahl, J (MAT 19)	107
Staszkow, E. (BIO 8)	63/64
Suddarth, S.A. (BIO 2)	56/57

Theis, I. (MAT 6)	41
Thiessenhusen, K.U. (EPI 4)	35
Todd, B.E. (BIO 2)	56/57
Tomanek, B. (BIO 8)	63/64
Tzalmona, A. (DIF 2)	46
Urbanski, A. (MET 12)	85
Valerius, K.-P. (BIO 12)	121
Veeman, W.S. (MET 8)	30
Vyver, F. van de (MAT 11)	99
Vyver, F. van de (BIO 20)	130
Walton, N. (MAT 4)	39
Wang, C.Y. (PLA 4)	69
Wang, P.C. (PLA 4)	69
Wang, P.C. (PLA 5)	132
Wark, U. (BIO 11)	119/120
Wark, U. (BIO 16)	125/126
Wiggins, C.J. (MAT 4)	39
Williamson, B. (PLA 3)	68
Woodford, J.A.T. (BIO 14)	123
Wu, Y. (RAI 3)	72
Xia, Y. (DIF 9)	50
Xia, Y. (MAT 14)	102
Xia, Y. (DIF 10)	112
Xia, Y. (DIF 11)	113
Xia, Y. (DIF 12)	114
Yao, S. (DIF 14)	116/117
Zelaya, F.O. (DIF 13)	115
Zhou, X. (Opening Lecture)	
Zhou, X. (MET 14)	87
Zhou, X. (MET 15)	88
Zhou, X. (BIO 17)	127
Zhou, X. (PLA 6)	133
Zschunke, A. (BIO 21)	131

# Participants

Ackerman, Prof. J.J.H.  
Washington Univ., Dept. of Chemistry  
  
St. Louis, MO 63130-4899  
USA

Ackerman, Prof. J.L.  
NMR Center, Dept. of Radiol., Mass. Gen. Hosp  
149th Street  
Charlestown, MA 02129  
USA

Albert, Dr. Klaus  
Inst. für Organische Chemie  
Auf der Morgenstelle 18  
7400 Tübingen  
Germany

Altenmüller, Andreas  
FHG-Medizintechnik  
Ensheimerstr. 48  
6670 St. Ingbert  
Germany

Andrew, Prof. E. Raymond  
Depart. of Physics/Univ. of Florida  
215 Williamson Hall  
Gainesville  
32611 Florida - USA

Antz, Christof  
MPI für Med. Forschg., NMR Gruppe Kalbitzer  
Jahnstr. 29  
6900 Heidelberg  
Germany

Armstrong, Prof. R.L.  
Univ. of New Brunswick  
P.O. Box 4400  
Fredericton, N.B., E3B 5A3  
Canada

As, Dr. Henk van  
Agric. Univ., Dept. Mol. Physics  
Dreyenlaan 3  
6703 HA Wageningen  
Netherlands

Atzori, Marco  
Poly bios/IBT research centre  
Padriciano 99, Area di Ricerca  
Trieste  
Italy

Bachert, Peter  
Dt. Krebsforschungszentrum  
Im Neuenheimer Feld 280  
6900 Heidelberg  
Germany

Back, Philip  
Department of Physics and Biophysics  
Massey University  
Palmerston North  
New Zealand

Barth, Peter  
FHG-IzfP-Mt  
Ensheimer Str. 48  
6670 St. Ingbert  
Germany

Bartuska, Victor J., Ph. D.  
Chemagnetics Inc.  
2555 Midpoint Drive  
Fort Collins, CO 80525  
USA

Baumann, Dr. Joachim  
Siemens AG München  
Otto-Hahn-Ring 6  
8000 München  
Germany

Beauvallet, Dr. Christian  
INRA-Centre de Recherches  
Zootechniques et Vétérinaires  
63122 Ceyrat  
France

Bele, Petra  
MPI f. Med. Forschg. AG Molekülkristalle  
Jahnstr. 29  
6900 Heidelberg  
Germany

Bellemann, Matthias  
DKZ, Inst. f. Radiol. u. Pathophysiол.  
Im Neuenheimer Feld 280  
6900 Heidelberg  
Germany

Bendel, Dr. Peter  
Weizmann Institute  
  
Rehovot  
Israel

Beringhelli, Prof. Tiziana  
Univ. di Milano, Dept. Chemistry  
Via Venezian 9  
20133 Milano  
Italy

Berliner, Lawrence J.  
The Ohio State Univ, Dept. of Chemistry  
120 W. 18th Avenue  
Columbus, OH 43210-1173  
USA

Bernhard, Thomas  
MPI f. Med. Forschg.  
Jahnstr. 29  
6900 Heidelberg  
Germany

Blümich, Dr. Bernhard  
MPI für Polymerforschg.  
Postfach 3148  
W-6500 Mainz  
Germany

Beynon, Peter J.  
Kodak Ltd. Research Div.  
Headstone Drive  
Marrow, Midd.  
Uk HA1 1Pf

Blümmler, P.  
MPI - Polymerforschung  
Postfach 3148  
6500 Mainz  
Germany

Bijl, G.  
University of Nijmegen, Physical Chemistry  
Toernooiveld 1  
Nijmegen  
The Netherlands

Boeffel, Christine  
MPI für Polymerforschg.  
Ackermannweg 10  
6500 Mainz  
Germany

Blackband, Dr. Stephen J.  
Depart. of Radiology and Radiological Sc.  
600 N. Wolfe Street  
Baltimore, MD 21205  
USA

Bogda, Dr. Mircea  
Inst. for Isotopic and Molecular Technology  
65-103 Donath Street, Box 700  
3400 Cluj Napoca  
Romania

Blankenstein, Christiane  
FHG, Medizintechnik  
Ensheimer Str. 48  
6670 st. Ingbert  
Germany

Brancolini, Dr. Alberto  
Agip  
Milano  
Italy

Brandl, Matthias  
Univ. Würzburg, EP V  
Am Hubland  
W-8700 Würzburg  
Germany

Brill, Roland  
FHG-IzfP-Mt  
Ensheimer Str. 48  
6670 St. Ingbert  
Germany

Bronnimann, Charles E.  
Chemagnetics/Otsuka Electronics  
2555 Midpoint Drive  
Fort Collins, CO 80525  
USA

Budzylek, Dietmar  
Oxford Instruments HT GmbH  
Kreuzberger Ring 38  
6200 Wiesbaden  
Germany

Callaghan, Prof. Paul  
Department of Physics and Biophysics  
Massey University  
Palmerston North  
New Zealand

Canet, Prof. Daniel  
Université de Nancy I, Lab. Method. RMN  
BP 239  
54506 Vandoeuvre-Nancy  
France

Carpenter, Dr. T. Adrian  
Univ. of Cambridge, Herchel Smith Lab.  
University Forvie Site, Robinson Way  
Cambridge  
England, U.K. Cb2 2PZ

Chingas, G.C.  
Lawrence Berkeley Lab.,  
Materials and Chemical Sciences Div.  
Berkeley, California 94720  
USA

Churchill, Simon  
SMIS LTD.  
Alan Turing Road Surrey Research Park  
Guildford  
U.K. Surrey GU2 5YF

Cory, David G.  
Bruker Instruments, Inc.  
19 Fortune Drive  
Billerica, MA 01821  
USA

Coy, Andrew  
Dept. of Physics and Biophysics  
Massey University  
Palmerston North  
New Zealand

Dommissie, R.  
University of Antwerp  
Groenen Borgerlaan 171  
2020 Antwerp  
Belgium

Crestana, Dr. Silvio  
NPDIA-EMBRAPA  
P.O. Box 741  
13560 Sao Carlos-Sao Paulo  
Brazil

Doran, Simon J.  
Univ. of Cambridge  
University Forvie Site, Robinson Way  
Cambridge  
England, U.K. CB2 2PZ

Datema, Dr. K.P.  
KSLA-Shell Research  
Badhuisenweg 3  
Amsterdam 1003 AA  
The Netherlands

Ende, Gabriele  
DKFZ Heidelberg  
INF 280  
6900 Heidelberg  
Germany

Dereppe, J.M.  
Univ. Louvain  
Place L. Pasteur 1 Bte 3A  
B-1348 Louvain la Neuve  
Belgium

Ermark, Frank  
MPI f. Med. Forschg.  
Jahnstr. 29  
6900 Heidelberg  
Germany

Doddrell, D.M.  
University of Queensland  
St. Lucia  
Brisbane, Queensland  
Australia

Feio, Gabriel  
ICTPOL/INIC  
Av. Prof. Gama Pinto 2  
Lisboa Codex  
Portugal-1699

Fichtner, Klaus-Peter  
Dt. Krebsforschungszentrum, Zentrale Spekt.  
Im Neuenheimer Feld 280  
6900 Heidelberg  
Germany

Filsinger, Bernd  
MPI f. Med. Forschg.  
Jahnstr. 29  
6900 Heidelberg  
Germany

Fujii, Hirotada  
The Tokyo Metropol. Inst. of Medical Sciences  
3-18, Honkomagome, Bunkyo-Ku  
Tokyo, 113  
Japan

Fujioka, Mikihiro  
FHG-IzfP-MT  
Ensheimer Str.  
6670 St. Ingbert  
Germany

Fukushima, Eiichi  
Lovelace Medical Foundation  
2425 Ridgecrest Dr., SE  
Albuquerque, NM 87108  
USA

Gairing, Hariolf  
Univ. Würzburg, Lehrst. f. Biophysik, A. Haas  
Am Hubland  
W-8700 Würzburg  
Germany

Garroway, A.N.  
Naval Research Laboratory  
Code 6120  
Washington DC 20315-5000  
USA

Gersonde, Prof. Dr. Klaus  
FHG-IzfP-MT  
Ensheimer Str. 48  
6670 St. Ingbert  
Germany

Geschke, Doz. Dr. D.  
Universität Leipzig, Physik  
Linnestr. 5  
O - 7010 Leipzig  
Germany

Gneiting, Thomas  
Univ. Würzburg, Phys. Inst.  
Am Hubland  
W-8700 Würzburg  
Germany

Gonord, Patrick  
I.E.F., Inst. d'Electronique Fondamentale  
Université Paris Sud - Bât. 220  
91405 Orsay  
France

Gries, Wolfgang  
FHG  
Ensheimer Str. 48  
6670 St. Ingbert  
Germany

Grimmer, Dr. Arnd-Rüdiger  
Zentralinstitut für Anorgan. Chemie  
Rudower Chaussee 5  
O - 1199 Berlin  
Germany

Gross, Dieter  
Bruker  
Silberstreifen  
7512 Rheinstetten  
Germany

Groza, Eng  
Inst. for Isotopic and Molecular Technology  
65-103 Donath Street, Box 700  
3400 Cluj Napoca 5  
Romania

Grucker, Prof. D.  
Inst. Physique Biologique  
4 Rue Kirschléger  
67085 Strasbourg CEDEX  
France

Gründer, Dr. Wilfried  
Univ. Leipzig, Inst. f. Biophysik  
Liebigstr. 27  
O-7010 Leipzig  
Germany

Guillot, Geneviève  
CNRS - IEF, Inst. d'Electronique Fondamentale  
Université Paris Sud - Bât. 220  
91405 Orsay  
France

Günther, Ewald  
MPI - Polymerforschung  
Postfach 3148  
6500 Mainz  
Germany

Haase, Prof. Dr. A.  
Univ. Würzburg, Physikal. Inst.  
Am Hubland  
8700 Würzburg  
Germany

Haeberlen, Prof. Dr. Ulrich  
Max-Planck-Inst. f. Med. Forschung  
Jahnstr. 29  
6900 Heidelberg  
Germany

Herrling, Dr. Thomas  
Zentrum für Wissenschaftl. Gerätebau  
Rudower Chaussee 6  
O-1199 Berlin  
Germany

Hall, Prof. L.D.  
Herchel Smith Lab. of Med. Chem., Univ. Forvi  
Robinson Way  
Cambridge, CB2 2PZ  
United Kingdom

Heuer, Andreas  
MPI f. Med. Forschg., AG Molekülkristalle  
Jahnstr. 29  
6900 Heidelberg  
Germany

Hausser, Prof. Dr. Karl-Hermann  
Max-Planck-Inst. f. Med. Forschung  
Jahnstr. 29  
6900 Heidelberg 1  
Germany

Hoffmann, Dr. Wolf-Dieter  
Sektion Physik der Uni. Leipzig  
Linnéstr. 5  
O - 7010 Leipzig  
Germany

Hennecke, Dr. M.  
BAM  
Unter den Eichen 87  
1000 Berlin 45  
Germany

Honkonen, R.S., Ph. D.  
The Procter & Gamble Co.  
P.O. Box 398707  
Cincinnati. OH 45239-8707  
USA

Hennel, Franciszek  
Jagellonian University Krakow  
Ul. Reymonta 4  
30-059 Krakow  
Poland

Hull, Dr. William E.  
Zentrale Spektroskopie/Dt. Krebsf.inst.  
Neuenheimer Feld 280  
6900 Heidelberg  
Germany

Ikeya, Prof. Motoji  
Osaka Univ., Dept. of Physics  
Toyonaka 560  
Osaka  
Japan

Ilg, Dr. Martin  
Bruker Medizintechnik  
Silberstreifen  
7512 Rheinstetten  
Germany

Jansen, J.  
MPI - Polymerforschung  
Postfach 3148  
6500 Mainz  
Germany

Jeffrey, Kenneth R.  
Massey Univ. Dept. of Physics  
  
Palmerston North  
New Zealand

Jelinski, Lynn W.  
AT&T Bell Laboratories  
600 Mountain Avenue, Room 1C-427  
Murray Hill, NJ 07974  
USA

Jezowski, Iwana, M.Sc  
Jagellanian University Inst. of Physics  
Reymonta 4  
Krakow 30-059  
Poland

Johnson, G. Allan  
Duke University Medical Center, Dept. of Radio  
Box 3302  
Durham, North Carolina 27710  
USA

Jonsen, Dr. Paul  
Chemagnetics  
7, Claro Court Business Center, Claro Road  
Harrogate, HG1 4BA  
England

Kabalka, Prof. George W.  
Chemistry Department  
University of Tennessee  
Knoxville, Tennessee  
USA

Kalbitzer, Hans Robert  
MPI für Med. Forschg.  
Jahnstr. 29  
6900 Heidelberg  
Germany

Kan, Siew  
Inst. d'Électronique Fondamentale  
Université Paris XI - Batiment 220  
F 91405 Orsay Cedex  
France

Kärger, Prof. Dr. Jörg  
Univ. Leipzig, Sektion Physik  
Linnéstr. 5  
O - 7010 Leipzig  
Germany

Kimmich, Prof. Dr. R.  
Univ. Ulm, Sekt. Kernresonanz  
Albert-Einstein-Allee  
7900 Ulm  
Germany

Knaus, Robert  
FHG  
Ensheimer Str. 48  
6670 St. Ingbert

Knauss, Robert  
Fraunhofer Institut  
Ensheimer Str. 48  
6670 St. Ingbert  
Germany

Köckenberger, Walter  
Botanisches Inst./Universität Bayreuth  
Universitätsstr. 30  
8580 Bayreuth  
Germany

Koeller, Elmar  
FHG  
Ensheimer Str. 48  
6670 St. Ingbert  
Germany

Koenig, Jack L.  
Case Western Univ., Dept. Macromoleculart Sci  
  
Cleveland, Ohio 44106  
USA

Kollath, Heidemarie  
  
Haldenstr. 26  
4300 Essen 12  
Germany

Komoroski, Richard A., Ph.D.  
University of Ark. for Med. Sci.  
4301 West Markham, Slot 582  
Little Rock, AR 72205  
USA

Konstanczak, Paul  
TU Berlin, Iwan-N.-Stranski-Inst.  
Str. d. 17. Juni 112  
1000 Berlin 12  
Germany

Körperich, Hermann  
FHG-Izfp-MT  
Ensheimer Str. 48  
6670 St. Ingbert  
Germany

Kotitschke, Klaus  
Univ. Würzburg, Phys. Inst.  
Am Hubland  
W-8700 Würzburg  
Germany

Krishnan, Bala S.  
Bristol-Myers Squibb Company Dept. #902  
5 Research Parkway  
Wallingford, CT 06492  
USA

Kuhn, Dr. Winfried  
FHG-Izfp-MT  
Ensheimer Str. 48  
6670 St. Ingbert  
Germany

Kwiecinski, Stanislaw, MSc  
Inst. of Nucl. Physics  
ul. Radzikowskiego 152  
31-342 Kraków  
Poland

Lauterbur, Prof. Paul C.  
University of Illinois  
1307 West Park Street  
Urbana, Illinois 61801  
USA

Lehmann, Volker  
Bruker  
Silberstreifen  
7512 Rheinstetten  
Germany

Lienhart, Klaus  
MPI für med. Forschg.  
Jahnstr. 40  
6900 Heidelberg  
Germany

Link, Alexander  
Physikal. Inst.  
Am Hubland  
8700 Würzburg  
Germany

Link, Dr. Jürgen  
Spectrospin AG  
Industriestr. 26  
8117 Fällanden  
Switzerland

Liße, Antje  
MPI f. Med. Forschg.  
Hans-Thoma-Str.  
6900 Heidelberg  
Germany

Lloyd, Dr. Charles M.  
Dental Scienc., Dent. School, Univ. of Dundee  
  
Dundee UK (DDI 4HN)  
Scotland

Lohman, Dr. Joost A.B.  
Bruker Spectrospin Ltd.  
Banner Lane  
Coventry, CV1 GGH  
England

Lutz, Dr. Norbert  
Zentrale Spektroskopie/Dt. Krebsf.inst.  
Im Neuenheimer Feld 280  
6900 Heidelberg  
Germany

MacConnachie, Celeste A.  
EMR/CRI  
Oil Patch Drive  
Devon Alta  
Canada TOC IEO

Macho, Dr. Volker  
MPI für Polymerforschung  
Ackermannsweg 10  
6500 Mainz  
Germany

Maffei, Pablo  
Université de Nancy I, Lab. Method. NMR  
BP 239  
54506 Vandoeuvre les Nancy Cedex  
France

Mansfield, Prof. Dr. Peter  
Univ. of Nottingham, Dept. of Physics  
University Park  
Nottingham NG7 2RD  
Great Britain

Manz, Bertram  
MPI f. Med. Forschg.  
Jahnstr.  
6900 Heidelberg  
Germany

Maraviglia, Prof. Bruno  
Univ. La Sapienza, Dipt. di Fisica  
P. le Aldo Moro, 2  
Roma, 00185  
Italy

Mehr, Knut  
Fhg-IzfP-MT, NMR  
Ensheimer Str. 48  
6670 St. Ingbert  
Germany

Maresch, Günter G.  
MPI für Polymerforschung  
Ackermannweg 10  
6500 Mainz  
Germany

Metzler, Alexander  
Uni. Würzburg / Physikal. Inst. V  
Am Hubland  
8700 Würzburg  
Germany

Mateescu, G.D., Ph. D.  
Case Western Reserve University  
10900 Euclid Avenue  
Cleveland, Ohio  
USA

Moreaux, C.  
Univ. Louvain  
Place L. Pasteur 1 Bte 3A  
B-1348 Louvain la Neuve  
Belgium

Mattingly, Mark, Ph. D.  
Bruker Instruments Inc  
Manning Park  
Billerica, Mass. 018121  
USA

Mügge, Dr. Clemens  
Humboldt-Universität  
Hessische Str. 1-2  
O-1040 Berlin  
Germany

Mehlkopf, A.F.  
Delft University of Technology  
Lorentzweg I  
2628 CJ Delft  
Netherlands

Neeman, Michal, Ph.D.  
Los Alamos  
National Lab., Life Sci. Div.  
Los Alamos, MS M888  
USA

Nesbitt, Dr. G.J.  
Shell Research  
Badhuisweg 3, 1031 cm  
Amsterdam  
The Netherlands

Päuser, Sabine  
Humboldt-Universität  
Hessische Str. 1-2  
O-1040 Berlin  
Germany

Neue, Dr. Günther  
Univ. Dortmund, Physikal. Chemie  
Otto-Hahn-Str. 6  
4600 Dortmund 50  
Germany

Pfleiderer, Dr. Bettina  
MGH-NMR Center  
Building 149, 13th Street  
Charlestown, MA 02129  
USA

Nordén, Bo, Ph. D.  
Department of organic chemistry  
University of Umea  
S-90187 Umea  
Sweden

Pines, A.  
Lawrence Berkeley Lab./ Univ. of Calif. Berk.  
  
Berkeley  
USA

Nunes, Teresa  
ICTPOL/LNETI  
Av. Prof. Gama Pinto 2  
Lisboa Codex  
Portugal-1699

Pittard, Dr. Simon  
MAGNEX SCIENTIFIC LTD.  
13, 15 + 19 Blacklands Way  
Abingdon, Oxon OX14 1DY  
England

Palstra, W. D.  
Agric. Univ., Dept. Mol. Physics  
Dreyenlaan 3  
6703 HA Wageningen  
Netherlands

Pope, Prof. J.M.  
University of N.S.W.  
School of Physics P.O. Box 1  
Kensington N.S.W. 2033  
Australia

Popp, Dipl.-Ing. Matthias  
Fa. Wemhöner & Popp oHG  
Jülicher Str. 342  
5100 Aachen  
Germany

Porzel, Dr. Andrea  
Inst. f. Biochemie der Pflanzen  
Weinberg 3  
O - 4050 Halle/Saale  
Germany

Pschorn, Dr. Dr. Uwe  
Boehringer Ingelheim KG  
Dept. of Pharmacology  
W-6507 Ingelheim  
Germany

Randell, Chris  
SMIS LTD.  
Alan Turing Road Surrey Research Park  
Guildford  
U.K., Surrey GU2 5YF

Reichert, Ingmar  
MPI für med. Forschg.  
Jahnstr. 40  
6900 Heidelberg  
Germany

Rofe, Craig  
Department of Physics and Biophysics  
Massey University  
Palmerston North  
New Zealand

Rohr, Dr. Dr. Gerhard  
Klinikum d. Stadt Mannheim, Fak. der. Uni HD  
Theodor-Kutzer-Ufer, Postf. 10 00 23  
6800 Mannheim  
Germany

Rydzynski, Dr. M.  
Institute of Nuclear Physics  
Radzikowskiego 152  
31-342 Krakow  
Poland

Samoilenko, Dr. A.A.  
c/o Bruker Analyt. Meßtech. z.H. Fr. Eichhoff  
Silberstreifen  
7512 Rheinstetten  
Germany

Sarafis, Vassilios  
University of Western Sydney  
Hawkesbury, New South Wales  
Australia

Sarkar, S.K., Ph.D.  
Smithkline Beecham, L-940  
109 Swedeland Road  
King of Prussia PA 19406  
USA

Schuff, Dr. Norbert  
Varian Ass.  
3120 Hansenway D-317  
Palo Alto, CA 94304-1030  
USA

Schaumburg, Kjeld  
Inst. of Chemistry (5)  
H.C. Ørsted Inst.-Universitets Parken 5  
Copenhagen Ø  
DK-2100-Denmark

Scrimgeour, Dr. Sheelagh N.  
Univ. of Dundee, Chemistry Dept.  
  
Dundee  
Scotland, UK. DD1 4HN

Schauß, G.  
MPI - Polymerforschung  
Postfach 3148  
6500 Mainz  
Germany

Shedd, Carol C.  
Dt. Krebsforschungszentrum  
Im Neuenheimer Feld 280  
6900 Heidelberg  
W.-Germany

Scholl, Stefan  
Fraunhofer Institut  
Ensheimer Str. 48  
6670 St. Ingbert  
Germany

Sobottka, Dr. Joachim  
Humboldt-Univ. Berlin, FB 24  
Postfach 56  
0-1120 Berlin  
Germany

Schuck-Hahn, Dr. Regina  
Varian GmbH  
Alsfelderstr. 6, P.O. Box 111435  
6100 Darmstadt  
Germany

Soma, Dr. Mauricio  
Uni. degli studi di Milano, Fac. di Farmacia  
Via Balzaretti 9  
20133 Milano  
Italy

Sonderegger, Markus  
Univ. Zürich, Physik. Inst.  
Schönberggasse 9  
CH-8001 Zürich  
Schweiz

Spiess, Prof. Dr. H.W.  
MPI - Polymerforschung  
Postfach 3148  
6500 Mainz  
Germany

Staemmler, Martin  
Fraunhofer-Institut IzfP-MT  
Ensheimer Str. 48  
6670 St.Ingbert  
Germany

Sulek, Dr. Zenon  
Inst. of Nucl. Physics, Kraków  
ul. Radzikowskiego 152  
31-342 Kraków  
Poland

Tesche, Bernd  
MPI f. Med. Forschg.  
Jahnstr. 29  
6900 Heidelberg  
Germany

Theis, Dr. Isolde  
Fraunhofer-Institut, IzfP-MT  
Ensheimer Str. 48  
6670 St. Ingbert  
Germany

Tilgner, Dr. Rainer  
Siemens AG, HL MT E  
Otto-Hahn-Ring 6  
8000 München 83  
Germany

Tzalmona, Prof. Dr. A.  
Univ. of Toronto, Dept. of Physics  
  
Toronto, Ontario  
Canada, M5S 1A7

Urbanski, Andrzej, MSc  
Inst. of Nucl. Physics  
ul. Radzikowskiego 152  
31-342 Kraków  
Poland

Valenzuela, Alejandro  
Siemens AG, ZFE ME MS 43  
Otto-Hahn-Ring 6  
8000 München 83  
Germany

Veeman, Prof. W.S.  
Univ. of Nijmegen  
Toernooiveld  
Nijmegen 6525 ED  
Netherlands

Vijayaragavan, Dr. Visalakshi

Römerweg 17  
6750 Kaiserslautern  
Germany

Visintainer, Dr. James  
Goodyear Research  
142 Goodyear Blvd.  
Akron, Ohio 44305  
USA

Voelkel, Dr. R.  
BASF AG  
ZKM - Bau G 201  
6700 Ludwigshafen  
Germany

Volke, Dr. Frank  
Univ. Leipzig, WB Molekülphysik, Sekt. Physik  
Linnéstr. 5  
7010 Leipzig  
Germany

Wang, Paul C., Ph.D.  
Howard University, Dept. of Radiology  
2041 Georgia Avenue, N.W.  
Washington, DC. 20060  
USA

Wehrle, Dr. Bernhard  
Bayer AG, ZF-DZA-SF, Geb. Q 18  
Kaiser-Wilhelm-Allee  
5090 Leverkusen-Bayerwerke  
Germany

Wirthlin, Dr. Toni  
Varian International AG  
Kollerstr. 38  
CH-6303 Zug  
Switzerland

Xia, Yang  
Massey University  
Dept. of Physics and Biophysics  
Palmerston North  
New Zealand

Zamir, Dr. David  
SOREQ Research Center  
Yavne 70 600  
Israel

Zetta, Dr. Lucia  
C. N. R., Univ. di Milano  
Via Ampere 56  
20131 Milano  
Italy

Zhou, Xiaohong, Ph.D.  
University of Illinois  
1307 W. Park Street  
Urbana, IL. 61.801  
USA

Zimmermann, Herbert  
MPI F. Med. Forschg.  
Jahnstr. 29 6  
6900 Heidelberg  
Germany